Master's thesis

NTNU
Norwegian University of Science and Technology
Faculty of Natural Sciences
Department of Physics

Ingvild Straumsheim Hoem

Automatic VMAT planning in RayStation for locally advanced cervical cancer

Master's thesis in Applied Physics and Mathematics
Supervisor: Anne Beate Langeland Marthinsen
Co-supervisor: Marit Funderud and Anette Guleng
June 2022

NTNU
Kunnskap for en bedre verden

ST. OLAVS HOSPITAL
UNIVERSITETSSYKEHUSET I TRONDHEIM

Ingvild Straumsheim Hoem

Automatic VMAT planning in RayStation for locally advanced cervical cancer

Master's thesis in Applied Physics and Mathematics
Supervisor: Anne Beate Langeland Marthinsen
Co-supervisor: Marit Funderud and Anette Guleng
June 2022

Norwegian University of Science and Technology
Faculty of Natural Sciences
Department of Physics

NTNU
Norwegian University of
Science and Technology

Abstract

Purpose: This study aimed to develop an automatic volumetric modulated arc therapy (VMAT) planning script for use in RayStation to replace manual VMAT planning for locally advanced cervical cancer (LACC) in the clinic. The automatic VMAT plans should follow the new dose constraints for cervical cancer published by the Norwegian Directory of Health in 2021 and contribute to reduced planning time without negative effects on plan quality.

Materials and methods: The automatic VMAT planning script was designed to follow the new dose constraints and to deliver just enough doses to target volumes and as low doses as possible to organs at risk (OARs). Manual VMAT plans from 25 retrospective LACC patients with and without lymph node metastasis treated at St. Olavs Hospital in 2020-2021 were used for script optimisation and quality assessment of the automatic VMAT plans. The automatic VMAT plans were quantitatively compared to the manual VMAT plans by dose statistics from RayStation and VMAT quality assurance (QA) measurements with the Delta^4 phantom. The plans were qualitatively compared in a blind test with 10 patients performed by physicists and dose planners in the clinic.

Results: The automatic VMAT planning script generated one plan in 30-45 minutes. From the dose statistics, the automatic VMAT plans delivered high enough but lower doses to target volumes than the manual VMAT plans. Doses to most OARs were similar or lower with automatic than with manual VMAT planning. The automatic VMAT plans had a significantly higher conformity index than the manual VMAT plans for all target volumes, mainly caused by less dose leakage to healthy tissue. In the QA measurements, the larger number of monitor units in the automatic VMAT plans compared to the manual VMAT plans had no negative effect on the linac's delivering quality of the plans. For 8/10 patients in the blind test, at least 7/8 respondents preferred the automatic VMAT plan over the manual VMAT plan.

Conclusion: The automatic VMAT planning script developed for LACC patients did reduce planning time without reducing plan quality.

Sammendrag

Formål: Denne studien hadde som mål å utvikle et automatisk planleggingsskript for volumetrisk modulert bueterapi (VMAT) av lokalavansert livmorhalskreft (LACC) for bruk i RayStation, for å erstatte manuell VMAT-planlegging i klinikken. De automatiske VMAT-planene skulle følge de nye retningslinjene for gynekologisk kreft publisert av Helsedirektoratet i 2021 og bidra til redusert planleggingstid uten å påvirke plankvaliteten negativt.

Materialer og metoder: Det automatiske planleggingsskriptet for VMAT ble designet til å gi akkurat nok dose til målvolumene i følge de nye retningslinjene, og redusere dosen til risikoorganer (OARs) så mye som mulig. Manuelle VMAT-planer fra 25 LACC-pasienter med og uten lymfeknutemetastase som har mottatt behandling ved St. Olavs Hospital ble brukt som utgangspunkt for skriptoptimalisering og kvalitetsvurdering av de automatiske VMAT-planene. De automatiske VMAT-planene ble kvantitativt sammenlignet med de manuelle VMAT-planene ved hjelp av dosestatistikk fra RayStation og VMAT-kvalitetssikringsmålinger (QA) med Delta^4 fantomet. Planene ble kvalitativt sammenlignet i en blindtest med 10 pasienter utført av fysikere og doseplanleggere i klinikken.

Resultater: Det automatiske VMAT-planleggingsskriptet genererte én plan på 30-45 minutter. Fra dosestatistikken leverte de automatiske VMAT-planene høye nok, men lavere doser til målvolumer enn de manuelle VMAT-planene. Dosen til de fleste OARs var lik eller lavere med automatisk planlegging enn med manuell planlegging. De automatiske VMAT-planene hadde en signifikant høyere konformitetsindeks enn de manuelle VMAT-planene for alle målvolumer, hovedsakelig forårsaket av mindre doselekkasje til friskt vev. QA-målingene viste at flere monitorenheter i de automatiske enn de manuelle VMAT-planene ikke påvirket linacens planleveringskvalitet negativt. For 8/10 pasienter i blindtesten foretrakk minst 7/8 respondenter den automatiske fremfor den manuelle VMAT-planen.

Konklusjon: Det automatiske planleggingsskriptet for VMAT utviklet for LACC-pasienter reduserte planleggingstiden uten å redusere plankvaliteten.

Preface

This master's thesis concludes the study program biophysics and medical technology at the Norwegian University of Science and Technology (NTNU) in Trondheim. The work was carried out during the spring semester of 2022 at the radiotherapy department at St. Olavs Hospital in Trondheim. This thesis aimed to develop a script for RayStation to automatise VMAT planning in the clinic for locally advanced cervical cancer patients. Automatic VMAT planning should reduce planning time, improve plan quality and reduce plan variability between different dose planners.

The abstracts attached in Appendix F and G were accepted for oral presentations at MedFys 2022 and the Biophysics and Medical Physics Spring Meeting 2022.

I want to thank my supervisor Marit Funderud for her excellent guidance on scripting for Raystation, motivational talks, patience, and always believing in me. Thanks to my supervisors Anne Beate Langeland Marthinsen and Anette Guleng, for organising meetings, good theoretical discussions and feedback during the finalisation of the thesis. I would also like to thank Jomar Frengen at the radiotherapy department who gave crucial advises to good dose planning strategies. Also, thanks to the head of the radiotherapy department, Anne Dybdahl Wanderås, for letting me write my master's thesis at the department.

At last, I want to thank my family for always supporting my choices and believing in me. Thanks to my friends at Physics and Mathematics at NTNU for long motivational lunch breaks and for always making the best of each other. Especially thanks to Lene for our many adventures during these five years. Finally, thanks to Kristoffer for being so patient and for biking to Scotland to let me finish the master's thesis in peace.

Ingvild Straumsheim Hoem
June 2022

Abbreviations

AI - Artificial intelligence

BT - Brachytherapy

CN - Conformation number

CT - Computed tomography

CTV - Clinical target volume

DSB - Double-strand break

DVH - Dose-volume histogram

EBRT - External beam radiation therapy

EUD - Equivalent uniform dose

GTV - Gross tumour volume

Gy - Gray

HPV - Human papillomavirus

IMRT - intensity-modulated radiation therapy

IQR - Inter quartile range

ITV - Internal target volume

LACC - Locally advanced cervical cancer

linac - Linear accelerator

LN - Lymph node

MCO - Multi-criteria optimisation

MLC - Multi leaf collimators

MRI - Magnetic resonance imaging

MU - Monitor unit

NTCP - Normal tissue complication probability

OAR - Organ at risk

PET - Positron emission tomography

PTV - Planning target volume

Q1 - first quartile

Q3 - third quartile

QA - Quality assurance

RF - Radio frequency

RT - Radiation therapy

SIB - Simultaneous integrated boost

SSB - Single-strand break

TPS - Treatment planning system

VMAT - Volumetric modulated arc therapy

Contents

1 Introduction

Cervical cancer caused 311.000 deaths worldwide in 2018 and is the fourth most common cancer type in women [1]. Screening programs and vaccination in developed high-income countries provide earlier detection and prevention, resulting in higher survival rates. In low-income and middle-income countries, the death rate is 18 times higher than in high-income countries. The leading cause of cervical cancer is the sexually transmitted human papillomavirus (HPV) which is present in 99% of the cases. Between 2012 and 2016, on average 355 patients were annually diagnosed with cervical cancer in Norway [2]. In the same period, the number of annually registered deaths was 75. This corresponds to 2.3% of all cancer cases and 1.5% of all cancer deaths. Cervical cancer has an associated risk of spreading to nearby lymph nodes (LNs) in the pelvic area. 45% of all cervical cancer patients are diagnosed with LN metastases which is associated with a reduced probability of long-term survival [3].

Patients with a large tumour (>2cm in diameter) within the cervix or a tumour that has grown into the tissue surrounding the cervix are diagnosed with locally advanced cervical cancer (LACC) [4]. The standard treatment regimen for LACC patients consists of external beam radiation therapy (EBRT), brachytherapy (BT) and concomitant chemotherapy. LN metastases receive an additional external radiation boost. This boost was traditionally given sequentially after the EBRT of the primary tumour, but with modern techniques, EBRT of the primary tumour and the LN boost may be given simultaneously.

In radiotherapy (RT), treatment planning aims to deliver a high radiation dose to cancerous tissue while limiting the radiation dose to surrounding organs at risk (OARs). Intensity-modulated radiation therapy (IMRT) and volumetric modulated arc therapy (VMAT) are modern RT techniques that use inverse treatment planning to reach this aim. In inverse planning, the input parameters are a set of dose objectives, and the required beam setup to meet the dose objectives are given as the output. This computationally heavy process requires a treatment planning system (TPS) such as RayStation. Manual treatment planning is a repetitive trial-and-error process of manually defining or redefining input parameters in RayStation and running plan optimisations. This process is time-consuming and resource-demanding. Although the treatment planners are well qualified in their field, different preferences and experiences will cause variability in the performance and consistency of the resulting plans. These challenges may be resolved by automating the VMAT planning procedure.

Automatic VMAT planning is an ongoing research topic, and many studies have presented possible solutions to automate the treatment planning procedure [5–10]. Classical automatic planning solutions include dose planner mimicking, multi-criteria optimisation, and knowledge-based planning [11]. Many classical automatic planning solutions have shown similar or superior plan quality to manual treatment planning. Modern artificial intelligence (AI) solutions that address the remaining challenges of classical automatic planning solutions have also been presented [12–14]. Although both classical and modern automatic planning solutions have shown novel results, large-scale clinical implementations of automatic VMAT planning have not yet been seen.

In June 2021, St. Olavs Hospital implemented an in-house-developed automatic dose planner mimicking solution for breast and prostate cancer in the clinic. The automatic planning method was initiated and developed by Marit Funderud, Jomar Frengen and Sigrun Saur Almberg at the RT department. The automatically made VMAT plans for breast and prostate cancer were of similar or better quality as manually made VMAT plans and significantly reduced the planning time. It is desirable to develop similar automatic VMAT planning solutions for other cancer sites such as LACC to improve treatment planning efficiency further.

This project aims to produce automatic VMAT plans in RayStation for LACC patients of similar or better quality as manually made VMAT plans. Up to now, VMAT plans for LACC patients treated at St. Olavs Hospital have followed the dose constraints from the EMBRACE II protocol [15]. The automatic VMAT planning method should follow the new dose constraints from the Norwegian Directorate of Health published in June 2021 [4].

This complete project consists of three phases; the pre-phase, the project thesis phase and the master's thesis phase. In the pre-phase Marit Funderud developed a Python script that automatically created VMAT plans for LACC patients. This script was built with similar working principles as the automatic VMAT planning scripts for breast and prostate cancer. The project thesis phase involved further development of the automatic VMAT planning script, mainly by testing different combinations and orders of optimisation functions until the automatic plan quality matched the manual plan quality. The script was tested on 15 LACC patients with positive LNs from the EMBRACE study and compared against non-clinical manual VMAT plans. This thesis finishes the master's thesis phase. The master's thesis phase involved improvement of weaknesses of the automatic VMAT planning script from the project thesis phase and comparing

the quality of the automatic plans generated by the automatic VMAT planning script to 25 manual VMAT plans used in the clinic. The plan quality was examined with dose statistics from RayStation, VMAT quality assurance (QA) measurements and a blind test.

2 Theory

Parts of the theory section overlaps with the project thesis written in 2021 [16].

In this thesis, the term *dose* refers to the absorbed dose. The absorbed dose is defined as the amount of radiation energy absorbed per unit mass of an organ or tissue [17]. The unit of absorbed dose is Grey (Gy) which is equal to one joule of absorbed radiation energy per kilogram of matter.

2.1 Cell damage by photon radiation

Photon radiation is used for cancer treatment because it induces DNA strand breaks which cause cell damage. If the damage to the DNA strands is irreparable, the cells lose their ability to proliferate and die [18]. Ionising photon radiation can damage DNA strands by two main mechanisms: direct action and indirect action, illustrated in Figure 1. For photon energies used in RT, both mechanisms include incident photons which transfer parts of their energy to free electrons, mostly through Compton scattering. These electrons interact directly with the DNA or indirectly by first interacting with a water molecule to produce a water radical that interacts with the DNA.

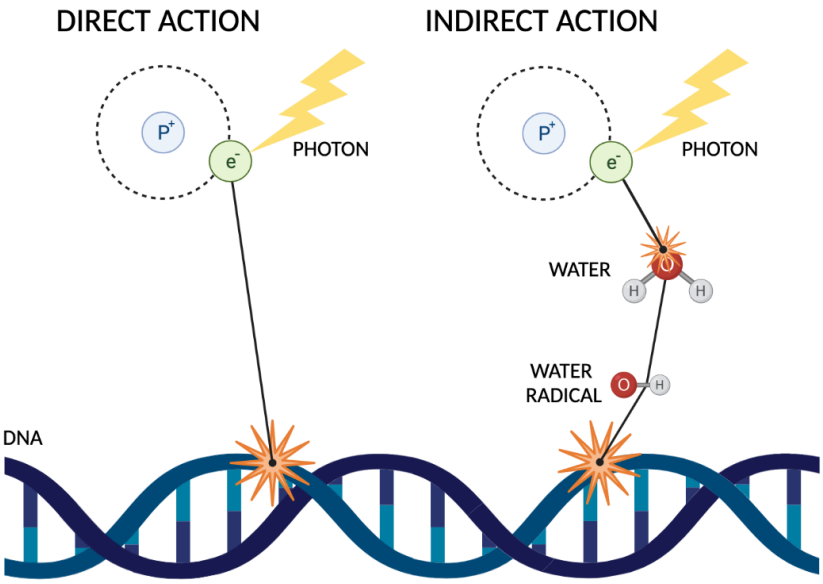

Figure 1: Schematics of direct and indirect action which induce DNA damage.

Ionising photon radiation damage DNA by single-strand breaks (SSB) and double-strand breaks (DSB). 1 Gy of radiation dose induces around 1000 SSBs, and around

25-40 DSBs per cell [19]. Lethal damage is primarily induced by DSBs, as SSBs are often repaired by copying the undamaged DNA strand. DSBs either occur if one ionisation damages both DNA strands, referred to as *single-hit* events, or if two SSB occur on opposing DNA strands close to each other, referred to as *multiple-hit* events [20]. The probability of a single-hit event, α, is linearly proportional to the dose, and the probability of a multiple-hit event, β, is proportional to the square of the dose. This results in a linear-quadratic relationship between cell survival and dose. The radiosensitivity differs widely between different cell types, also between normal cells and cancer cells, and is characterised by the ratio between α and β. The difference in radiosensitivity is mainly caused by differences in the cells' ability to repair DNA damage. Cell types with a high repair capacity, such as many healthy cell types, are often characterised with a low α/β-ratio. Cancer cells are often characterised with a higher α/β-ratio as they tend to have lower repair capacity. This difference can be exploited in fractionated RT. In fractionated RT cells are irradiated with a dose that may be lethal to cancerous tissue but is more tolerable for normal tissues.

The effect of irradiating normal tissues depends on the structure of the organs' functional sub-volumes. Sub-volumes are organ compartments that perform part of an organ's function. They can be arranged in a parallel or a serial structure or somewhere in between [21]. In parallel organs, the sub-volumes function relatively independently, and radiation-induced complications only occur after a critical volume of the organ has been damaged. Therefore, parallel organs have a significant volume effect, meaning that the organ's tolerance dose is related to the irradiated organ volume. For organs with a significant volume effect, the mean radiation dose gives predictions of the normal tissue complication probability (NTCP). The kidneys are an example of a parallel organ. In serial organs, damage to any one sub-volume cause a complication expressed by the whole volume. Serial complications are most affected by the highest dose received by the organ, and the maximum radiation dose can thus predict the NTCP. The spinal cord, bladder, rectum, sigmoideum and bowel are examples of serial organs.

2.2 External beam radiotherapy

EBRT is the most widely used RT technique and aims to transfer ionising radiation from outside the body to cancerous tissue inside the body for either cure or palliation purposes. The workflow behind every EBRT treatment includes many steps performed by a large variety of specially trained personnel. EBRT is most commonly delivered by a medical linear accelerator (linac) that produces high energy electrons or photons

focused directly toward cancerous tissue in the patient.

2.2.1 The radiotherapy workflow

RT is a resource demanding treatment technique that requires personnel from different professions in every stage of the workflow. The RT workflow can be divided into five stages: patient assessment, image acquisition, treatment planning, treatment delivery and follow-up [22]. Figure 2 shows a schematic overview of the RT workflow. Once the patient assessment concludes to proceed with RT, a 3D computed tomography (CT) scan is taken of the treatment site. In a CT image, the voxel intensity is proportional to the tissue's electron density, which is proportional to the dose. Hence, CT based treatment planning makes it possible to customise the treatment to each patient's unique anatomy. Before the CT scan, the patient must be in a stable, reproducible position to ensure reproducible treatments over many fractions. After the CT acquisition is completed and reviewed, the CT images are transferred to a TPS for delineation of target volumes and OARs. In addition to the CT images, magnetic resonance images (MRI) or positron emission tomography (PET) images can provide additional tissue characteristics to obtain accurate volume delineations. The RT workflow continues with the treatment planning stage, where an appropriate treatment technique is selected, and target volumes and OARs are assigned dosimetric planning goals. Specially trained treatment planners generate the treatment plan by modifying the radiation beams and weights of the planning goals in the TPS until the goals are met. Treatment planning is always a compromise between high doses to target volumes and low doses to OARs. The final treatment plan is reviewed by a physician and a physicist and may be tested on the linac for QA. For every fraction during the treatment delivery stage, daily CT images may be taken to ensure accurate positioning relative to the treatment plan. A surface scan can also be done at the treatment site for setup verification. After ended RT, the patient is followed up by a physician.

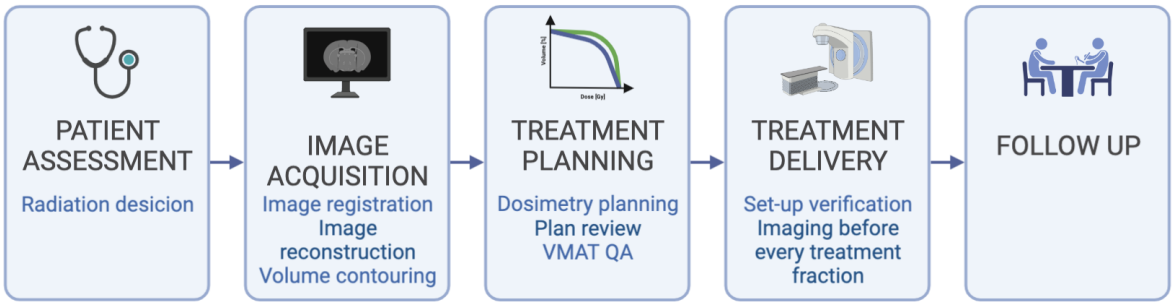

Figure 2: The five stages of the radiotherapy workflow, including patient assessment, image acquisition, treatment planning, treatment delivery and follow-up.

The outcome of a RT treatment depends on the quality of all five steps in the RT workflow. Numerous processes in the RT workflow can affect the quality of a treatment plan, such as incorrect image representation of the patient, incorrect delineation of target volumes and OARs, radiation delivery errors, or that the planner fails to meet the achievable plan quality. This master's thesis will mainly focus on the third step: treatment planning, which will be described in more detail in Section 2.3.

2.2.2 The linear accelerator

As illustrated in Figure 3, the linac is composed of the electron gun, the radiofrequency (RF) power generator, the accelerating waveguide, the electron beam transport system, and the x-ray target [23]. The electron gun consists of a thermionic material that works as a cathode which emits electrons when heated. Emitted electrons are then focused into a pencil beam and accelerated towards the anode and the accelerating waveguide. The accelerating waveguide is a copper pipe with cavities throughout its length. The RF power generator produces strong electric and magnetic fields in each cavity, allowing the electrons to accelerate between each cavity through the accelerating waveguide. At the end of the accelerating waveguide, the bending magnet leads the high energy electrons onto either an x-ray target to produce a photon beam or onto a scattering foil to produce an electron beam. The x-ray target for photon production is composed of a material with a high atomic number to produce bremsstrahlung photons from electron energy. Typical photon energies from a linac are 6, 10 or 15 MV. A photon beam consists of an energy spectrum, and the photon energy (i.e. 6 MV) represents the peak energy of the spectrum. The photon beam can be shaped by multileaf collimators (MLCs) in the linac head to fit the patient's tumour and anatomy. The radiation can be delivered from 360° around the patient by rotating the gantry. The rotating gantry and moving MLCs are the main principles of modern RT where high energy radiation can be delivered to defined concave target volumes while sparing nearby OARs. IMRT and VMAT are two modern RT techniques that will be explained in Section 2.3.3.

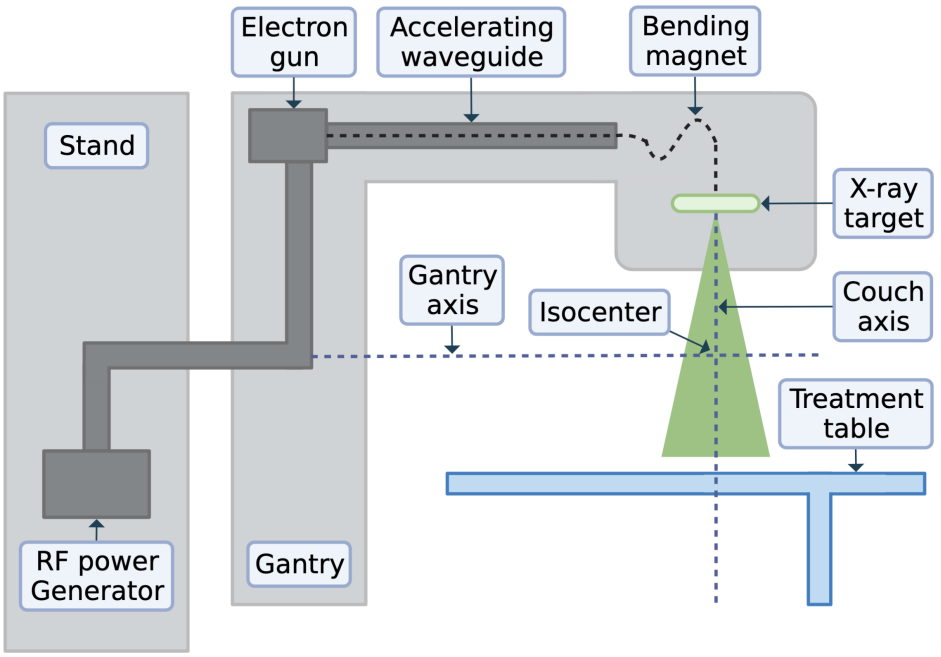

Figure 3: Schematic diagram of a linear accelerator including the RF power generator, electron gun, accelerating waveguide, the bending magnet and the x-ray target.

2.2.3 Monitor units

The machine output of the linac is measured in monitor units (MU) by ionisation chambers located in the linac head between the x-ray target and the MLCs. The linac is calibrated for a specific energy so that a machine output of 100 MU delivered with a 10 cm · 10 cm field deposit a radiation dose of 1 Gy at a point located 100 cm away from the source and at a water depth of 10 cm [24]. As the number of MUs is counted before the MLCs shape the beam, the number of MUs is not a measure of dose. A narrow beam heavily modulated by the MLCs requires more MUs to dissipate a specific dose than an open field beam.

2.3 Treatment planning

Treatment planning in RT maps where the high energy radiation from the linac is absorbed inside the patient's body to control the dose received by target volumes and OARs. Successful treatment plans maximise the therapeutic ratio, i.e. the ratio between cancer tissue damage and normal tissue damage, for the individual patient. In contrast, unsuccessful treatment plans fail to meet achievable clinical goals [25]. When the linac was introduced in the 1960s, treatment planning involved two opposing fields. In modern RT, the treatment planning must consider a much larger parameter space

due to the rotating gantry and continuous modulation of MLC positions. The increased size of the parameter space makes successful treatment planning more complicated but enables dose delivery to defined concave target volumes while sparing nearby OARs.

2.3.1 Treatment planning volumes

In RT treatment planning, target volumes are volumes with a prescribed high dose, and OARs are volumes that should receive as little radiation as possible. There are four main target volumes in RT treatment planning: the gross tumour volume (GTV), the clinical target volume (CTV), the internal target volume (ITV) and the planning target volume (PTV) shown in Figure 4. The GTV is the visible extension of the malignant growth in diagnostic images [26]. It might sometimes be relevant to split the GTV into GTVp (primary tumour), GTVn (lymph nodes) and GTVm (other metastases). The CTV contains the GTV and areas with subclinical malignant disease. Such malignant disease is difficult to identify, and the CTV is therefore often defined based on discretion. The ITV contains the CTV and an internal margin to include potential volume changes of the CTV and physiological movements such as breathing. The ITV or the CTV is the volume that should receive the prescribed dose. The definition of the GTV, CTV and ITV are similar for any treatment technique, including EBRT and BT. The PTV includes the ITV and a setup margin that accounts for patient movements during irradiation and uncertainties due to patient positioning and field settings for each treatment. The sizes of the internal margin and setup margin can vary in different directions.

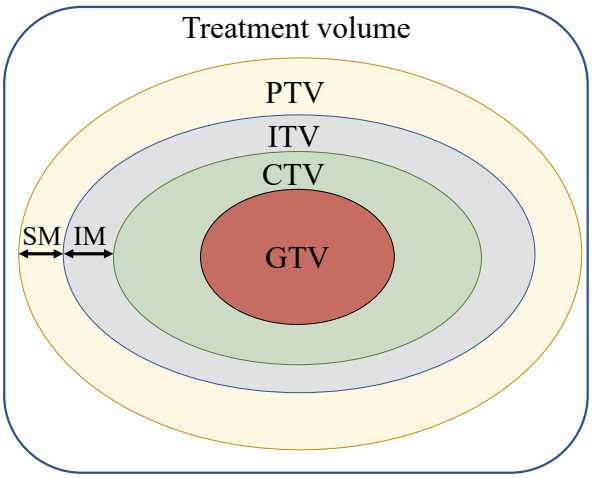

Figure 4: Location of the gross tumour volume (GTV), clinical target volume (CTV), internal target volume (ITV) and planning target volume (PTV) inside the treatment volume. The internal margin (IM) and setup margin (SM) are also shown.

Similarly to target volumes, OARs are defined by contouring the visible extension of the OAR in diagnostic images, followed by adding margins to account for uncertainties [26]. The OARs of the highest interest are the organs that receive a relatively high radiation dose by being located near a target volume. Due to the structure and sensitivity of the OARs' functional sub-units, different OARs have different tolerance doses.

2.3.2 Dose volume histograms

Cumulative dose-volume histograms (DVHs) are graphical representations of the radiation dose delivered to any defined volume, and is a good tool to compare dose distributions from different treatment plans [27]. The height of a DVH curve at a certain dose represents the volume that receives a dose equal to or greater than that dose. Figure 5 shows a DVH curve with the associated DVH parameters D_{98} and D_{50} defined as the minimum dose received by the hottest 98% and 50% of the volume, respectively. Other parameters related to DVHs are D_{max} and V_{dose}. D_{max} is the maximum dose received by a certain volume and V_{dose} is the volume percentage that receive a certain dose. As an example, V_{30Gy} is the volume percentage that receive 30 Gy or more. Similarly, $V_{95\%}$ is the volume percentage that receive at least 95% of the prescribed dose. The figure also shows the ideal DVH curve for target volumes that should have a homogeneous dose distribution.

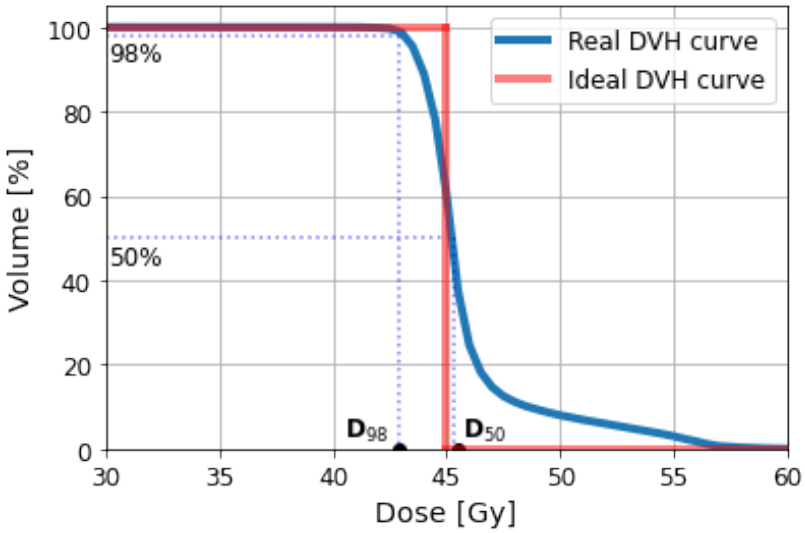

Figure 5: Cumulative dose volume histogram (DVH) showing the percentage of a specific volume that receive a specific dose or higher. The blue curve represents a real DVH curve, and the red curve represents the ideal DVH curve for a target volume with a prescribed homogeneous dose of 45 Gy. D_{98} and D_{50} is the dose received by 98% and 50% of the volume, respectively.

2.3.3 Modern treatment planning and VMAT

The most considerable development from conventional to modern RT is the shift from forward to inverse planning [23]. In forward planning, the beam characteristics are given as input to the TPS. The TPS then calculates a dose distribution as the output from several radiation beams of different weights aimed from different angles towards the target volume. This approach is interactive and depends strongly on the experience and knowledge of the person producing the plan. Computer-aided planning methods have become dominating with the advances in computer technology and increased complexity of radiation delivery- and planning techniques. This revolution has introduced inverse planning that works backwards relative to forward planning. With inverse planning, the input parameters are the desired dose results, referred to as dose objectives, and the output is the required radiation beam setup to produce the desired dose distribution. The inverse TPS has built-in iterative inverse planning algorithms which works to meet the dose objectives by optimising the radiation delivery. The software relies on many input parameters that can be adjusted for each patient to obtain the optimal treatment plan. IMRT and VMAT are two modern RT techniques based on inverse planning.

IMRT delivers multiple beamlets with non-uniform fluency from angles designed by inverse planning algorithms [23]. By reducing the fluence for delivery angles that affect OARs and increasing the fluence for delivery angles where OARs are less affected, IMRT obtains a high therapeutic ratio. To concentrate the irradiation to the tumour volume, the MLCs shape the radiation field to fit the tumour projection. IMRT can produce concave-shaped dose distributions, beneficial for sparing OARs.

VMAT is an advanced version of IMRT in which the gantry and the MLCs' positions are in continuous movement during irradiation [23]. During a VMAT treatment, dose rate and gantry speed change simultaneously as the gantry rotates around the patient. Continuous dose delivery improves conformity and significantly shortens treatment time compared to IMRT.

Inverse VMAT planning requires a compromise between maximising the dose conformity to target volumes and maximising the probability of accurate treatment delivery [28]. The conformity to target volumes increases with increased plan complexity. Characteristics of treatment plans with high complexity are plans with narrow and irregularly shaped beams that require a high number of MUs [29]. Limitations in linac

performance, dose calculations and accurate positioning of the MLCs contribute to inaccurate treatment delivery. These limitations have greater significance in complex treatment plans.

2.4 VMAT plan optimisation in RayStation

RayStation is a TPS from RaySearch Laboratories in Stockholm, Sweden, used to compute the dose distribution from a set of input instructions [30]. The computations are based on an objective function with associated optimisation functions.

2.4.1 The objective function

Treatment planning goals, such as the dose constraints that will be presented in Tables 2 to 4 in Section 2.9.3, are referred to as objectives in RayStation. An objective function describes how far away the current treatment plan is from meeting the given objectives [31]. Inverse dose planning in RayStation aims to find the optimal objective function for each individual patient, which is the function that finds the best balance between all the given objectives. In practice, this means finding the optimal balance between target coverage and organ sparing. The TPS's first optimisation round begins with an initial guess for the objective function. The initial guess is based on the objectives and geometry of target volumes and OARs. With manual planning, the plan resulting from the initial guess of the objective function is analysed by a treatment planner to find areas of improvement. After modifying the objective function based on the areas of improvement, re-optimisation of the plan gives a new dose distribution for the new objective function. This iterative process repeats until there is an acceptable compromise between target coverage and organ sparing which satisfies the dose objectives. Section 2.5 includes closer explanations on manual and automatic VMAT planning.

2.4.2 Optimisation functions

Optimisation functions further modifies the objective function and are built-in functions in RayStation that work to meet the given objectives. A good optimisation function should be as similar as possible to the quantity used to state the corresponding dose objective and cause as little conflict as possible with other optimisation functions [31].

Max dose, min dose, max DVH, min DVH, max equivalent uniform dose (EUD), min EUD and dose fall-offs are frequently used optimisation functions, and are explained

below. Each optimisation function includes a function weight that defines its importance relative to other optimisation functions. In addition, every optimisation function has an assigned function value during and after an optimisation round. The function value quantifies how far away the TPS is from meeting the objective that the optimisation function represents. Conflicts occur when two or more optimisation functions work against each other. One example of a conflict is if the PTV overlaps with an OAR and two optimisation functions simultaneously work to decrease and increase dose to the OAR and PTV respectively inside the overlapping volume. Conflicting optimisation functions will dominate the optimisation problem, which makes it more difficult to solve other conflicts. One way to work around such conflicts is to create optimisation volumes that do not intersect with other volumes with contradictory associated optimisation functions. One example of a help volume would be an OAR volume without its intersection with a target volume. This will be illustrated later, in Figure 14 in Section 2.9.3.

2.4.3 Uniform dose, min dose and max dose optimisation functions

The uniform dose function works to achieve a specified dose in every voxel in a specified volume [31]. It penalises the deviation from the specified dose in both directions and is a good optimisation function for volumes that aim for a homogeneous dose distribution. The min dose function penalises doses below a specified dose level in a specific volume and is suitable for target volumes that aim for high doses. Similarly, the max dose function penalises doses above a specified dose level in a specific volume. The max dose function is a good optimisation function for OARs with low hot-spot tolerance.

2.4.4 Max DVH and min DVH optimisation functions

The max DHV and min DVH functions works quite similarly to the max dose and min dose functions, respectively, but they only penalise a fraction of the specified volume [31]. As an example, if a dose constraint says that 75% of the rectum should receive less than 40 Gy, 75% max DVH of 40 Gy will work to reduce the dose to 40 Gy in 75% of the rectum volume. Exactly where the dose is reduced in the organ is not specified, but RayStation will choose the volume where the least amount of conflicts occur.

2.4.5 Max EUD and min EUD optimisation functions

The EUD is calculated according to Niemierkos generalised EUD formulation (gEUD) from 1999 given by

$$\text{gEUD} = \left(\sum_i v_i D_i^a \right)^{\frac{1}{a}} \tag{1}$$

where v_i is the fraction of the volume that receives the dose D_i, and a is a tissue specific parameter that describes the volume effect of the organ [31,32]. The max EUD function penalises doses above the specified EUD level, and the min EUD function penalises doses below the specified EUD level. If $a = 1$, the EUD equals the volume's mean dose. Increasing or decreasing a in a max EUD function will prioritise to reduce high or low doses, respectively.

2.4.6 Dose fall-off optimisation functions

Ideally, the dose should fall immediately at the border between a target volume and healthy tissue. Due to mechanical and physical limitations, immediate dose falls are not possible, which causes conflicts at the target volume border. To reduce these conflicts, one can accept higher doses near the target volume and lower doses as the distance to the target volume increases. The dose fall-off function works as a max dose function, but with different dose levels at different distances from the target [31]. User-specified parameters for selecting the dose levels are the high dose level, the low dose level and the low dose-distance. For example, the dose fall-off function can be used to reduce the dose from 55 Gy at the border of a PTVn to 30 Gy over a distance of 1 cm. The high dose level acts at the target border, and the dose level linearly decreases with distance to the low dose level at the low dose-distance. Outside the low dose-distance, the fall-off function works as a max dose function with the low dose level as the max dose.

2.5 Manual and automatic VMAT planning

Manual treatment planning for VMAT is a complicated and time-consuming process which consumes hours, or even days, of human effort [25]. Most manual VMAT plans are made by an interactive trial-and-error process where the dose planner tries to steer the TPS (i. e. RayStation) towards the dose objectives for every patient. A

schematic overview of the working procedure for manual VMAT planning is shown in Figure 6. The working procedure includes definition of optimisation functions, TPS optimisation and plan evaluation [11]. This procedure is repeated until the plan is clinically acceptable.

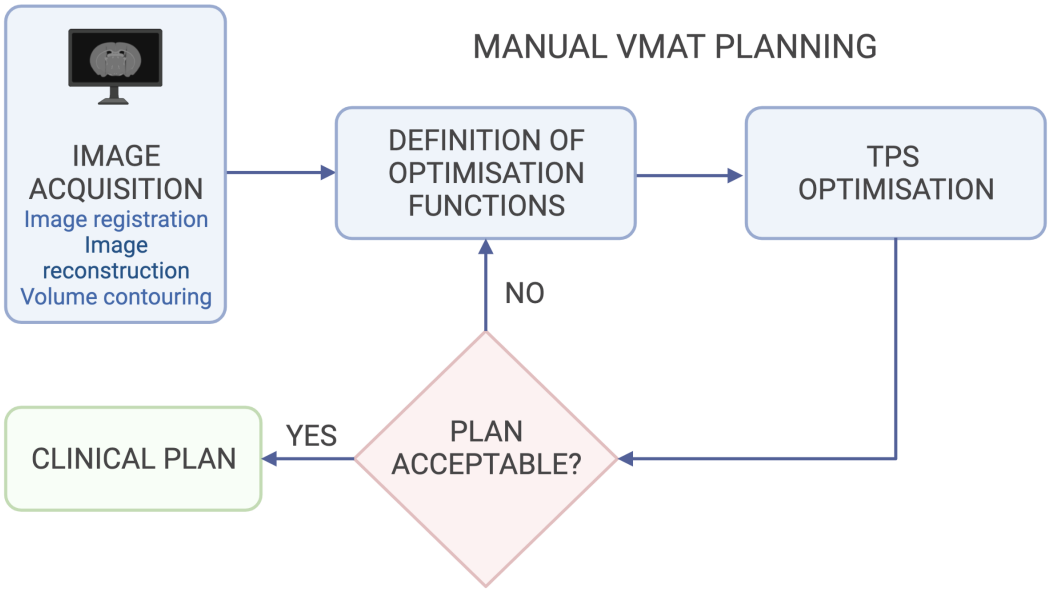

Figure 6: Schematic of the manual VMAT planning procedure. After image registration, optimisation functions are defined for optimisation in the treatment planning system (TPS). This is repeated until the plan is clinically acceptable. Figure adapted from [11].

To increase the effectiveness of the treatment planning process, manual VMAT planning can be automated. Automatic planning is rapidly improving, and several research projects and in-house solutions have been developed worldwide [11]. Most commercial TPSs have also implemented some automatic planning tools, but large-scale clinical implementations have not yet been seen. Automatic VMAT planning can be divided into three categories: treatment planner mimicking, multi-criteria optimisation (MCO), and knowledge-based planning. This project involves the development of a treatment planner mimicking solution.

In treatment planner mimicking, the decision-making of successful treatment planners has been systematised over time and converted into computer logic [11]. The computer logic aims to tune the optimisation functions iteratively to steer the TPS similarly as if done manually. Modern TPSs allow scripting, which can be used for in-house development of treatment planner mimicking solutions. These solutions are not as lim-

ited by time as manual VMAT planning, and allow to perform more iterations which potentially lead to higher plan quality. Throughout this thesis, automatic VMAT planning refers to treatment planner mimicking. The automatic VMAT planning solution that is implemented for breast and prostate cancer patients at St. Olavs hospital in Trondheim is an in-house developed treatment planner mimicking solution.

With MCO, treatment plans are automatically generated by exploring Pareto-optimal plans [11]. The Pareto space includes one dimension for each optimisation function. In a multi-criteria problem, such as treatment planning, it typically does not exist one solution that simultaneously minimises all optimisation functions. Pareto-optimal plans are plans that are on the so-called Pareto surface which consists of treatment plans that cannot be improved in any objectives without degrading one or more of the other objectives. Not all plans on the Pareto surface are clinically acceptable, but the most clinically acceptable plan will be on the Pareto surface. MCO can be divided into *a posteriori* MCO and *a priori* MCO [10]. In *a posteriori* MCO, many plans on the Pareto surface are generated and the treatment planner has to navigate through the plans to find a plan that is clinically acceptable. The TPS RayStation supports *a posteriori* MCO for VMAT planning [33]. In *a priori* MCO, a prioritised list of dose objectives contribute to produce the one Pareto-optimal plan which best balances the objectives. The Erasmus MC Cancer Institute has developed and implemented the "Erasmus-iCycle" software which uses *a priori* MCO [5, 34, 35].

Knowledge-based planning can be either atlas-based or model-based, of which both methods use a library of high-quality clinical treatment plans to aid the planning process for new patients [11]. An atlas-based system recognises a new patient's geometrical and anatomical features and copies the plan setup for the closest matching patient in the library. Model-based systems use the library to train a model that automatically predicts the parameters required to automatically generate plans for new patients.

2.6 Treatment plan evaluation tools

Dose volume histograms (DVH) explained in Section 2.9.3, box plots, paired t-tests and the conformity index are statistical tools that can be used to present dose data graphically and to evaluate and compare plan quality.

2.6.1 Box plots

A box plot is a standardised way of displaying the locality, spread and skewness of a data set, and gives a summary of the minimum, first quartile (Q1), median, third quartile (Q3) and the maximum value of the data set [36]. Figure 7 illustrates the characteristics of a box plot. The interquartile range (IQR) constitutes the box with size equal to the distance between Q1 and Q3. The whiskers extend to the most extreme data point in the range Q1 - 1.5 · IQR and Q2 + 1.5 · IQR. Data points outside this range are regarded as outliers and are marked with small circles. The orange line inside the box is the median, and the positioning of the median inside the box along with the size of the box and the whiskers provide information on the location, spread and skewness of the data set.

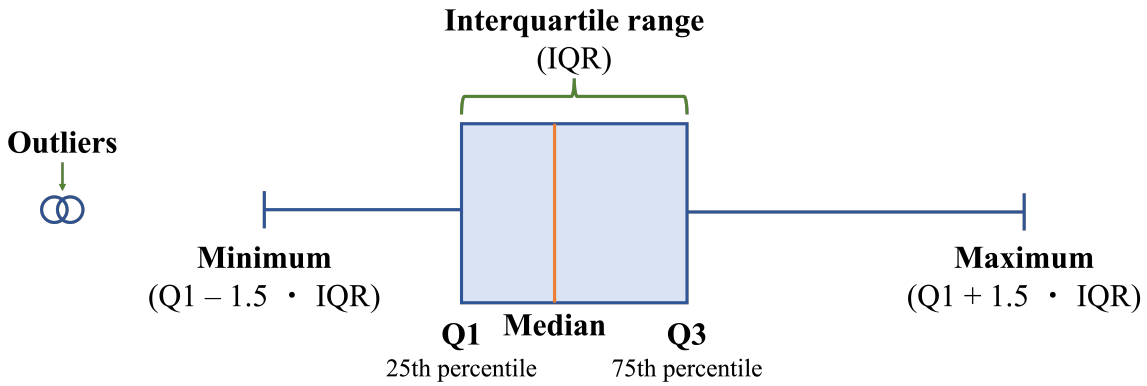

Figure 7: Box plot showing the minimum value, first quartile (Q1), median value, interquartile range (IQR), third quartile (Q3), maximum value and outliers.

2.6.2 Student's t-test

A Student's t-test is a statistical hypothesis test used to determine if the mean of two different data sets are significantly different from each other [37]. The ratio between the difference between two groups and the difference within the groups is called the t-score [38]. A large t-score represents large differences between the two data sets. Associated to a t-score is the p-value. The p-value represents the probability that the results from the two data sets occurred by chance. Hence, a low p-value represents a low probability that the results occurred by chance and a high probability that the mean of the two data sets are different from each other.

2.6.3 Conformity index

The conformity of a treatment plan provides information on how well the dose is confined to a designated volume. The conformity index can quantify this by a number between 0 and 1 where 1 represents perfect conformity. Many different definitions of the conformity index has been published of which some provides more, or different, information about the treatment plan than others [39]. The conformity index is calculated from one reference isodose around one target volume. The reference isodose is defined as the volume that receive the reference dose expressed by the isodose or more. For example, the 40 Gy reference isodose is the volume that receive minimum 40 Gy. One definition of the conformity index is the conformation number (CN) by A. Riet et al. defined by

$$CN = \frac{TV_{RI}}{TV} \times \frac{TV_{RI}}{V_{RI}} \tag{2}$$

where TV is the target volume, TV_{RI} is the volume of the target volume covered by the reference isodose, and V_{RI} is the volume of the reference isodose [40]. The first term of the CN equation represents the volume fraction of the target volume covered by the reference isodose. The second term refers to the volume fraction of the reference isodose that covers the target volume. Consequently, the second term also provides information about the volume of healthy tissue that receives the reference isodose. If CN=1, the dose distribution has perfect conformity, and the reference isodose covers the target volume precisely without irradiating any healthy tissue.

2.7 Quality assurance of VMAT plans

Complex RT treatment plans such as VMAT plans require dosimetric verification before clinical delivery [41]. This dosimetric verification is referred to as patient QA. Patient QA provides information on how well the linac delivers the VMAT plan. The dose distribution measured in the patient QA and the dose distribution calculated by the TPS will be referred to as the the measured dose distribution and the calculated dose distribution, respectively.

One method for performing patient QA is with the Delta^4 phantom (ScandiDos, Uppsala, Sweden) illustrated on the treatment table in Figure 8 (left). The phantom consists of 1069 p-type silicon diodes of 0.00004 cm^2 arranged in a crossed array. As

shown in Figure 8 (right), the diodes are positioned more densely in the center of the phantom. At the central 6 cm · 6 cm the diodes are placed in 0.5 cm intervals, and in 1 cm intervals at the remaining 20 cm · 20 cm. The phantom itself is cylindrical and consists of the water substitute polymethylmethacrylate [42]. The phantom comes with computer software that allows the user to compare the calculated and measured dose distributions. Dose distribution comparisons through the software can be achieved both qualitatively and quantitatively with parameters such as the dose difference, distance-to-agreement and the gamma index.

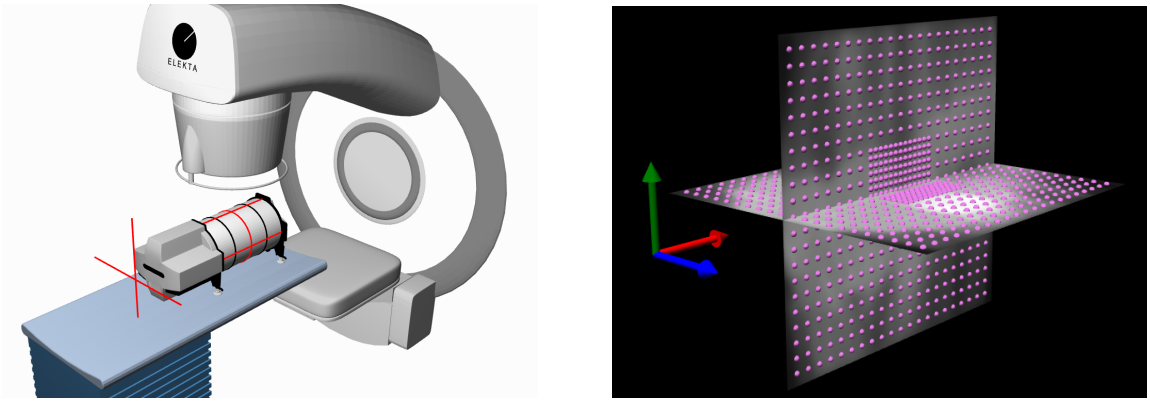

Figure 8: Illustration of the Delta^4 Phantom+ by ScandiDos. Left: the phantom is positioned at the isocenter of the linear accelerator. Right: the location of the 1096 silicon diodes along the two crossed planes inside the phantom. The images are taken from the Delta^4 software [43].

The dose difference is the difference in the dose of a measured data point and and its corresponding calculated data point [44]. In regions with high dose gradients, minor errors in the calculated or measured dose distribution result in large dose differences [45]. Large dose differences in such regions are relatively unimportant because the correct dose will be close to the calculated or measured point. The distance-to-agreement is therefore introduced as the distance between a measured data point and the nearest point in the calculated dose distribution that exhibits the same dose. When determining the difference between a calculated and measured dose distribution, the dose difference and distance-to-agreement evaluations compliment each other, and can be combined into the gamma index.

2.7.1 Formalisation of the gamma index

The gamma index, γ is a technique used to quantitatively compare two dose distributions, and can be done with the Delta^4 phantom. In conjunction with Figure 9, the

formalism of the γ index will be described in the following section.

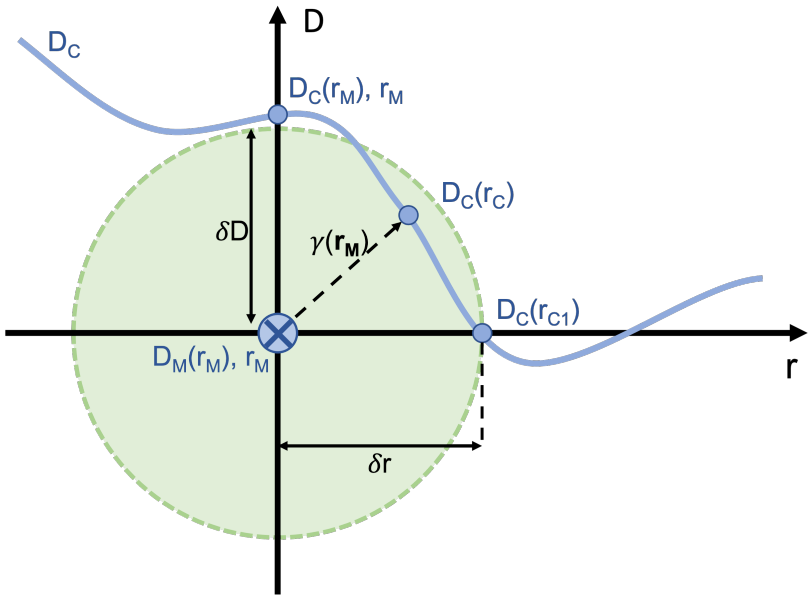

Figure 9: 1D schematic representation of the gamma index method adapted from [45]. The y-axis represents dose, D, and the x-axis is distance, r. The cross, $D_M(r_M), r_M$ at the origin is the measured refernece point and the blue line represents the calculated dose distribution with discrete points marked as solid circles. The green ellipse around the measured point originates from the distance δr and dose δD acceptance criteria. In this diagram, point $D_C(r_M), r_M$ lies outside the acceptance ellipsoid, and would thus have Γ >1. $D_C(r_C)$ lies inside the acceptance ellipsoid and would have Γ <1. $D_C(r_{C1})$ on the acceptance ellipsoid border would have Γ=1. The resulting γ <1 for the measured reference point $min\{\Gamma\}$ <1.

For each measured point, the dose difference and distance-to-agreement should be calculated against each point in the calculated dose distribution [44]. The dose difference, $\Delta D(r_M, r_C)$, is calculated by

$$\Delta D(r_M, r_C) = D_C(r_C) - D_M(r_M)$$

where $D_C(r_C)$ is the dose at a point in the calculated dose distribution and $D_M(r_M)$ is the measured point dose. The vector $\Gamma(r_M, r_C)$ is then calculated for each point in the calculated dose distribution by the equation

$$\Gamma(\mathbf{r}_M, \mathbf{r}_C) = \sqrt{\frac{\Delta r^2(\mathbf{r}_M, \mathbf{r}_C)}{\delta r^2} + \frac{\Delta D^2(\mathbf{r}_M, \mathbf{r}_C)}{\delta D^2}}$$

where δr and δD are the distance- and dose difference acceptance criteria. Finally, the γ is found as the minimum Γ calculated over all the points from the calculated dose distribution:

$$\gamma(\mathbf{r}_M) = min\{\Gamma(\mathbf{r}_M, \mathbf{r}_C)\} \forall \{\mathbf{r}_C\}.$$

As shown in Figure 9, the distance- and dose difference criteria form an ellipsoid around the measured point. This ellipsoid determines the pass region of the calculated points. If a calculated point is within the ellipsoid, the measured point will pass since γ <1. The passing criteria is normally reported in the format δD(%)/δr(mm), and 3%/3mm is most commonly used for standard VMAT plans.

2.8 Cervical cancer

Cervical cancer refers to abnormal cell growth in the cervix, which is the lower and most inferior part of the uterus, an essential organ of the female reproductive tract illustrated in Figure 10 [46]. The upper part of the cervix, called the endocervix, consists of glandular cells and forms the cervical channel connecting the vagina to the lower inner part of the uterus. The ectocervix consists of squamous cells and is the lower and outer part of the cervix which faces the inner lumen of the vagina. The separation between these two cervical regions constitutes the transformation zone, being the location with the most frequent abnormal cell development.

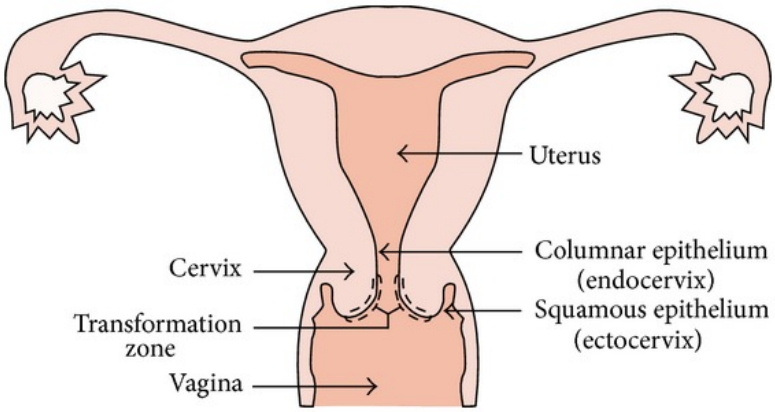

Figure 10: The female reproductive tract including the uterus, cervix, columnar epithelium (endocervix), squamous epithelium (ectocervix), transformation zone and vagina [46].

Primarily, cervical cancer develops due to the HPV that in some cases encode proteins essential for viral replication, such as E6 [47]. E6 inactivates the tumour suppressor gene p53 and the check points of the cell cycle. HPV type 16 encodes for this exact protein and accounts for 60% of cervical cancers [48]. The most common type of cervical cancer is squamous cell carcinoma, of which 90% of the cases contain HPV DNA [49]. In other cases, cervical cancers can develop in glandular cells in the endocervix, called adenocarcinoma.

2.8.1 Lymph node metastases

Metastases is the process by which cancer cells break loose from their primary tumour site and settle at a secondary site [50]. Cervical cancer cells can break loose from the cervix, travel to the lymphatic system, and metastasese to nearby LNs. This resettlement is called LN metastases. The lymphatic system consists of a network of lymph vessels and LNs to carry lymph fluid around the body [51]. LNs are located at several sites in the body, such as the armpits, neck, chest and belly, and work as filters for foreign substances such as infections and cancer cells. The location of LNs in the pelvic region is shown in Figure 11. Lymphocytes will recognise and kill the majority of cancer cells entering a LN. However, one or two might attach to the LN wall, start to grow, and form a metastases. LNs with LN metastases will be referred to as positive LNs.

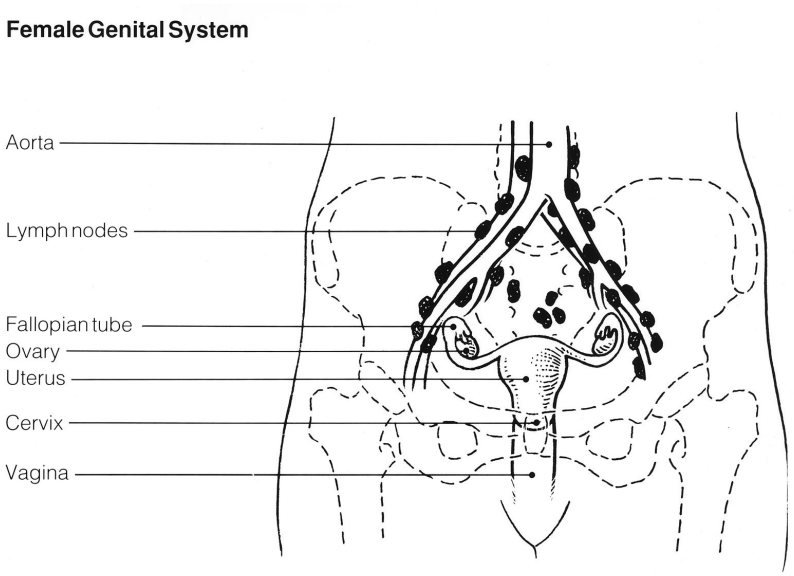

Figure 11: Lymph node location in the pelvis illustrated with the larger black dots [52].

2.8.2 FIGO staging and treatment of cervical cancer

Staging of cervical cancer was introduced by the International Federation of Gynecology and Obstetrics (FIGO) already in 1929 to determine the severity of the disease. Since then, it has been revised many times, most recently in 2018 [4]. Staging is an essential tool to ensure that patients with the same cancer profile receive the same treatment. For cervical cancer, there are four stages, I-IV, of which a higher stage often corresponds to larger tumour volume and more spread. Each stage has additional subgroups, labelled with a letter (i.e IA), that describe the disease in more detail. A higher subgroup letter (i.e IB) describes a more extensive disease within a give stage. Further, a subgroup can be labelled with a number (i.e. IB2) which is related to the tumour size. Table 1 describes the four FIGO stages and subgroups of cervical cancer in short.

Table 1: Description of the four (I-IV) FIGO stages and subgroups [4].

Stage		Description
I		The carcinoma is strictly confined to the cervix uteri
	IA	Deepest invasion depth < 5mm, only diagnosed with microscopy
	IB	Clinically visible lesion confined to the cervix
II		The carcinoma invades beyond the uterus, but not onto the lower third of the vagina or to the pelvic wall
	IIA	Involvement limited to the upper two thirds of the vagina without parametrial involvement
	IIB	With parametrial involvement but not up to the pelvic wall
III		Tumour involves the lower third of the vagina and/or extends to the pelvic wall
	IIIA	Involvement in the lower third of the vagina, no extension to the pelvic wall
	IIIB	Extension to the pelvic wall and/or hydronephrosis or non-functioning kidney
IV		Extension beyond the true pelvis or has involved the mucosa of the bladder or rectum
	IVA	Spread of the growth to adjacent organs
	IVB	Spread to distant organs

LACC refers to FIGO stage IB2-IVA [4]. Stage IB2 refers to a clinically visible lesion of < 2 cm confined to the cervix. The general treatment regimen for LACC patients is EBRT and BT combined with chemotherapy [53]. BT is an internal RT technique where a radioactive source is brought into the cervix and uterus via the vagina as close to the cancer site as possible. Internal radiation with BT is given at the end or towards the end of the EBRT and provides a highly conformal dose escalation to the tumour, with greater sparing of surrounding OARs than that achievable with EBRT [54]. Both the primary tumour and positive LNs should be treated with EBRT. EBRT to the LNs was conventionally given as a sequential boost that extended the overall treatment time, reducing the probability of local control [55]. The improved

precision of dose delivery with IMRT and VMAT, described in Section 2.3.3, enables simultaneous radiation delivery to the primary tumour and positive LNs, referred to as simultaneous integrated boost (SIB).

2.9 VMAT planning for locally advanced cervical cancer

VMAT planning for LACC patients is especially complicated due to the many nearby OARs and different target dose levels for cases with LN metastases. These difficulties also make manual VMAT planning of LACC patients particularly complicated. One study reported that manual VMAT plans for LACC patients on average took 6 hours, including 3 hours of hands-on planning time, which agrees with experiences at St. Olavs Hospital [5]. This section includes the definition of target volumes and OARs together with their associated planning aims used for treatment planning for LACC patients.

2.9.1 Target volumes in locally advanced cervical cancer

Figure 12 shows the target volumes for a LACC patient with LN metastases including GTVp, CTVp, PTVp, GTVn, CTVn and PTVn. Some target volumes are labelled with its associated prescribed physical dose, introducing i.e. PTV_45.

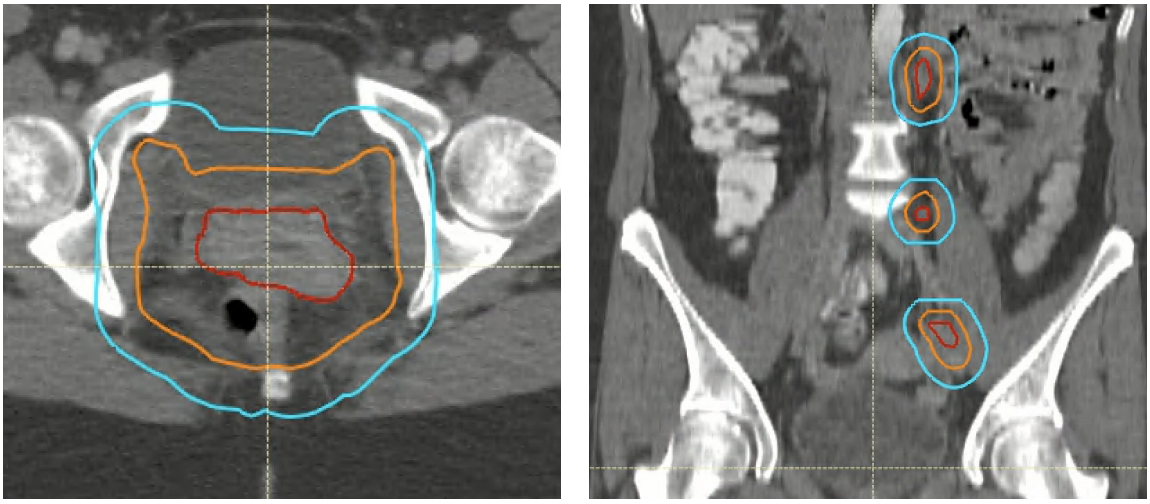

Figure 12: Left: primary target volumes GTVp (red), CTVp (orange) and PTVp (blue) of a LACC patient, viewed in the transverse plane. Right: target volumes GTVn (red), CTVn (orange) and PTVn (blue) of the lymph node metastases of a LACC patient, viewed in the coronal plane.

2.9.2 Organs at risk in locally advanced cervical cancer

The organs at highest risk for LACC patients are the rectum, bladder, sigmoideum, bowel, kidneys and femoral heads. Figure 13 shows the location of some of the OARs and their proximity to GTVp.

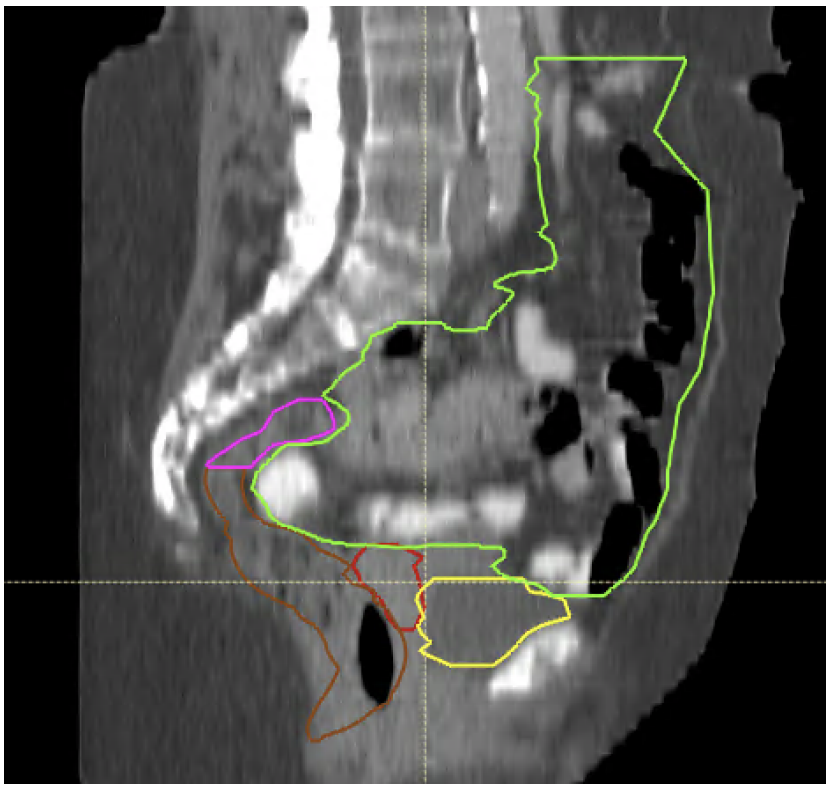

Figure 13: Organs at risk delineated on one patient showing the bladder (yellow), rectum (brown), bowel (green), sigmoideum (pink) and GTVp (red), viewed in the sagittal plane.

2.9.3 Planning aims

Finding the optimal compromise between high dose to target volumes and low dose to OARs for LACC patients is still an ongoing research topic. EMBRACE is the name of an extensive study on cervical cancer and is short for image-guided intensity-modulated **E**xternal beam radiochemotherapy and **M**RI based adaptive **BRA**chytherapy in locally advanced **CE**rvical cancer [53]. EMBRACE I was an international multicenter study initiated in 2008 to evaluate and benchmark MRI based adaptive BT. 27 international centres and 1416 patients were involved in the study, and St. Olavs Hospital in Trondheim participated with 37 patients. In EMBRACE II, the scope broadened to include image-guided RT and systemic treatment in the form of concomitant ra-

diochemotherapy [15]. The treatment outcome data from EMBRACE I was the basis for the EMBRACE II study protocol with dose constraints to target volumes and OARs. The EMBRACE II protocol suggest a total physical dose of 45 Gy in 25 fractions to PTVp, and 55 Gy and 57.5 Gy with SIB to positive LNs inside and outside the true pelvis, respectively. The dose to the positive LNs depends on the LN's proximity to PTVp that receive additional dose from the BT boost.

Until recently, the EMBRACE study results have been the guideline for implementation of cervical cancer treatment in Norway. In June 2021, new gynaecological cancer guidelines were published by the Norwegian Directorate of Health [4]. Hard- and soft dose constraints from the Norwegian Directory of Health in case of EBRT of cervical cancer with and without SIB are shown in Tables 2 to 4 for target volumes, OARs without SIB and OARs with SIB, respectively. The new dose constraints are based on the EMBRACE II protocol, but include additional maximum dose constraints to OAR volumes in areas 10-15 mm from PTVn. Figure 14 illustrates an OAR volume that is cropped 15 mm from PTVn which these dose constraints apply to. xCTVp_HR+10 correspond to the primary tumour (GTVp) and the remaining part of the cervix with a 10 mm margin.

Table 2: Hard and soft dose constraints to target volumes for EBRT of cervical cancer with and without simultaneously integrated boost given by the Norwegian Directory of Health [4].

Volume	**Hard dose constraints**	**Soft dose constraints**
ITV_45	D_{max} < 95 % (42.8 Gy)	D_{max} < 107 % (48.2 Gy)
PTV_45	$V_{95\%}$ > 95 % (42.8 Gy) D_{max} < 107 % (48.2 Gy)	$V_{95\%}$ = 95 % (42.8 Gy)
CTVn	D_{98} > 100 % of prescribed dose	D_{50} > 102 % of prescribed dose
PTVn	D_{98} > 90 % of prescribed dose D_{max} < 107 % of prescribed dose	D_{50} > 102 % of prescribed dose
xCTVp_HR+10		D_{max} < 103 % (46.4 Gy)

Table 3: Hard and soft dose constraints for organs at risk for EBRT of cervical cancer without simultaneously integrated boost given by the Norwegian Directory of Health [4].

Organ	**Hard dose constraints**	**Soft dose constraints**
Bowel	$D_{max} < 47.3$ Gy	$V_{40Gy} < 250$ cm^3 $V_{30Gy} < 500$ cm^3
Sigmoideum	$D_{max} < 47.3$ Gy	
Bladder	$D_{max} < 47.3$ Gy	$V_{40Gy} < 60\%$ $V_{30Gy} < 80\%$
Rectum	$D_{max} < 47.3$ Gy	$V_{40Gy} < 75\%$ $V_{30Gy} < 90\%$
Spinal cord	$D_{max} < 48$ Gy	
Femoral head	$D_{max} < 50$ Gy	
Kidney	$D_{mean} < 15$ Gy	$D_{mean} < 10$ Gy
Body	$D_{max} < 48.2$ Gy	
Duodenum	$V_{55\ Gy} < 15$ cm^3	

Table 4: Hard and soft dose constraints for organs at risk for EBRT of cervical cancer with simultaneously integrated boost given by the Norwegian Directory of Health [4].

Organ	**Hard dose constraints**	**Soft dose constraints**
Bowel	D_{max} < prescribed dose to PTVn	Pelvic radiation: V_{40Gy} < 250 cm^3 V_{30Gy} < 500 cm^3
	D_{max} < 47.3 Gy (in areas 10-15 mm from PTVn)	Paraortal radiation: V_{40Gy} < 300 cm^3 V_{30Gy} < 650 cm^3
Sigmoid	D_{max} < prescribed dose to PTVn D_{max} < 47.3 Gy (in areas 10-15 mm from PTVn)	
Bladder	D_{max} < prescribed dose to PTVn D_{max} < 47.3 Gy (in areas 10-15 mm from PTVn)	V_{40Gy} < 60 % V_{30Gy} < 80 %
Rectum	D_{max} < prescribed dose to PTVn D_{max} < 47.3 Gy (in areas 10-15 mm from PTVn)	V_{40Gy} < 75 % V_{30Gy} < 95 %
Spinal cord	D_{max} < 48 Gy	
Femoral head	D_{max} < 50 Gy	
Kidney	D_{mean} < 15 Gy	D_{mean} < 10 Gy
Body	D_{max} < 48.2 Gy (in areas 10-15 mm from PTVn)	
Duodenum	$V_{55\ Gy}$ < 15 cm^3	

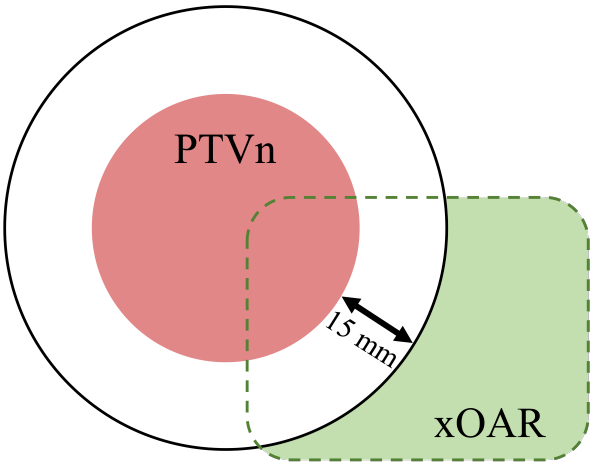

Figure 14: Illustration of xOAR (green volume), being the OAR volume that does not intersect with PTVn (red) + 15 mm. The original OAR volume is represented by the stippled green line.

The ideal DHV curve in Figure 5 applies to the primary target volume PTV_45 as the dose constraints say that a large volume fraction should receive a significant fraction of the prescribed dose and that the CTV should not have hot spots greater than 46.4 Gy. For the LN boost, the dose constraints assumes that CTVn is located in the central part of PTVn, and not at the edges [4]. With this assumption, the dose constraints aim for a heterogeneous dose inside PTVn with a central dose higher than 100% and a peripheral dose of 90% of the prescribed dose.

3 Materials and methods

Parts of the materials and methods section overlaps with the project thesis written in 2021 [16].

3.1 Patients and manual VMAT plans

This project included 25 patients from a retrospective patient group diagnosed and treated for LACC at St. Olavs hospital between december 2019 and december 2021. Table 5 shows the number of positive LNs inside and outside the true pelvis for every patient in the patient group. The group included 8 patients without positive LNs and 17 patients with 1-4 positive LNs inside the true pelvis and/or 1-5 positive LNs outside the true pelvis. All patients were treated with a combination of VMAT and BT with manually made VMAT plans uniquely designed for every patient. All patients were anonymised before being used in this study.

During a treatment course, several VMAT plans are generally made for one patient to account for changes in uterus position. The first plan often has large margins that cover possible uterus positions [26]. Further in the treatment course, more fine-tuned plans with adjusted margins are often made to fit the treatment to the current uterus position. To ensure a consistent comparative basis, the manual VMAT plans used in this project were chosen to be the first plan made for each patient, which had large margins. These are the VMAT plans delivered in the first fractions of the treatment. The plans may have been adjusted for later fractions. The same target volumes, with similar margins, were used for automatic VMAT planing. The manual VMAT plans follow the dose constraints from the EMBRACE II protocol, which were standard procedures at St. Olavs Hospital at the treatment time, not the new dose constraints from the Norwegian Directory of Health.

Table 5: Overview of patients included in this study and number of positive lymph nodes.

Patient	Number of LN inside true pelvis	Number of LN outside true pelvis
1	-	3
2	-	-
3	-	-
4	-	5
5	1	-
6	2	2
7	-	-
8	3	-
9	1	-
10	1	-
11	1	-
12	4	2
13	-	-
14	-	3
15	-	2
16	-	-
17	-	-
18	-	-
19	2	1
20	-	1
21	1	-
22	2	-
23	-	-
24	-	2
25	-	1

3.2 VMAT planning volumes

Volume delineations of OARs, GTVs, CTVs and PTVs on the planning CT images were done by a physician. St. Olavs Hospital generally use GTV, CTV and PTV for target definitions. Dose guidelines to the ITV has therefore not been addressed in this project. Volume delineations for OARs and target volumes used in the project are described

in Tables 6 and 7 respectively. This project did not address the dose constraint to the duodenum as most patients lacked delineation of this organ. The kidneys and spinal cord were generally not delineated on patients treated without SIB due to their distance from the target volume. The CTV to PTV margins of PTV_45 depend on the uterus position and predicted uterus movement of each individual patient, but was evaluated to approximately 1.2 cm in superior and posterior directions and 0.8 cm in the lateral direction by the physician.

Table 6: Delineations of organs at risk [4]

Organ at risk	**Volume description**
Bladder	Outer contour of the urine bladder including the bladder wall and bladder neck
Rectum	Outer contour of the rectum wall from the anorectal sphincter to the transition to sigmoideum
Bowel	Outer contour of the intestinal loops, including the mesentery
Sigmoideum	Outer contour of the sigmoideum from the rectum-sigmoid transition to the left fossa iliaca
Body	Outer contour of the patient
Kidneys	Outer contour of kidneys excluding the renal pelvis
Spinal cord	Outer contour of medulla spinalis
Femoral heads	Outer contour of the caput and collum femoris to the trochanter minor

Table 7: Delineations of target volumes [4]

Target volume	Volume description
GTVp	Gross tumour volume of the primary cervix tumour
GTVn_55	Pathological lymph nodes with possible extracapsular growth with a prescribed total dose of 55 Gy
GTVn_57.5	Pathological lymph nodes with possible extracapsular growth with a prescribed total dose of 57.5 Gy
CTV_45	GTVp + remaining part of the uterus that is not tumour infiltrated
CTVn_55	GTVn_55 + 5 mm margin
CTVn_57.5	GTVn_57.5 + 5 mm margin
PTV_45	CTV_45 + margin depending on uterus position and predicted uterus movement
PTVn_55	CTVn_55 + 8 mm margin
PTVn_57.5	CTVn_57.5 + 8 mm margin

Optimisation volumes were defined and used in the automatic VMAT planning script to avoid conflicting optimisation functions within a single volume. The optimisation volumes were labelled with the letter x in RayStation and are listed and explained in Table 8. Optimisation volumes to the OAR volumes outside PTVn + 15 mm were made to meet these dose constraints in Table 4 without conflicting with the high dose in PTVn. An illustration of xBowel, being the bowel volume without its intersection with PTVn + 15 mm, is provided in Figure 15. Delineating CTVp_HR, being the GTVp and the remaining part of the cervix, is not part of the standard procedure at St. Olavs Hospital. Instead, the optimisation volume xCTVp, being the CTVp + 10 mm minus PTVn + 7 mm, is used to avoid hot spots in the volume that receive additional dose from BT. Hence, in this project, the soft dose constraint to xCTVp_HR+10 in Table 2 will be applied to xCTVp instead of to xCTVp_HR+10.

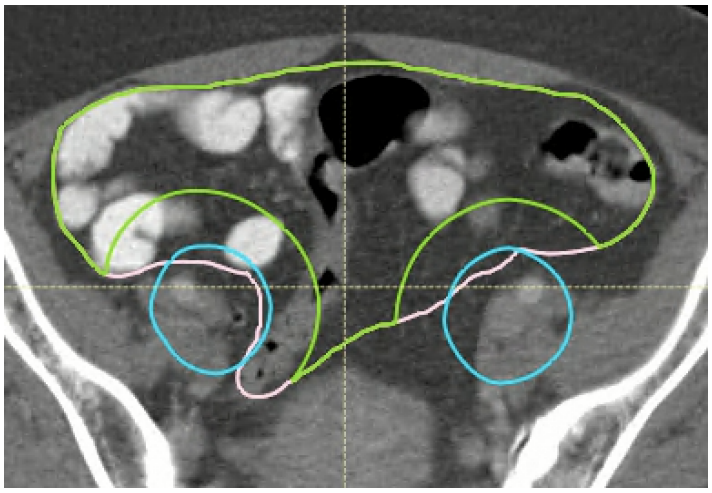

Figure 15: The optimisation volume xBowel in green is defined as the bowel - (PTVn + 15 mm). The pink volume shows how the contoured bowel volume extends outside xBowel and partly overlaps with the PTVn in blue.

Table 8: Optimisation volumes used in the automatic planning script. PTVn refers to both PTVn_55 and PTVn_57.5.

Optimization volume	**Volume description**
xRectum	Rectum volume minus PTVn + 15 mm
xBladder	Bladder volume minus PTVn + 15 mm
xSigmoideum	Sigmoideum volume minus PTVn + 15 mm
xBowel	Bowel volume minus PTVn + 15 mm
xCTVp	GTVp + 10 mm minus PTVn + 7 mm
xOAR47.3	Intersection of OARs and the 47.3 Gy isodose
x40 and x40-PTV	40 Gy isodose outside PTV_45
xRing0-1.5cm	Volume 1.5 cm outside PTV_45

3.3 The automatic VMAT planning script

3.3.1 Improvement areas of the script

The automatic VMAT planning script developed for the project thesis in the autumn of 2021 was used as a basis for this master project. The script from the project thesis

was initially tested on all the 25 patients to identify its weaknesses. Four improvement areas were identified:

1. script adaptation for patients without positive LNs

2. reduce optimisation function value for max EUD and max DVH functions for xBladder

3. reduce kidney doses

4. improve conformity by reducing dose to healthy tissue around PTV

3.3.2 Workflow for script development

The workflow for improving the weaknesses of the script from the project thesis was divided into three tasks:

1. identify improvement areas and adjust the script accordingly

2. run the improved script on selected patients

3. assess the outcome of the script adjustments

One round of this procedure took 45-60 minutes per patient. Improvement areas of the script were identified by either looking at the dose distribution in RayStation or by exporting dose statistics to Excel and evaluate the data. One example of dose statistics in Excel is provided in Figure A.1 in Appendix A. The script adjustments mainly involved tuning, adding or reordering optimisation functions. Tuning an optimisation function involved changing the dose-related input parameters or the input weight that determined the priority of the function. Adjustments were made for optimisation functions dedicated to volumes that had performed better in earlier script tests or if the adjustment was believed to give better results. Every workflow round included only minor script adjustments to control which adjustments caused changes to the dose distribution.

Testing the automatic VMAT planning script on a small number of patients provided time to test more versions of the script. The script was mainly optimised for patients

2 without SIB and 19 with SIB. These two patients were chosen because meeting the dose constraints for these patients seemed challenging early in the process. The script was occasionally tested on other patients to see if the new optimisations gave similar results.

3.3.3 Script structure

The VMAT planning software used at St. Olavs Hospital was RayStation 11A SP1 (RaySearch Laboratories, Stockholm, Sweden) [30]. All plans made with the automatic VMAT planning script applied the RayStation settings shown in Table 9.

Table 9: RayStation settings

Setting	Parameter
VMAT technique	Dual arc
Energy	6 MV
Max gantry spacing	2 degrees
Start/stop angle of 1st arc	178/182 degrees
Start/stop angle of 2nd arc	182/178 degrees
Collimator angle	25 degrees
Leaf motion constraint	0.5 cm / degree

The automatic VMAT planning script's main design idea was decided to be to deliver just enough dose to target volumes according to Table 2 while reducing OAR doses as much as possible. Only optimisation functions that supported this design were included in the script.

The automatic VMAT planning script was divided into two phases which automatically modified and re-optimised the optimisation functions in RayStation. A flowchart of the script is provided in Figure 16. The optimisation functions dedicated to specific OARs, target volumes and optimisation volumes for one example patient are listed in order of function value in Figures B.1 and B.2 in Appendix B. In the next two paragraphs, a *step* refers to one of the four iterative step and an *iteration* refers to one of many optimisation iterations included in each step.

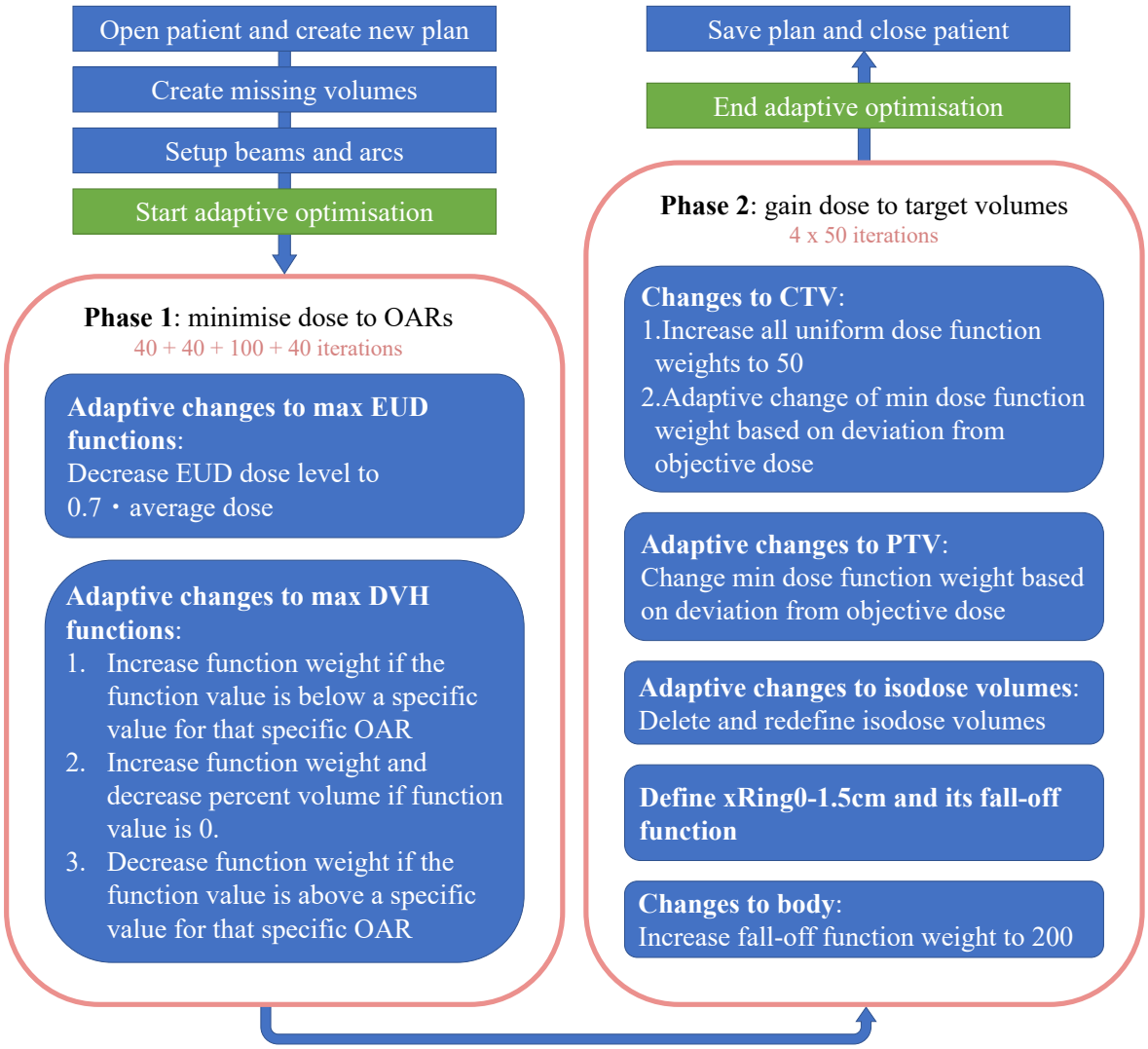

Figure 16: Flowchart of the automatic VMAT planning script. The script include entrance procedures, phase 1 that works to minimise dose to OARs, phase 2 that works to gain dose to target volumes, and exit procedures.

The first phase works to reduce dose to OARs and includes four steps that each contains 40 or 100 iterations that works with the optimisation functions. Before every new step, adaptive changes are made to the max EUD and max DVH optimisation functions. An optimisation function is adaptive if its input parameters are changed according to the dose distribution during the script's run-time. Thus, adaptive optimisation functions are tailored to each patient to obtain a high-quality VMAT plan. The adaptive changes to the max EUD and max DVH functions work to reduce the OAR dose as much as possible, supporting the script's design idea. Hard dose constraints to OARs in Tables 3 and 4 focus on D_{max}. To meet the hard dose constraints and reduce the higher doses

in the OARs, the tissue specific parameter for the max EUD function in Equation (1) is set to a=2. Adaptive functionality of the max EUD function is achieved by reducing the EUD dose level to 70% of the average OAR dose before every new step. The max DVH functions are adaptive by changing the function weight according to the function value before a new step. If the function value is below a set criteria, the function weight is increased to give the dose reduction to the OAR a higher priority. If the function value is above a set criteria, the function weight is decreased. These adaptive weight adjustments prevents the max DVH functions from getting a high function value that makes it dominate in the second phase. Evenly distributing the function value is essential to prioritise all optimisation functions and meet as many objectives as possible.

The second phase works to gain coverage to the target volumes in four steps that each contains 50 iterations. The function weight of the uniform dose functions of CTV is increased to 50 before the first step to increase the importance of a high homogeneous dose in the CTV. In agreement with the main design idea, min dose functions are used on target volumes to not increase the target dose beyond the hard dose constraints. Before all new steps, adaptive changes are made to optimisation functions for CTV, PTV, xOAR47.3, x40 and xRing0-1.5cm. Changes to the function weight of the min dose functions to CTV and PTV are based on the deviation from the objective dose. A large deviation gives a more significant increase in the function weight. The 47.3 isodose that intersects with an OAR, xOAR47.3, is deleted and redefined before every step to prevent newly emerged hot spots in the OARs. To increase conformity, a ring volume xRing0-1.5cm is made from the border to 1.5 cm outside PTV_45 + PTVn. The fall-off function of xRing0-1.5cm works to reduce dose from the highest dose level of PTVn (55 Gy or 57.5 Gy) to 30 Gy over a distance of 1.5 cm. The ring volume is defined before the second step and works for the remaining three steps. A max dose function is applied to the 40 Gy isodose volume outside PTV and PTVn in all steps to further increase conformity. This isodose volume was called x40-PTV for patients without positive LNs and x40 for patients with positive LNs. In the final two steps, the function weight of the fall-off function to the body is increased from 1 to 200, also to increase conformity.

The four improvement areas of the base script were solved by:

1. expanding the script to give satisfactory results also for patients without LNs

2. reducing input weight of the max DVH and max EUD functions for xBladder-PTVn and reduce the criteria for decreasing the function weight of the max DVH function.

3. Decrease kidney EUD dose level by 70% if kidney dose exceed 10 Gy.

4. Add a max dose function to the 42 Gy isodose outside PTV and PTVn (x40-PTV and x40)

3.4 Plan comparison and statistical analysis

The plan quality of the automatic VMAT plans were compared against manual VMAT plans both quantitatively and qualitatively. Quantitative comparison was performed by analysing dose statistics from RayStation and data from QA measurements. Qualitative comparisons were performed through a blind test sent to physicists, physicians and treatment planners at St. Olavs Hospital.

3.4.1 Statistical analysis

VMAT plans from automatic and manual planning were compared quantitatively with DVHs, box plots, paired t-tests and the conformity index. DVH and box plot data were retrieved from RayStation with a Python script that transferred data to Excel. All DVHs and box plots were plotted with matplotlib version 3.2.2 that retrieved the Excel dose statistics. D_{max} was defined as the dose delivered to the hottest 0.03 cm^3 of the volume.

Paired t-tests

Paired student t-tests were performed to conclude if the mean of a dose parameter deviated between automatic and manual VMAT planning. The paired t-test applies the null hypothesis that there is no difference between the automatic and manual VMAT plans in the dose statistics. Hence, the p-value represents the probability of observing the given results if the null hypothesis is true. The p-values from the paired t-tests were calculated using scipy version 1.5.2, and a p-value lower than 0.05 was considered statistically significant.

Conformity index

The conformity index was calculated according to Equation (2) and used to compare the

quality of the dose distributions from automatic and manual VMAT planning. Conformity indexes were calculated for the isodoses at 95% of the prescribed dose to PTV_45 (42.75 Gy) and 90% of the prescribed dose to PTVn_55 (49.5 Gy) and PTVn_57.5 (51.75 Gy). For patients with positive LNs and more than one target volume, the conformity index's isodose for one target volume might be present at other target volumes. For example, when calculating the conformity index for PTVn_57.5, the 51.75 Gy isodose is also present inside and around the fall-off region around PTVn_55. Consequently, the conformity index of PTVn_57.5 would be low and not provide the intended information. To compensate for this, the isodose intersection with other target volumes and a margin of 30 mm were subtracted from the total isodose volume. For example, when calculating the conformity index for PTVn_57.5, the 51.75 Gy isodose inside and around PTVn_55 was subtracted from the total isodose volume to only include the isodose volume that belongs to PTVn_57.5.

3.4.2 QA measurements

Both the manual and automatic VMAT plans were delivered by the linac to the Delta^4 Phantom+ and measured. The measurements took place at the RT department at St. Olavs hospital on an ELEKTA Versa HD linac (Elekta, Stocholm, Sweden). To ensure equal conditions for all VMAT plans, all measurements were done in one day with the same linac and phantom setup. The software ScandiDos Delta^4 (version 1.00.0180 November 2019) was used to record the measurements and collect data [43].

3.4.3 Blind test

The purpose of the blind test was to see if the quantitative results agreed with the physicists', physicians' and dose planners' qualitative VMAT plan evaluation. The blind test included 10 of the 25 patients, and to not reveal the planning procedure, relevant information was removed from RayStation. Which of the two cases represented which plan was randomised. Case 4, 5 and 9 were the patients with automatic VMAT plans anticipated to score worst against the manual plans. The remaining seven patients were selected to give an even distribution of LN situations. Figure 17 shows the distributed form for answering the blind test. The recipients should select the best quality plan based on qualitative assessment of the dose distributions and the dose objectives in Tables 2 and 4.

Case nr	Positive Lymph nodes	Plan 1	Plan 2	Does not matter	Comment (*What was crucial for selecting this plan? Would you ask for adjustments to the selected plan? What adjustments?)*
1	3 to 57.5 Gy				
2	3 to 55 Gy				
3	2 to 55 Gy and 1 to 57.5 Gy				
4	3 to 57.5 Gy				
5	2 to 55 Gy and 2 to 57.5 Gy				
6	2 to 55 Gy				
7	4 to 55 Gy and 2 to 57.5 Gy				
8	None				
9	None				
10	None				

Figure 17: Empty form for answering the blind test. The form was sent to physicists, physicians and dose planners working with LACC patients at St. Olavs Hospital.

4 Results

4.1 The automatic VMAT planning script

The script developed for RayStation produced VMAT plans for LACC patients automatically with a run-time of 30-45 minutes. VMAT plans without positive LNs treated without SIB had shorter run-time than plans with positive LNs treated with SIB.

The total number of MUs by automatic and manual VMAT planning is plotted in Figure 18. The automatic VMAT plans have a significantly higher number of MUs than the manual VMAT plans ($p < 10^4$).

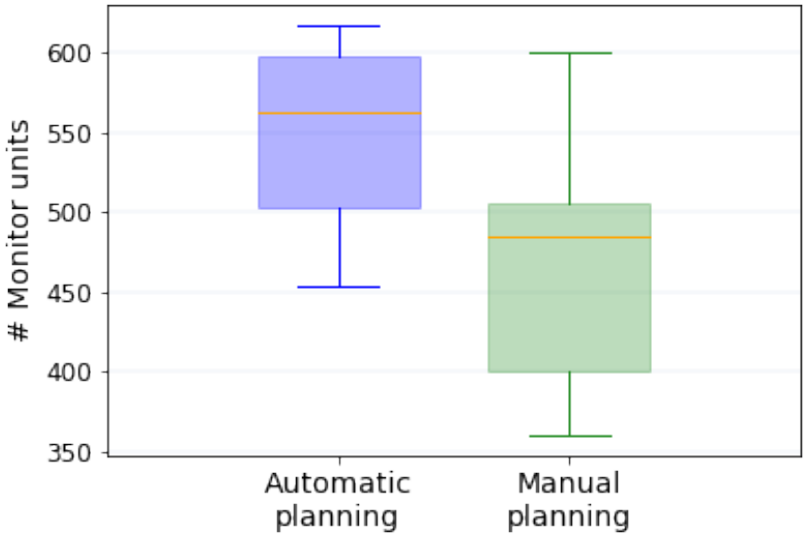

Figure 18: Total number of monitor units used for automatic VMAT planning (blue) and manual VMAT planning (green), N=25.

4.2 Dose statistics

This section provides dose statistics, including the conformity index, from the automatic- and manual VMAT plans for the 25 patients. The results are related to the dose-volume constraints from the Norwegian directory of health listed in Tables 2 to 4. The dose statistics are presented by DVH curves and box plots with associated p-values. The p-values are listed in Tables 10 to 13 at the end of each subsection.

4.2.1 Target volumes

Mean cumulative DVH curves for PTV_45 without SIB, PTV_45 with SIB, PTVn_55 and PTVn_57.5 are shown in Figure 19. Similar plots for CTV_45 without SIB, CTV_45 with SIB, CTVn_55 and CTVn_57.5 are shown in Figure 20. The results indicates that dose received by target volumes are generally lower with automatic than with manual VMAT planning.

The volume percentage of PTV_45that receive 95% of the prescribed dose (42.8 Gy), $V_{95\%}$, is shown in Figure 21 for the patients treated without SIB and with SIB. $V_{95\%}$ to both patient groups achieve the hard dose constraint, but are considerably higher than the soft dose constraint $V_{95\%}$ = 95% (42.8 Gy). The figure shows that automatic VMAT planning gives lower $V_{95\%}$ than manual VMAT planning, and Table 10 shows that automatic planning gives significantly lower $V_{95\%}$ to PTV_45 for the patient group treated with SIB.

The dose received by 98% of the target volumes PTVn and CTVn, D_{98}, are shown in Figures 22 and 23, respectively. The narrow boxes from automatic VMAT planning show less variability in dose delivery between patients than manual VMAT planning. All VMAT plans achieve the hard dose constraint for both PTVn and CTVn. From Table 10, automatic VMAT planning gives significantly lower D_{98} than manual VMAT planning for both PTVn and CTVn.

Figure 24 shows the maximum dose, D_{max}, received by PTV_45 treated without and with SIB, PTVn_55 and PTV_57.5. D_{max} is given as the percentage of the prescribed dose for each patient group. Except for outliers, all VMAT plans achieve the D_{max} hard dose constraint, except for PTV_45 treated with SIB and manual VMAT planning that have most data points outside and above hard dose constraint. Table 10 shows that D_{max} for PTV_45 treated with SIB and automatic VMAT planning is significantly lower than with manual VMAT planning.

The dose received by 50% of the target volumes PTVn and CTVn, D_{50}, are shown in Figure 25. The results show that it is easier to achieve the hard dose constraint for CTVn than for PTVn. Table 10 shows that D_{50} for the PTVns are significantly lower for automatic VMAT planning than for manual VMAT planning.

The maximum dose, D_{max}, to xCTVp for the patients treated without and with SIB is shown in Figure 26. The results show that neither the automatic nor the manual

VMAT plans meet the soft dose constraint for xCTVp. For the patients treated without SIB, Table 10 shows that the automatic VMAT plans have significantly higher D_{max} than the manual VMAT plans, but the difference is not very large (≈0.5 Gy).

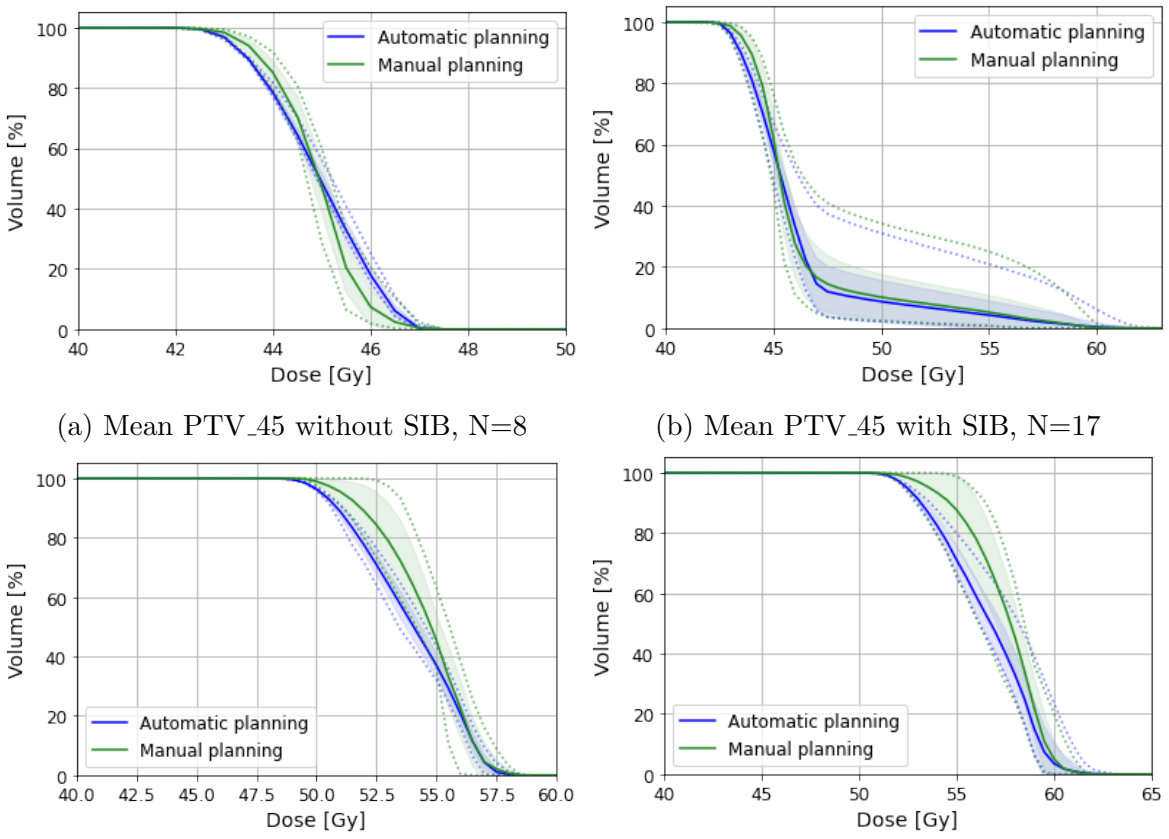

(a) Mean PTV_45 without SIB, N=8

(b) Mean PTV_45 with SIB, N=17

(c) Mean PTVn_55, N=10

(d) Mean PTVn_57.5, N=10

Figure 19: Mean cumulative dose volume histogram for (a) **PTV_45 without SIB**, (b) **PTV_45 with SIB**, (c) **PTVn_55** and (d) **PTVn_57.5** from N patients. Data from the automatic and manual VMAT plans are plotted in blue and green, respectively. The solid lines represent the mean, and the dotted lines represents the minimum and maximum values. The shaded areas are the first standard deviation. The horizontal axis starts at 40 Gy.

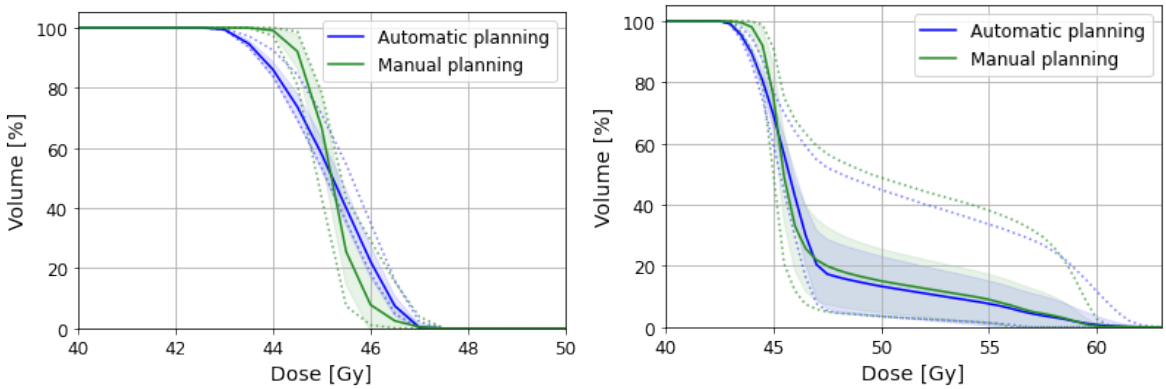

(a) Mean CTV_45 without LNs, N=8

(b) Mean CTV_45 with LNs, N=17

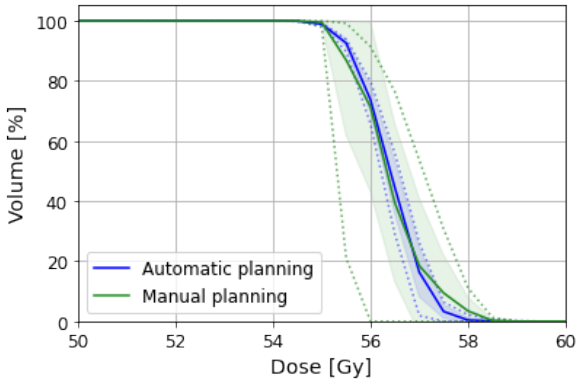

(c) Mean CTVn_55, N=8

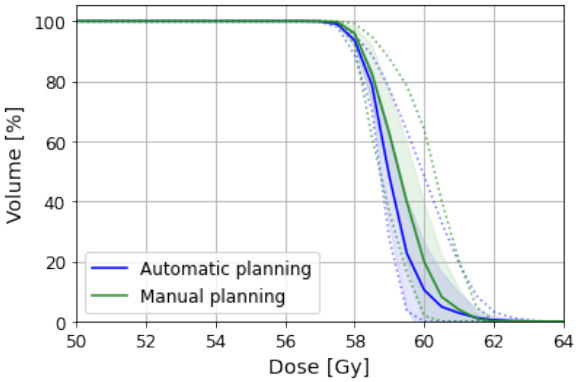

(d) Mean CTVn_57.5, N=7

Figure 20: Mean cumulative dose volume histogram for (a) **CTV_45 without SIB**, (b) **CTV_45 with SIB**, (c) **CTVn_55** and (d) **CTVn_57.5** from N patients. Data from the automatic and manual VMAT plans are plotted in blue and green, respectively. The solid lines represent the mean, and the dotted lines represents the minimum and maximum values. The shaded areas are the first standard deviation. The horizontal axis starts at 40 Gy for the CTVs and at 50 Gy for the CTVns.

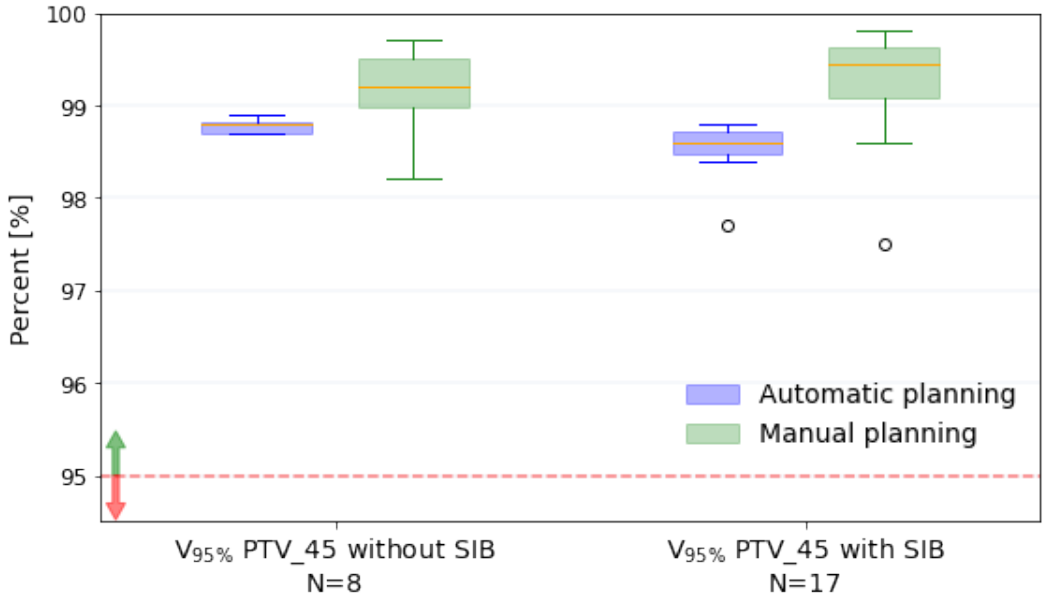

Figure 21: Box plots for $\mathbf{V_{95\%}}$ for **PTV_45** for N patients. Automatic and manual planning is plotted in blue and green, respectively. The red line represents the hard dose constraint $V_{95\%} > 95\%$ (42.8 Gy) with green and red arrows pointing in the accepted and not accepted direction.

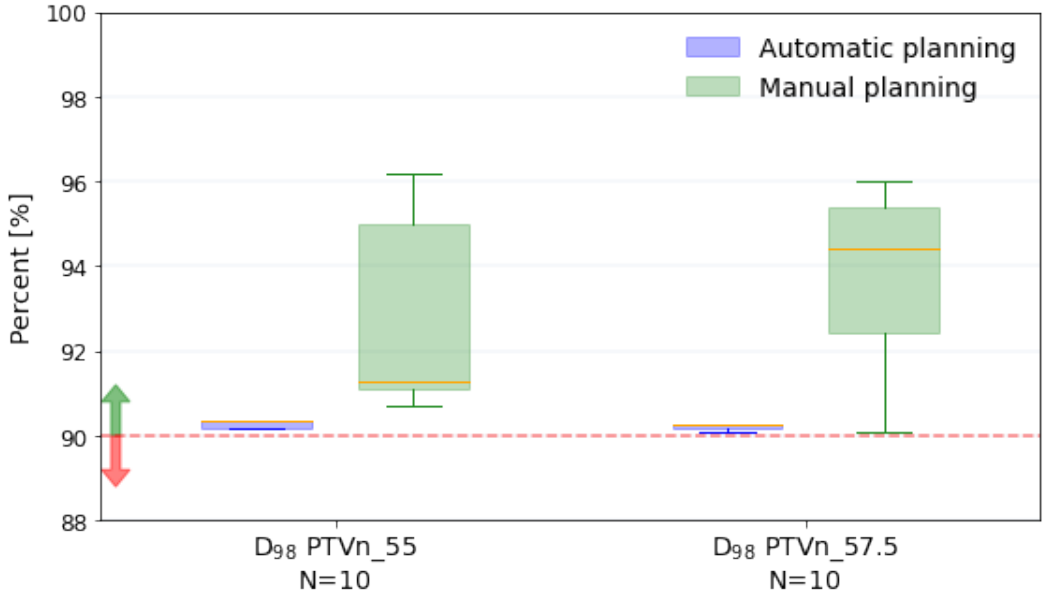

Figure 22: Box plots for $\mathbf{D_{98}}$ for **PTVn_55** and **PTVn_57.5** for N patients. Automatic and manual planning is plotted in blue and green, respectively. The red line represents the hard dose constraint $D_{98} > 90\%$ of prescribed dose with green and red arrows pointing in the accepted and not accepted direction.

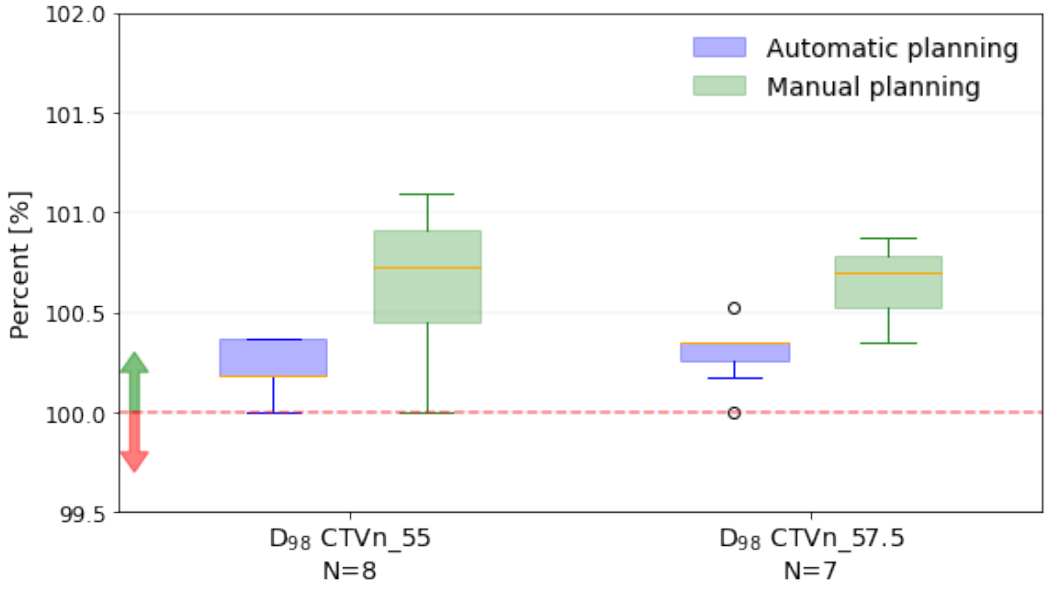

Figure 23: Box plots for $\mathbf{D_{98}}$ for **CTVn** for N patients. Automatic and manual planning is plotted in blue and green, respectively. The red line represents the hard dose constraint $D_{98} > 100\%$ of prescribed dose with green and red arrows pointing in the accepted and not accepted direction.

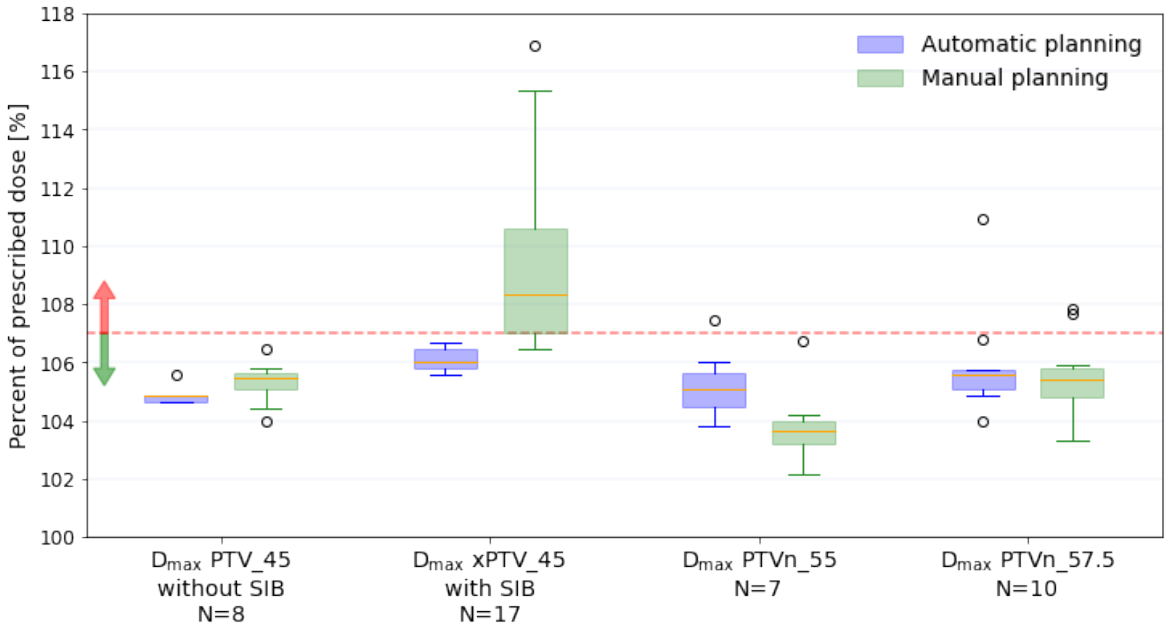

Figure 24: Box plots for $\mathbf{D_{max}}$ for **PTV_45** and **PTVn** for N patients. Automatic and manual planning is plotted in blue and green, respectively. The red line represents the hard dose constraint $D_{max} < 107\%$ of prescribed dose with green and red arrows pointing in the accepted and not accepted direction.

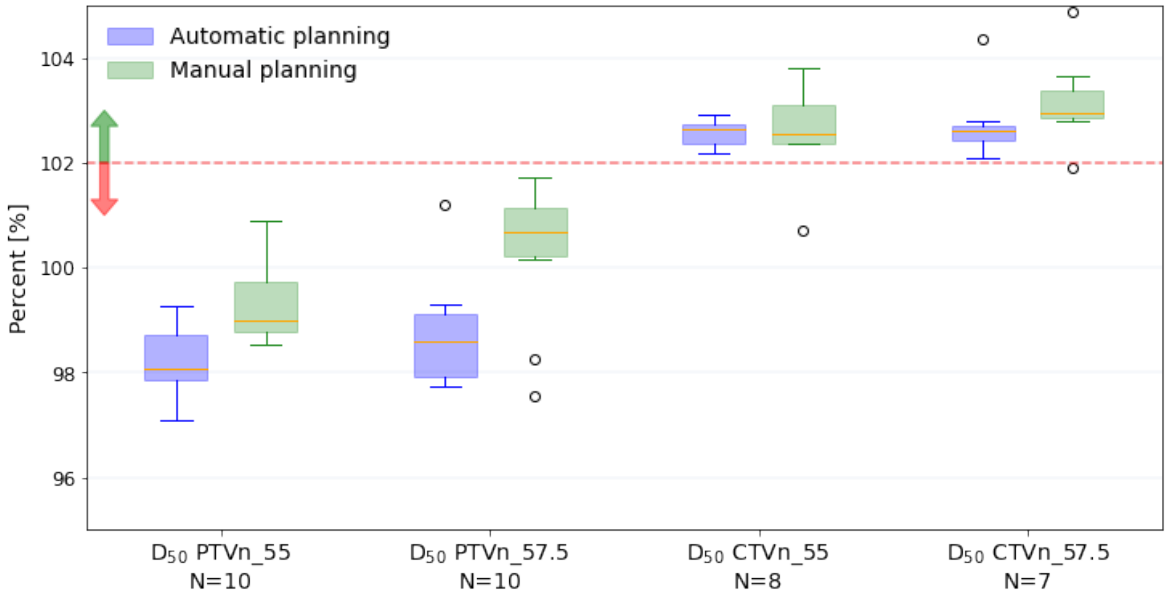

Figure 25: Box plots for $\mathbf{D_{50}}$ for **PTVn** and **CTVn** for N patients. Automatic and manual planning is plotted in blue and green, respectively. The red line represents the soft dose constraint $D_{50} > 102\%$ of prescribed dose with green and red arrows pointing in the accepted and not accepted direction.

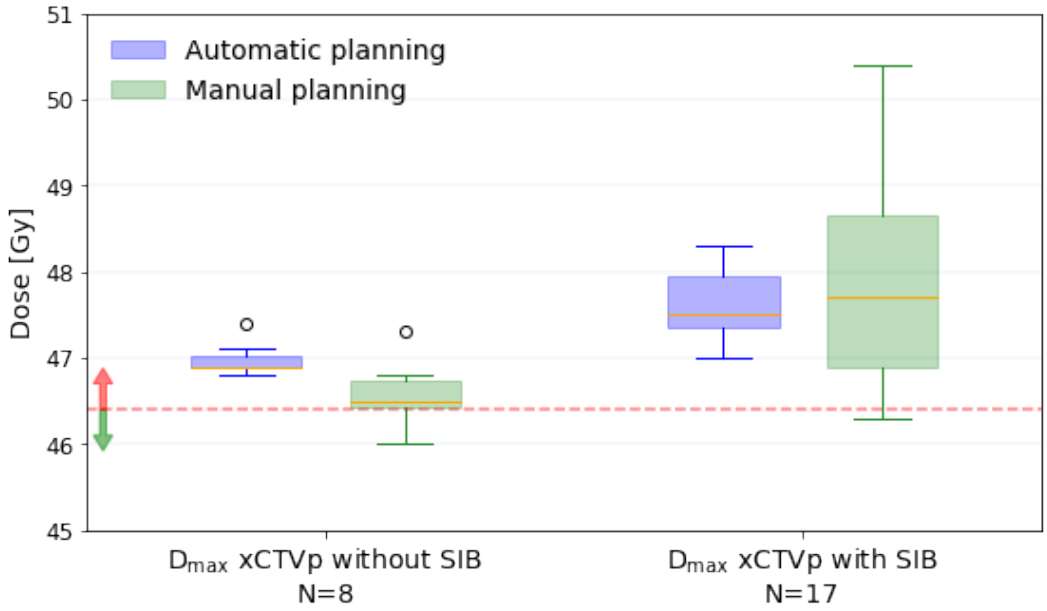

Figure 26: Box plots for $\mathbf{D_{max}}$ to **xCTVp** for N patients. Automatic and manual planning is plotted in blue and green, respectively. The red line represents the soft dose constraint $D_{max} < 103\%$ (46.4 Gy) of prescribed dose with green and red arrows pointing in the accepted and not accepted direction.

Table 10: p-values for the presented target volume dose statistics. Statistically significant results (p-value < 0.05) are in bold and labelled with a star.

Volume	**Figure**	***p*-value**
$V_{95\%}$ PTV_45 without SIB	fig. 21	0.0896
$V_{95\%}$ with SIB	fig. 21	**0.0008** ⋆
D_{98} PTVn_55	fig. 22	**0.0257** ⋆
D_{98} PTVn_57.5	fig. 22	**0.0077** ⋆
D_{98} CTVn_55	fig. 23	**0.0148** ⋆
D_{98} CTVn_57.5	fig. 23	**0.0006** ⋆
D_{max} PTV_45 without SIB	fig. 24	0.1051
D_{max} PTV_45 with SIB	fig. 24	**0.0007** ⋆
D_{max} PTVn_55	fig. 24	0.1232
D_{max} PTVn_57.5	fig. 24	0.5316
D_{50} PTVn_55	fig. 25	**0.0101** ⋆
D_{50} PTVn_57.5	fig. 25	**0.0089** ⋆
D_{50} CTVn_55	fig. 25	0.8904
D_{50} CTVn_57.5	fig. 25	0.3908
D_{max} xCTVp without SIB	fig. 26	**0.0427** ⋆
D_{max} xCTVp with SIB	fig. 26	0.3383

4.2.2 Organs at risk

The mean cumulative DVH curves for the rectum, bladder, sigmoideum, bowel and body are shown in Figures 27 and 28 for the patients treated without and with SIB, respectively. Figure 29 shows the DVH curves for xOAR volumes, being the OARs excluding the volumes 15 mm from PTVn. All five DVH curves inn all three figures show similar or lower received dose for automatic VMAT planning than for manual VMAT planning at any volume percentage. This result in seen for both the mean DVH curves, and the standard deviations.

The box plots in Figures 30 to 32 shows the maximum doses to rectum, bladder, sigmoideum and bowel for patients treated without SIB, with SIB to 55 Gy and with SIB to 57.5 Gy. The results show that automatic VMAT planning tends to give similar or higher dose to these OARs than manual VMAT planning for patients without SIB. From Table 11, a significant difference was found for the bladder. Doses to these OARs for patients with SIB to 55 Gy and 57.5 Gy show more similar results for automatic and

manual VMAT planning. Figure 33 shows the maximum dose to xRectum, xBladder, xSigmoideum and xBowel, being the OARs excluding PTVn + 15 mm, for the patients treated with SIB. From Table 12, automatic VMAT planning gives significantly lower maximum doses to xSigmoideum and xBowel than manual VMAT planning.

Box plots for the maximum dose to the spinal cord and the femoral heads are given in Figures 34 and 35. The spinal cord was only delineated on 7 patients, of which two were treated without SIB and five with SIB. All seven patients were included in one plot due to this small data sample. From Table 12, automatic VMAT planning gives significantly lower maximum dose to the femoral heads than manual VMAT planning.

The mean dose to the kidneys are plotted in Figure 36, and indicate that automatic VMAT planning gives higher kidney doses than manual VMAT planning. From Table 12, the result is significant for the right kidney. Maximum dose to the body for patients treated without SIB and xBody for patients treated with SIB are shown in Figure 37. The plot implies similar or lower doses to the body with automatic VMAT planning. From Table 12, automatic VMAT planning gives significantly lower maximum dose to xBody than manual VMAT planning. Images of how very low kidney doses create dose accumulations in the body are provided in Figures C.1 and C.2 in Appendix C. How the function weight of the kidney max EUD optimisation function affects the kidney and bowel doses is shown in Table C.1 in Appendix C.

Box plots for the soft dose constraints to V_{40Gy} and V_{30Gy} to rectum, bladder and bowel are shown in Figures 38 and 39 for patients treated without and with SIB, respectively. All sub plots show similar or lower dose with automatic VMAT planning than with manual VMAT planning. From Tables 11 and 12, V_{40Gy} to the rectum with and without SIB and V_{40Gy} to the bladder with SIB are the only V_{40Gy} or V_{30Gy} results that show no significant difference between automatic and manual VMAT planning.

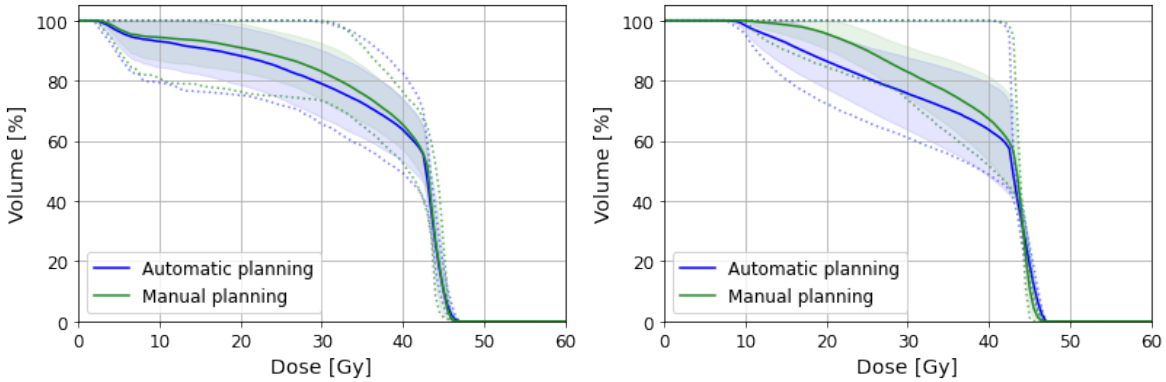

(a) Rectum without SIB

(b) Bladder without SIB

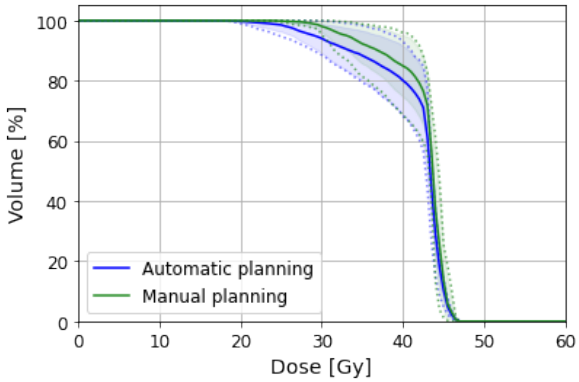

(c) Sigmoideum without SIB

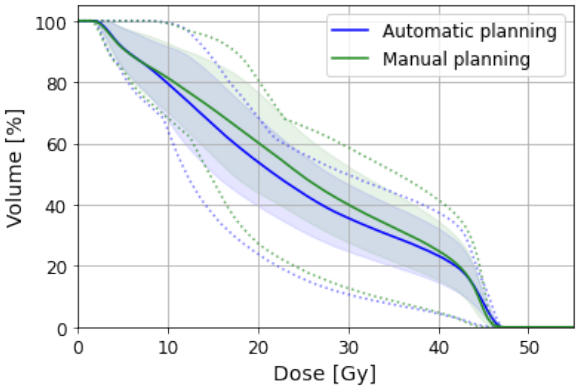

(d) Bowel without SIB

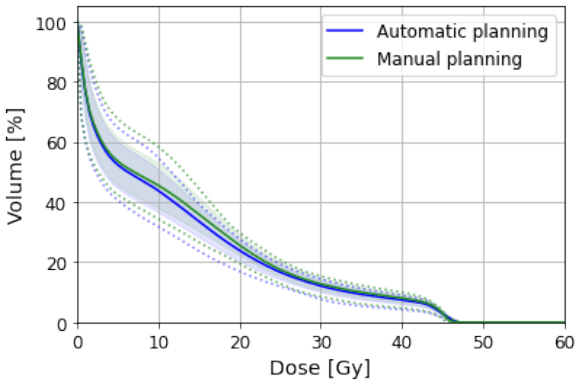

(e) Body without SIB

Figure 27: Mean cumulative dose volume histogram for (a) **Rectum**, (b) **Bladder**, (c) **Sigmoideum**, (d) **Bowel** and (e) **Body** for the patients treated **without SIB**, N=8. Data from the automatic and manual VMAT plans are plotted in blue and green, respectively. The solid lines represent the mean, and the dotted lines represents the minimum and maximum values. The shaded areas are the first standard deviation.

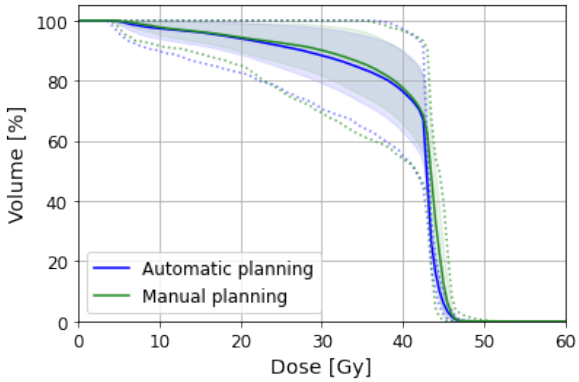

(a) Rectum with SIB

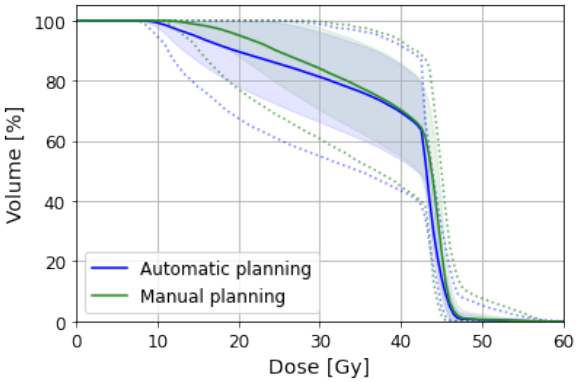

(b) Bladder with SIB

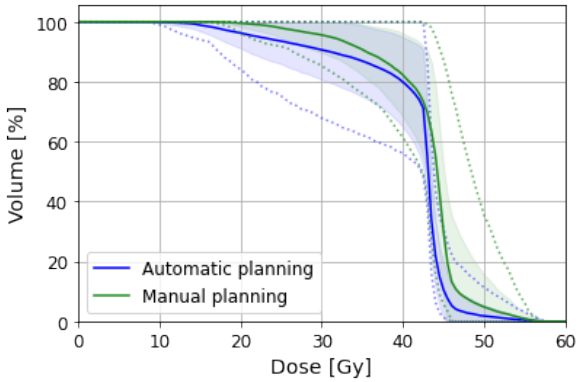

(c) Sigmoideum with SIB

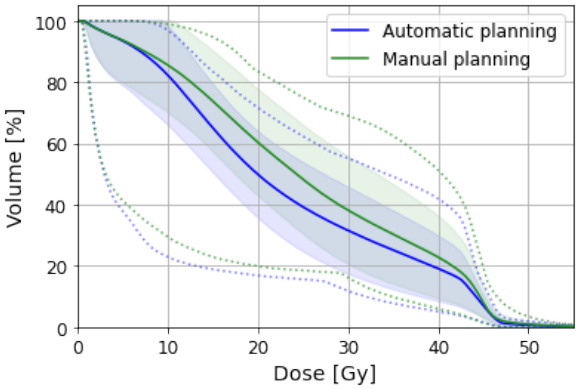

(d) Bowel with SIB

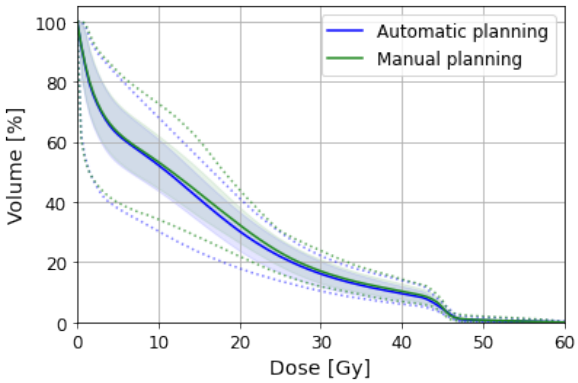

(e) Body with SIB

Figure 28: Mean cumulative dose volume histogram for (a) **Rectum**, (b) **Bladder**, (c) **Sigmoideum**, (d) **Bowel** and (e) **Body** of the patients treated **with SIB**. Data from the automatic and manual VMAT plans are plotted in blue and green, respectively. The solid lines represent the mean, and the dotted lines represents the minimum and maximum values. The shaded areas are the first standard deviation.

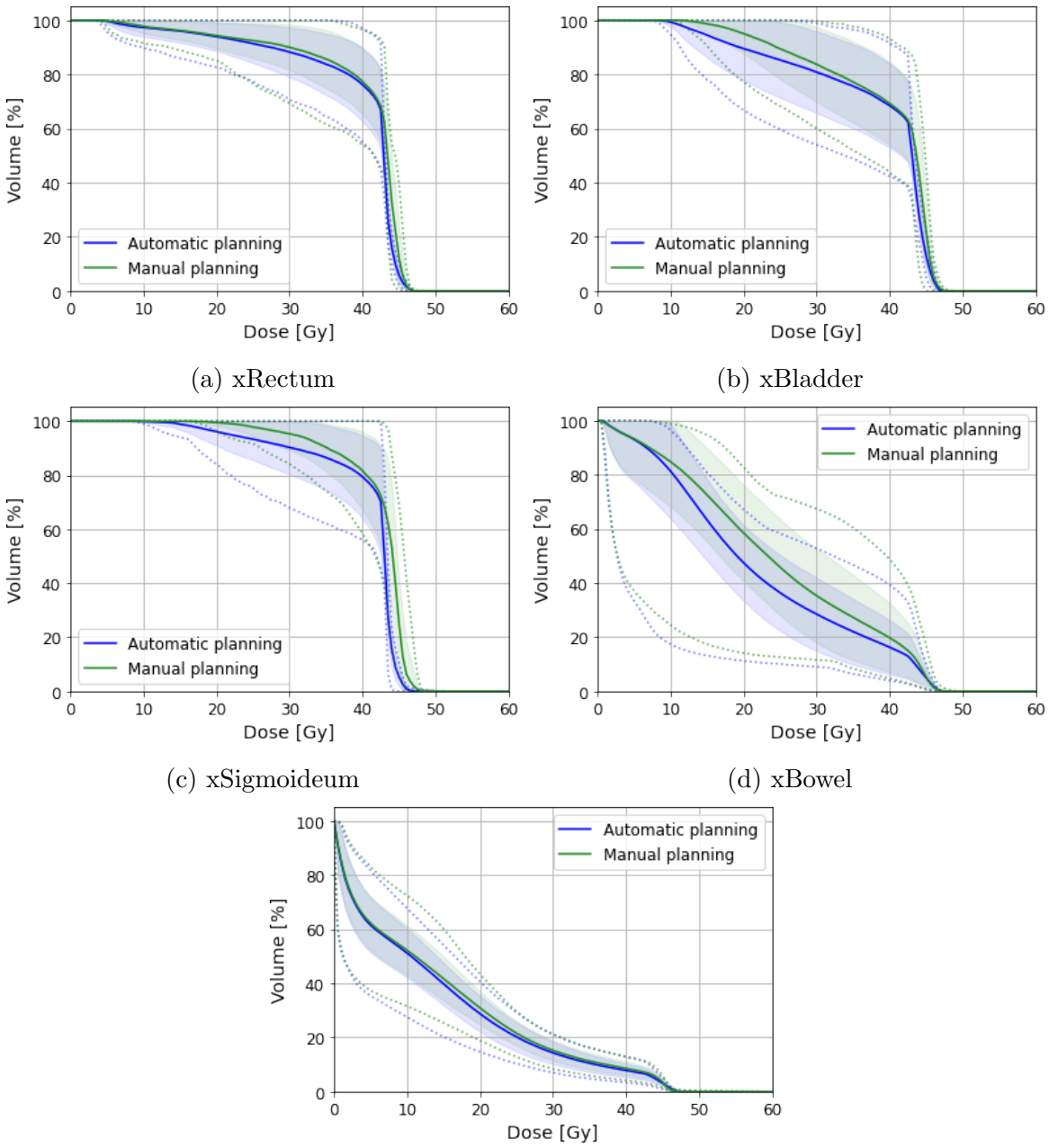

(a) xRectum

(b) xBladder

(c) xSigmoideum

(d) xBowel

(e) xBody

Figure 29: Mean cumulative dose volume histogram for (a) **xRectum**, (b) **xBladder**, (c) **xSigmoideum**, (d) **xBowel** and (e) **xBody** for the patients treated **with SIB**. Data from the automatic and manual VMAT plans are plotted in blue and green, respectively. The solid lines represent the mean, and the dotted lines represents the minimum and maximum values. The shaded areas are the first standard deviation.

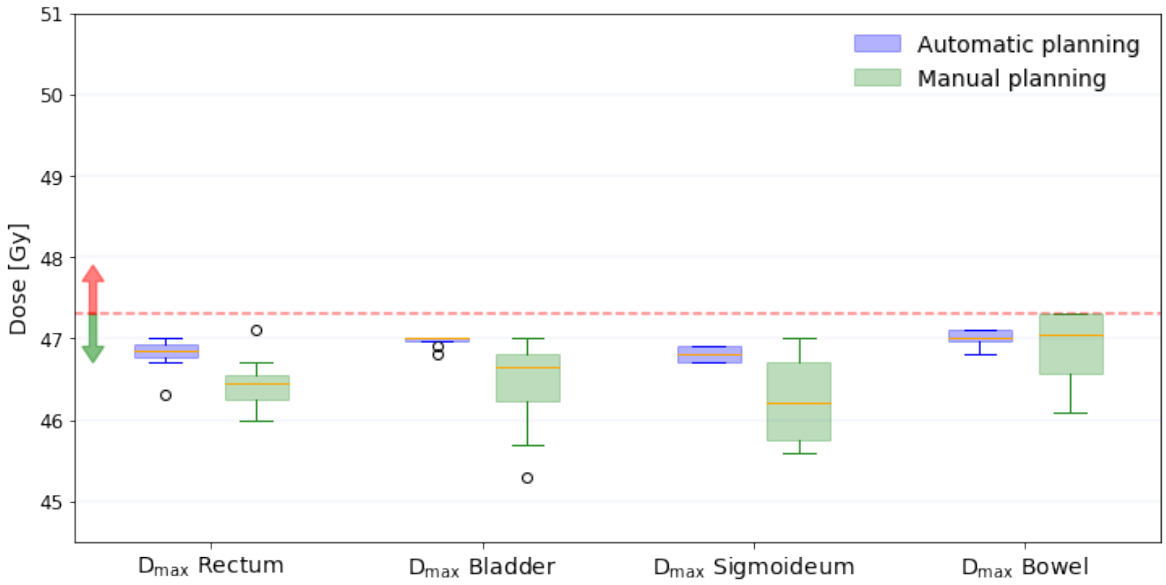

Figure 30: Box plots for $\mathbf{D_{max}}$ to **Rectum**, **Bladder**, **Sigmoideum** and **Bowel** for patients treated **without SIB**, N=8 . Automatic and manual planning is plotted in blue and green, respectively. The red line represents the hard dose constraint D_{max} < 47.3 Gy with green and red arrows pointing in the accepted and not accepted direction.

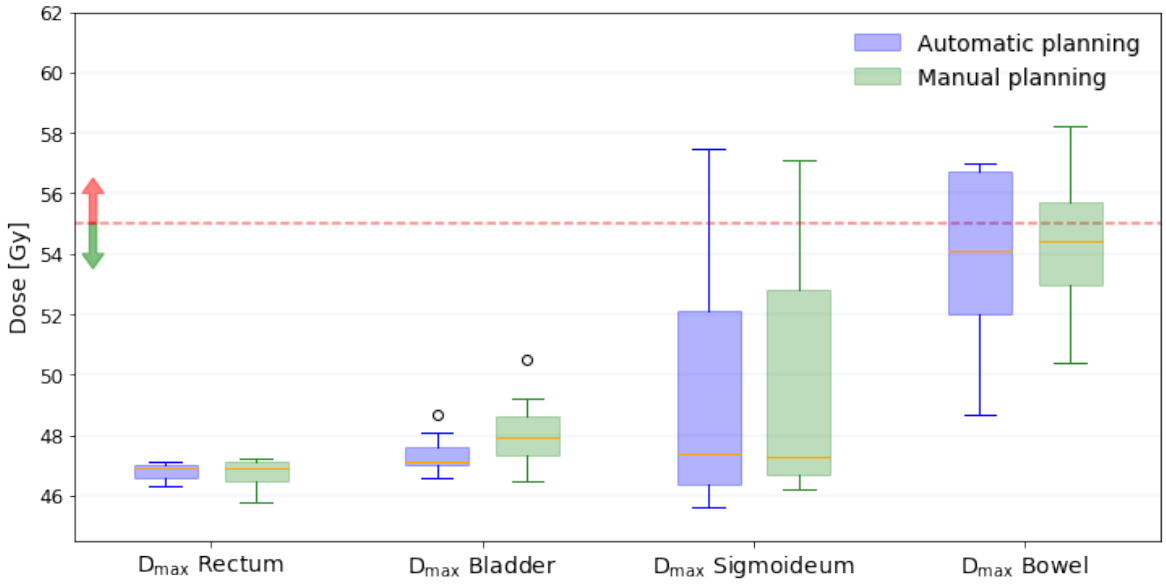

Figure 31: Box plots for $\mathbf{D_{max}}$ to **Rectum**, **Bladder**, **Sigmoideum** and **Bowel** for patients treated **with SIB to 55 Gy**, N=7. Automatic and manual planning is plotted in blue and green, respectively. The red line represents the hard dose constraint D_{max} < 55 Gy with green and red arrows pointing in the accepted and not accepted direction.

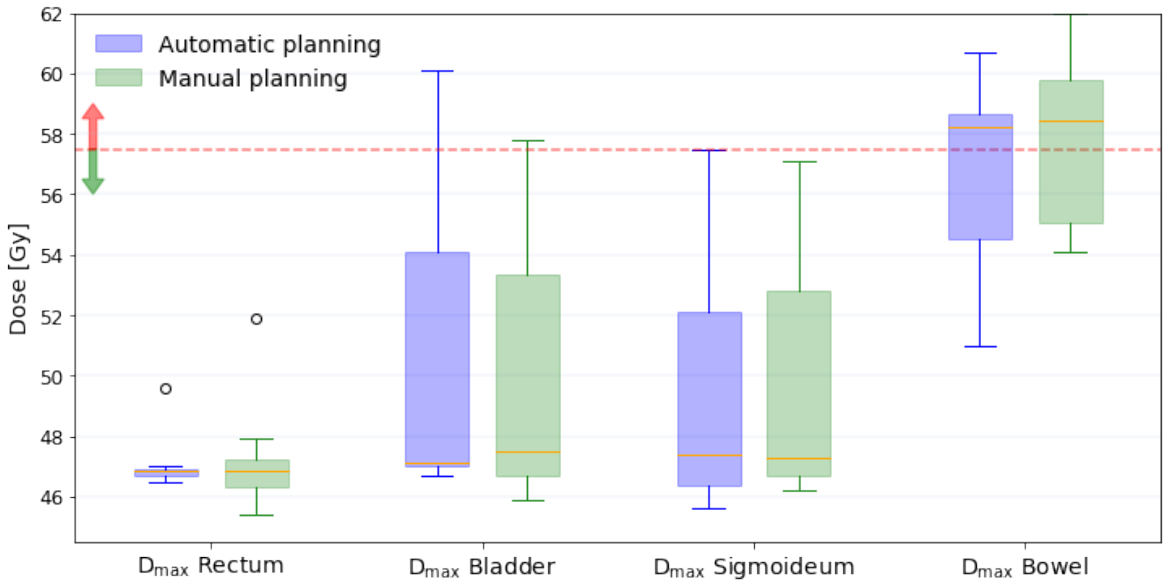

Figure 32: Box plots for $\mathbf{D_{max}}$ to **Rectum**, **Bladder**, **Sigmoideum** and **Bowel** for patients treated **with SIB to 57.5 Gy**, N=10. Automatic and manual planning is plotted in blue and green, respectively. The red line represents the hard dose constraint $D_{max} < 57.5$ Gy with green and red arrows pointing in the accepted and not accepted direction.

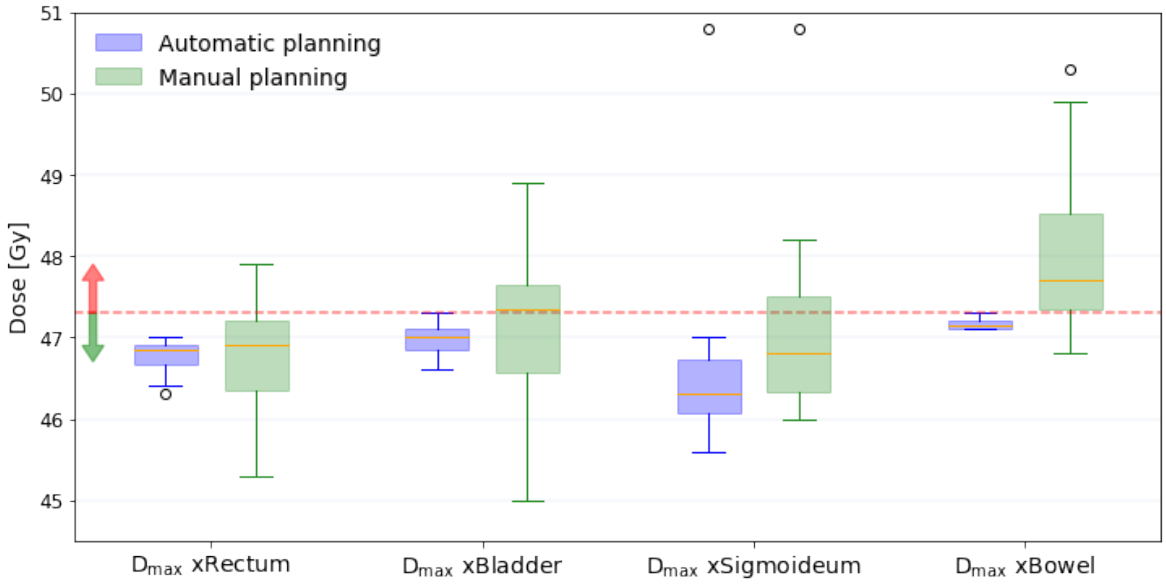

Figure 33: Box plots for $\mathbf{D_{max}}$ to **xRectum**, **xBladder**, **xSigmoideum** and **xBowel** for patients treated **with SIB**, N=17. Automatic and manual planning is plotted in blue and green, respectively. The red line represents the hard dose constraint $D_{max} < 47.3$ Gy with green and red arrows pointing in the accepted and not accepted direction.

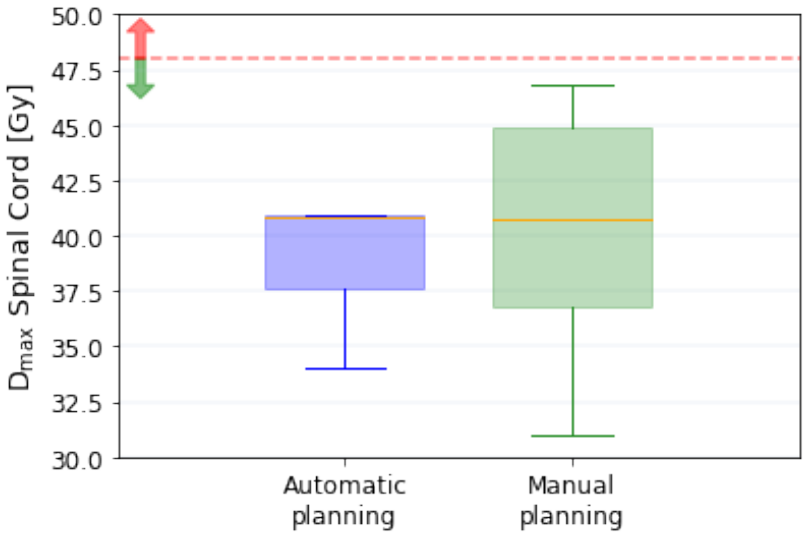

Figure 34: Box plots for $\mathbf{D_{max}}$ to the **Spinal Cord** for N=7 patients for automatic and manual VMAT planning. The red line represents the hard dose constraint D_{max} < 48 Gy with green and red arrows pointing in the accepted and not accepted direction.

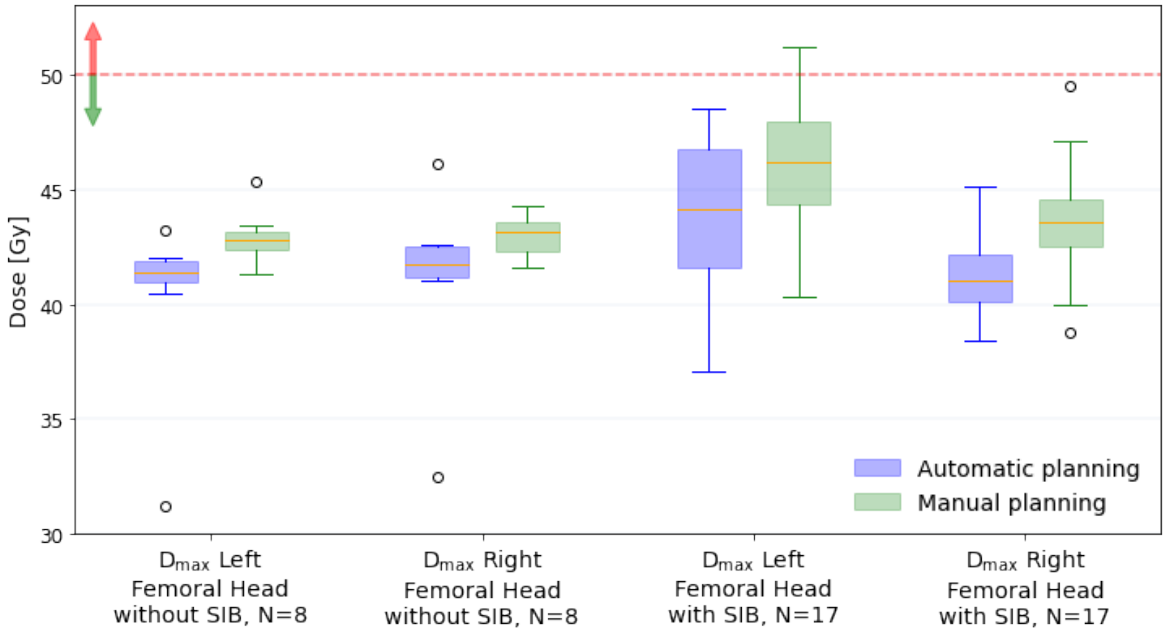

Figure 35: Box plots for $\mathbf{D_{max}}$ to the left and right **Femoral Heads** treated **without and with SIB** for N patients. Automatic and manual VMAT planning is plotted in blue and green, respectively. The red line represents the hard dose constraint D_{max} < 50 Gy with green and red arrows pointing in the accepted and not accepted direction.

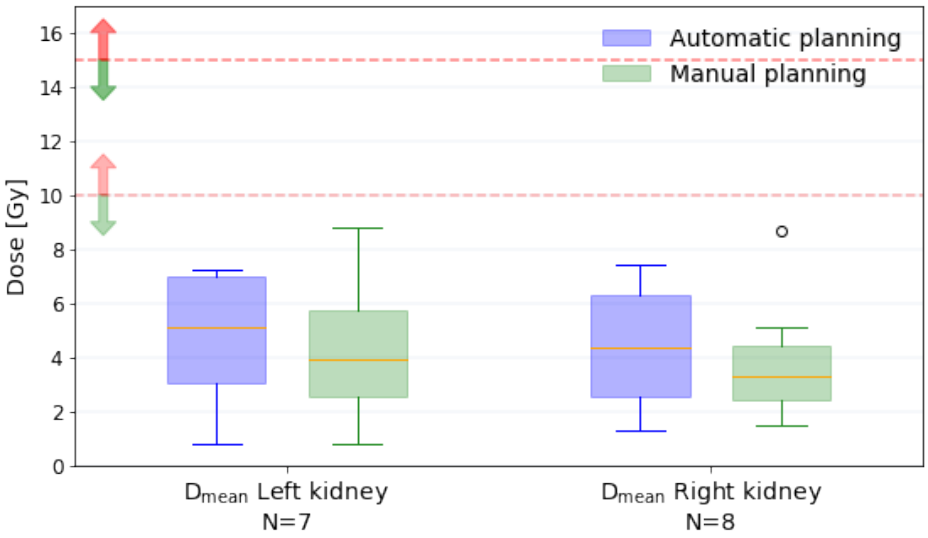

Figure 36: Box plots for $\mathbf{D_{mean}}$ to the left and right **Kidneys** for N patients. Automatic and manual VMAT planning is plotted in blue and green, respectively. The red lines represents the hard dose constraint $D_{mean} < 15$ Gy and the soft dose constraint $D_{mean} < 10$ Gy with green and red arrows pointing in the accepted and not accepted direction.

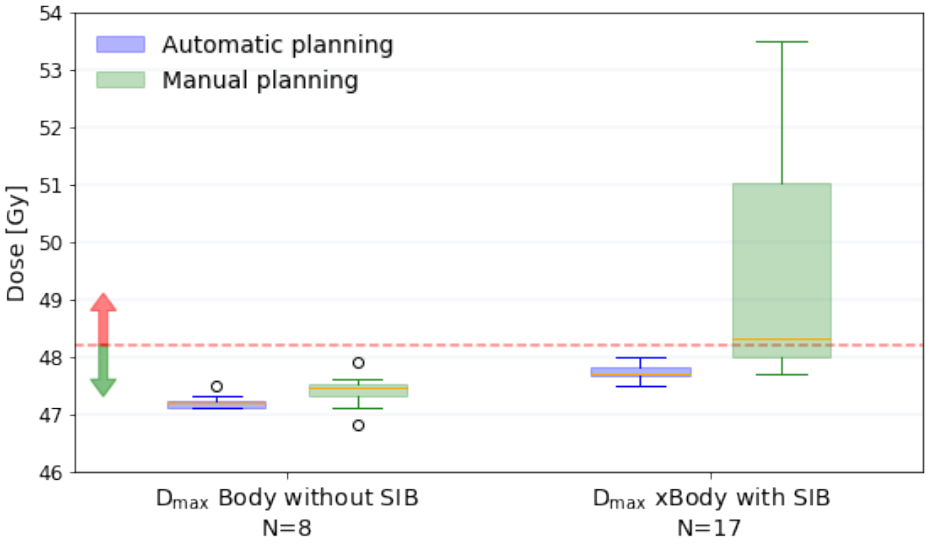

Figure 37: Box plots for $\mathbf{D_{max}}$ to the **Body without SIB** and **xBody with SIB** for N patients. Automatic and manual VMAT planning is plotted in blue and green, respectively. The red line represents the hard dose constraint $D_{max} < 48.2$ Gy with green and red arrows pointing in the accepted and not accepted direction.

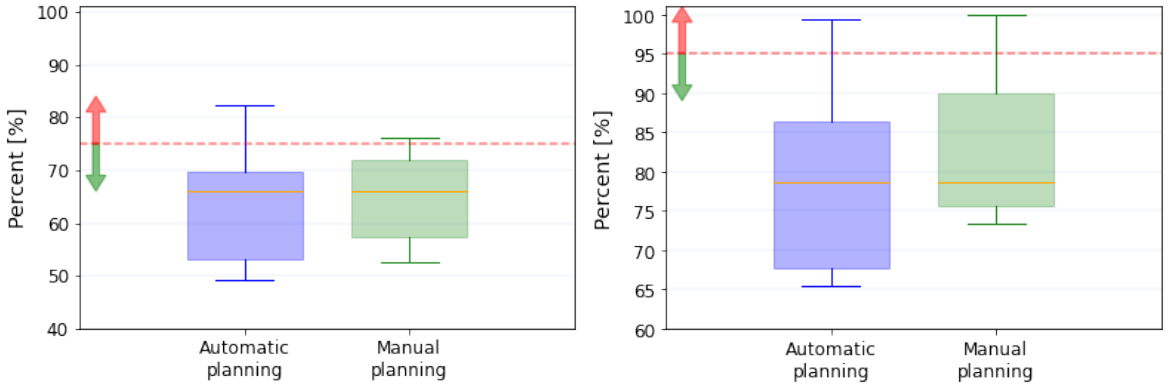

(a) $\mathbf{V_{40\ Gy}}$ rectum (< 75%)

(b) $\mathbf{V_{30\ Gy}}$ rectum (< 95%)

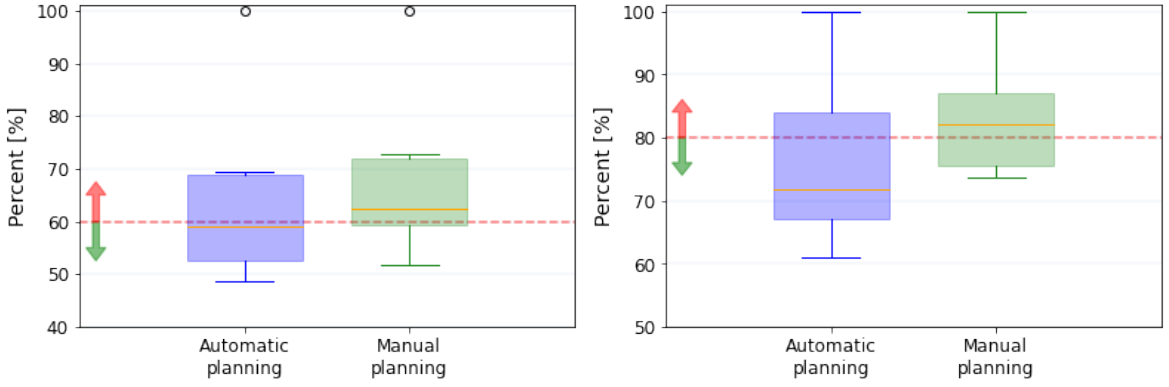

(c) $\mathbf{V_{40\ Gy}}$ bladder (< 60%)

(d) $\mathbf{V_{30\ Gy}}$ bladder (< 80%)

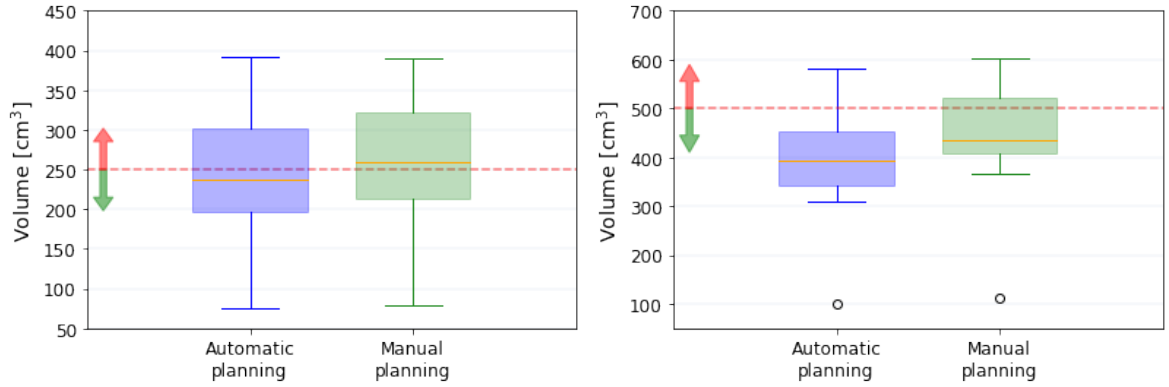

(e) $\mathbf{V_{40\ Gy}}$ bowel (< 250 cm^3)

(f) $\mathbf{V_{30\ Gy}}$ bowel (< 500 cm^3)

Figure 38: Box plots for $\mathbf{V_{40\ Gy}}$ and $\mathbf{V_{30\ Gy}}$ to **Rectum**, **Bladder** and **Bowel** for N=8 patients **without SIB** for automatic and manual VMAT planning. The red line represents the soft dose constraints with green and red arrows pointing in the accepted and not accepted direction.

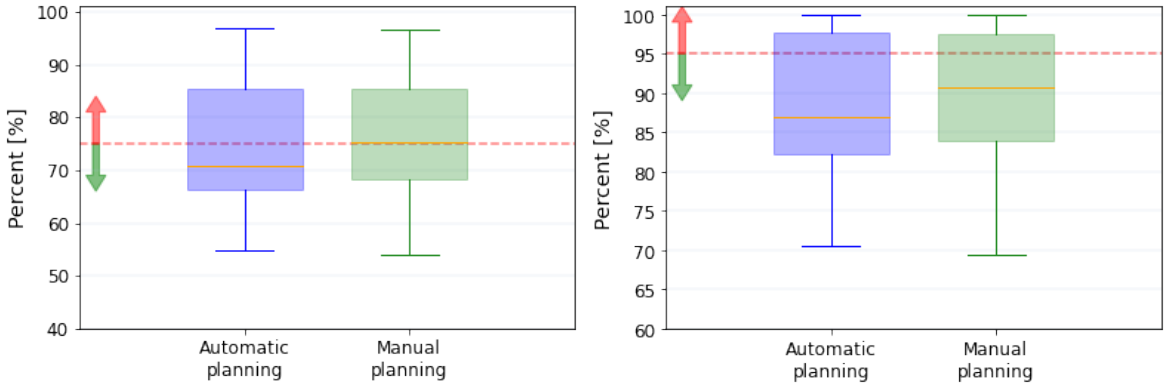

(a) $\mathbf{V_{40\ Gy}}$ rectum (< 75%)

(b) $\mathbf{V_{30\ Gy}}$ rectum (< 95%)

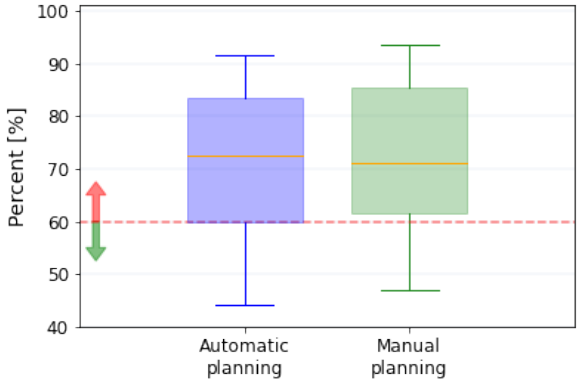

(c) $\mathbf{V_{40\ Gy}}$ bladder (< 60%)

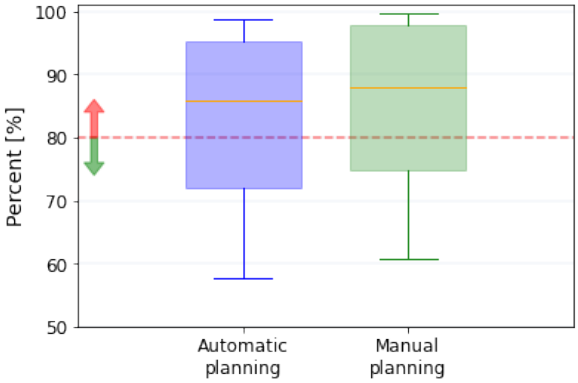

(d) $\mathbf{V_{30\ Gy}}$ bladder (< 80%)

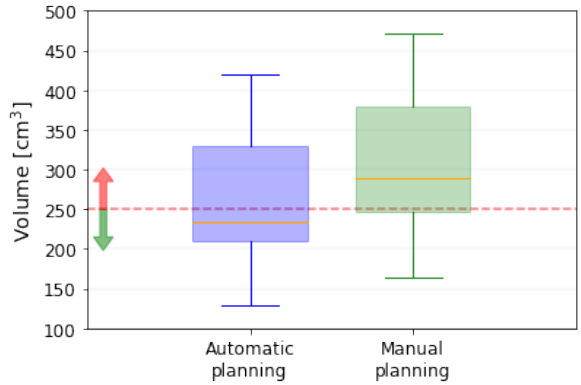

(e) $\mathbf{V_{40\ Gy}}$ bowel (< 250 cm^3)

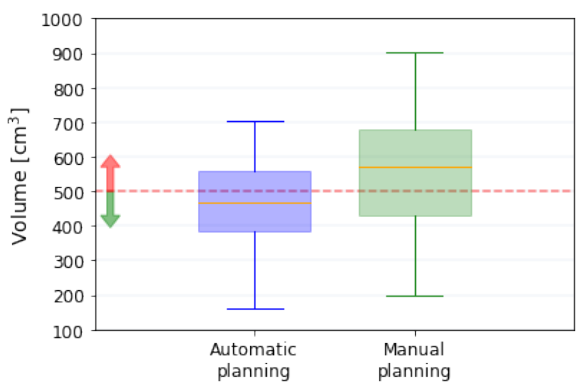

(f) $\mathbf{V_{30\ Gy}}$ bowel (< 500 cm^3)

Figure 39: Box plots for $\mathbf{V_{40\ Gy}}$ and $\mathbf{V_{30\ Gy}}$ to **Rectum**, **Bladder** and **Bowel** for N=17 patients **with SIB** for automatic and manual VMAT planning. The red line represents the soft dose constraints with green and red arrows pointing in the accepted and not accepted direction.

Table 11: p-values for the presented OAR dose statistics for EBRT **without SIB**. Statistically significant results (p-value < 0.05) are in bold and labelled with a star.

Volume	**Figure**	***p*-value**	**Volume**	**Figure**	***p*-value**
D_{max} Rectum	fig. 30	0.0596	V_{40Gy} Rectum	fig. 38a	0.2938
D_{max} Bladder	fig. 30	**0.0423** ⋆	V_{30Gy} Rectum	fig. 38b	**0.0291** ⋆
D_{max} Sigmoideum	fig. 30	0.1843	V_{40Gy} Bladder	fig. 38c	**0.0040** ⋆
D_{max} Bowel	fig. 30	0.5325	V_{30Gy} Bladder	fig. 38d	**0.0095** ⋆
D_{max} Body	fig. 37	0.0847	V_{40Gy} Bowel	fig. 38e	**0.0090** ⋆
D_{max} Left FemoralHead	fig. 35	0.0771	V_{30Gy} Bowel	fig. 38f	**0.0007** ⋆
D_{max} Right FemoralHead	fig. 35	0.1733			

Table 12: p-values for the presented OAR dose statistics for EBRT **with SIB**. Statistically significant results (p-value < 0.05) are in bold and labelled with a star.

Volume	Figure	p-value	Volume	Figure	p-value
D_{max} Rectum SIB to 55 Gy	fig. 31	0.7752	D_{max} Left FemoralHead	fig. 35	**0.0070** ⋆
D_{max} Bladder SIB to 55 Gy	fig. 31	**0.0429** ⋆	D_{max} Right FemoralHead	fig. 35	**0.0001** ⋆
D_{max} Sigmoideum SIB to 55 Gy	fig. 31	0.2355	D_{max} Spinal Cord	fig. 34	0.6098
D_{max} Bowel SIB to 55 Gy	fig. 31	0.3189	V_{mean} Left Kidney	fig. 36	0.3853
D_{max} Rectum SIB to 57.5 Gy	fig. 32	0.7374	V_{mean} Right Kidney	fig. 36	**0.0086** ⋆
D_{max} Bladder SIB to 57.5 Gy	fig. 32	0.2192	D_{max} xBody	fig. 37	**0.0086** ⋆
D_{max} Sigmoideum SIB to 57.5 Gy	fig. 32	0.2356	V_{40Gy} Rectum	fig. 39a	0.1198
D_{max} Bowel SIB to 57.5 Gy	fig. 32	0.1217	V_{30Gy} Rectum	fig. 39b	**0.0258** ⋆
D_{max} xRectum	fig. 33	0.8132	V_{40Gy} Bladder	fig. 39c	0.1777
D_{max} xBladder	fig. 33	0.4259	V_{30Gy} Bladder	fig. 39d	**0.0270** ⋆
D_{max} xSigmoideum	fig. 33	**0.0205** ⋆	V_{40Gy} Bowel	fig. 39e	**0.0001** ⋆
D_{max} xBowel	fig. 33	**0.0042** ⋆	V_{30Gy} Bowel	fig. 39f	**0.0003** ⋆

4.3 Conformity index

The conformity index defined by the *CN* in Equation (2) for automatic and manual VMAT planning for PTV_45 with and without SIB, PTVn_55 and PTVn_57.5 are plotted in Figure 40. Automatic VMAT planning gives a higher *CN* than manual VMAT planning for all target volumes. Figure 41 shows the contribution from the first term of the *CN* equation which concerns how much of the target volume that is covered by the reference isodose. Figure 42 shows the contribution from the second term of the *CN* equation which concerns how much of the reference isodose that covers the target volume. Associated p-values are given in table Table 13. Figures 43 and 44 shows screenshots of the 42.75 Gy isodose around PTV_45 and the 49.5 Gy isodose around PTVn_55 in patient 7 and 21, respectively.

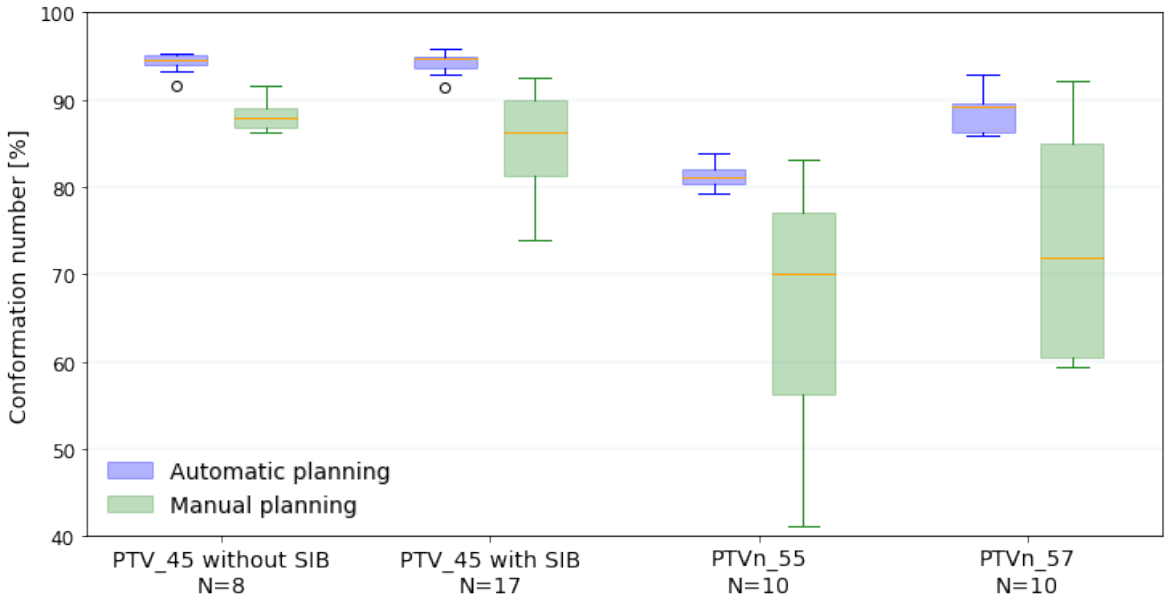

Figure 40: Box plot of the **conformation number** of PTV_45 without SIB, PTV_45 with SIB, PTVn_55 and PTVn_57.5 for N patients. Automatic and manual planning is plotted in blue and green, respectively.

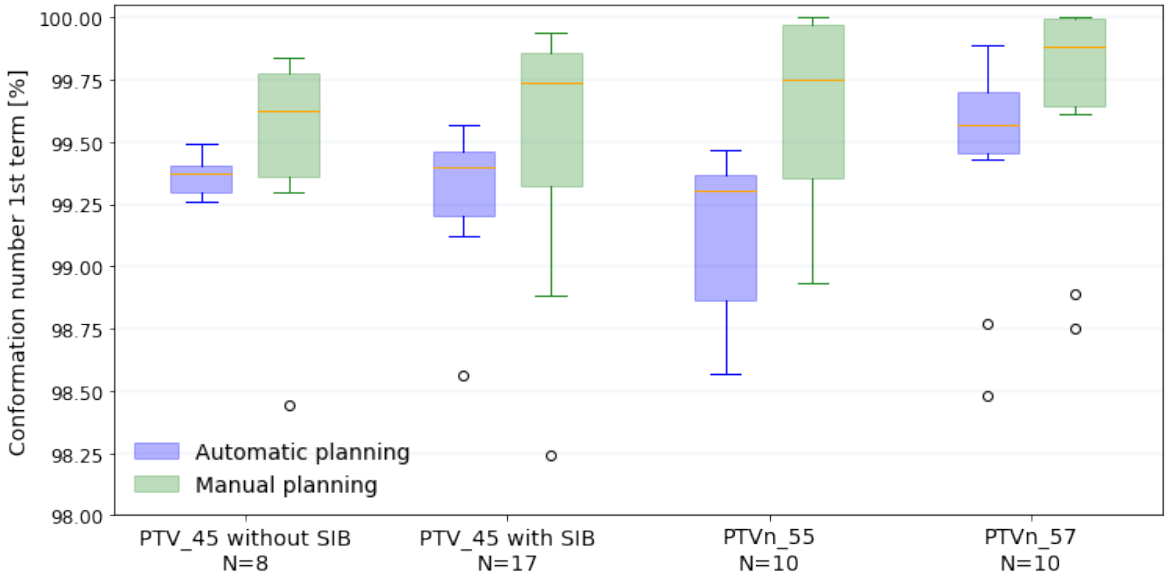

Figure 41: Box plot of the **first term** of the conformation number in Equation (2) for PTV_45 without SIB, PTV_45 with SIB, PTVn_55 and PTVn_57.5 for N patients. The first term concerns the fraction of the target volume that is covered by the reference isodose. Automatic and manual planning is plotted in blue and green, respectively.

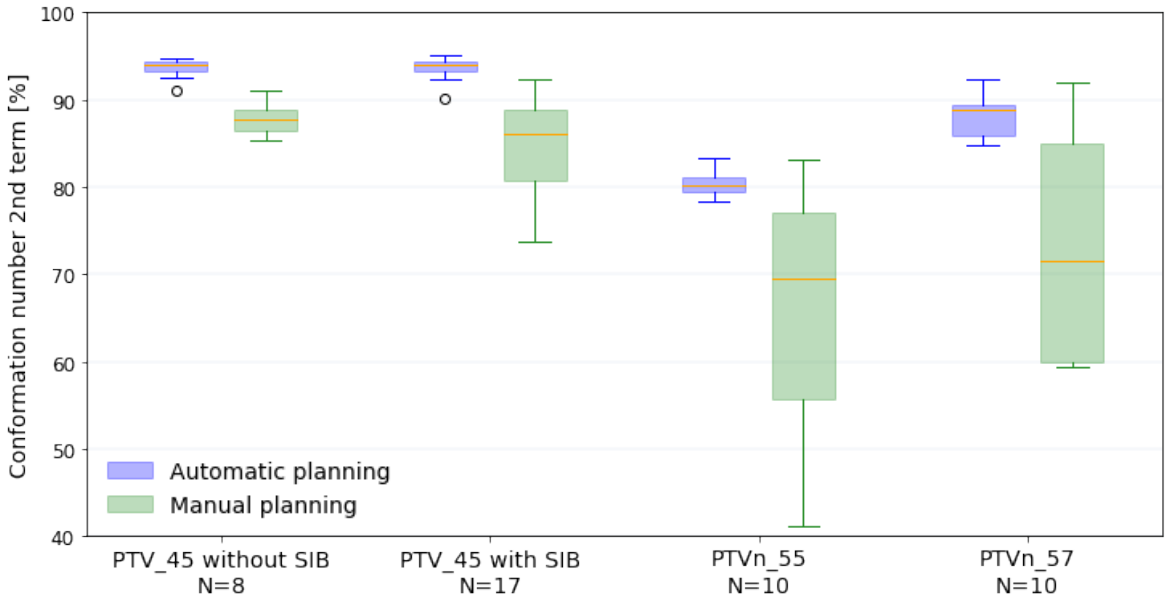

Figure 42: Box plot of the **second term** of the conformation number in Equation (2) for PTV_45 without SIB, PTV_45 with SIB, PTVn_55 and PTVn_57.5 for N patients. The second term concerns the fraction of the reference isodose that covers the target volume. Automatic and manual planning is plotted in blue and green, respectively.

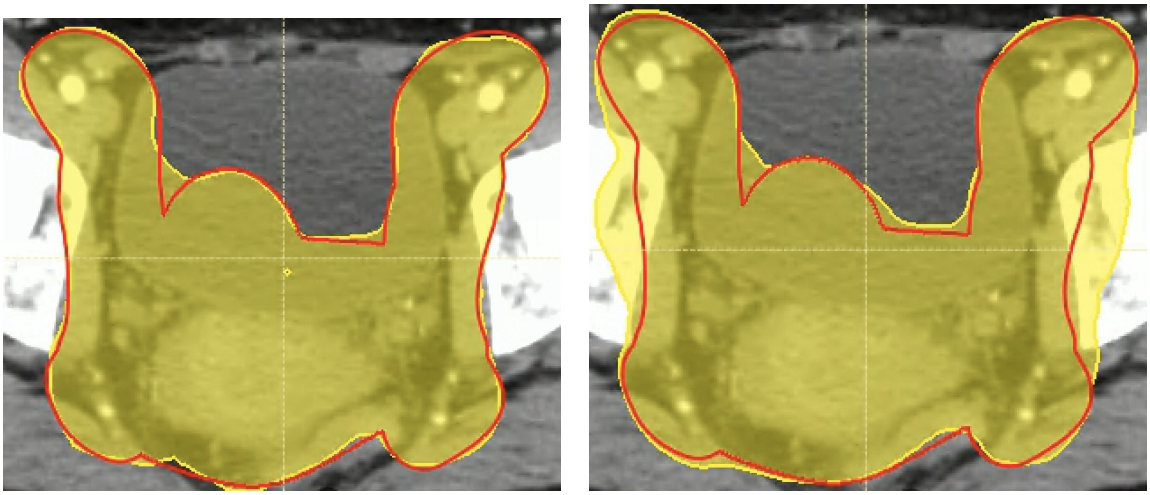

(a) Automatic planning (b) Manual planning

Figure 43: Image of the conformity of PTV_45 in red for patient 7 treated without SIB. The yellow volume represents the 42.75 Gy reference isodose. Automatic planning: $CN = 0.943$, 1st term = 0.994, 2nd term = 0.949. Manual planning: $CN = 0.867$, 1st term = 0.998, 2nd term = 0.869.

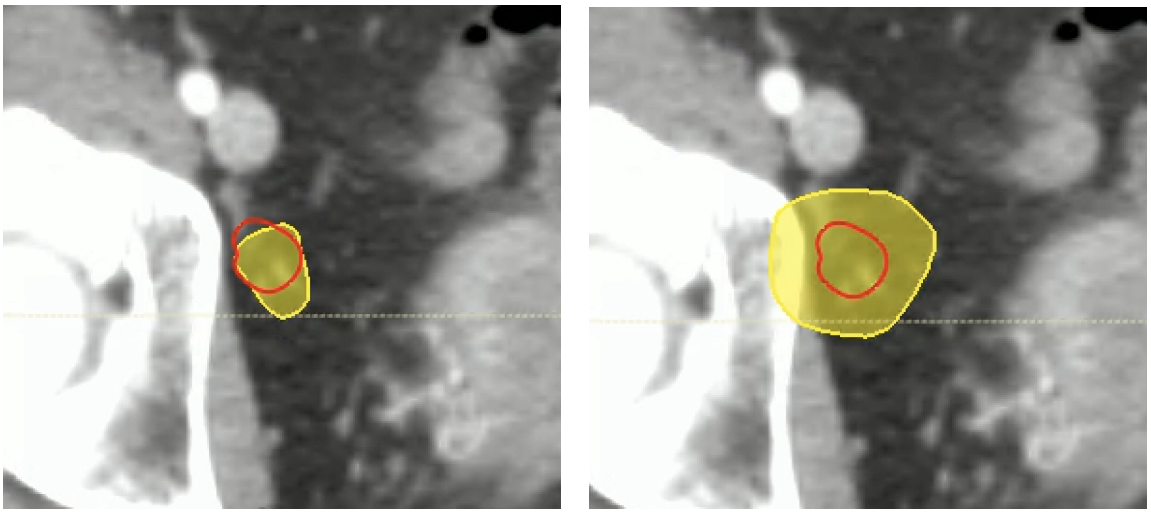

(a) Automatic planning (b) Manual planning

Figure 44: Image of the 49.5 Gy reference isodose in yellow with a positive LN in red with SIB to 55 Gy for patient 21. Automatic planning: $CN = 0.794$, 1st term = 0.988, 2nd term = 0.804. Manual planning: $CN = 0.535$, 1st term = 0.993, 2nd term = 0.539.

Table 13: p-values for the conformation number (CN) and the isolated 1st term (TV_{RI}/TV) and 2nd term (TV_{RI}/V_{RI}) in the CN Equation (2). Statistically significant results (p-value < 0.05) are in bold and labelled with a star.

Volume	***CN*** (fig. 40)	***CN* 1st term** (fig. 41)	***CN* 2nd term** (fig. 42)
PTV_45 without SIB	**0.0009** ⋆	0.5343	**0.0007** ⋆
PTV_45 with SIB	< **10^{-4}** ⋆	0.1284	< **10^{-4}** ⋆
PTVn_55	**0.0072** ⋆	< **10^{-4}** ⋆	**0.0061** ⋆
PTVn_57.5	**0.0040** ⋆	**0.0007** ⋆	**0.0038** ⋆

4.4 QA measurements

Gamma passing rates and maximum gamma for the passing criteria 3% 3mm and 2% 2mm are plotted in Figure 45. From the associated p-values, no difference in gamma passing rate or maximum gamma between automatic and manual VMAT planning were found.

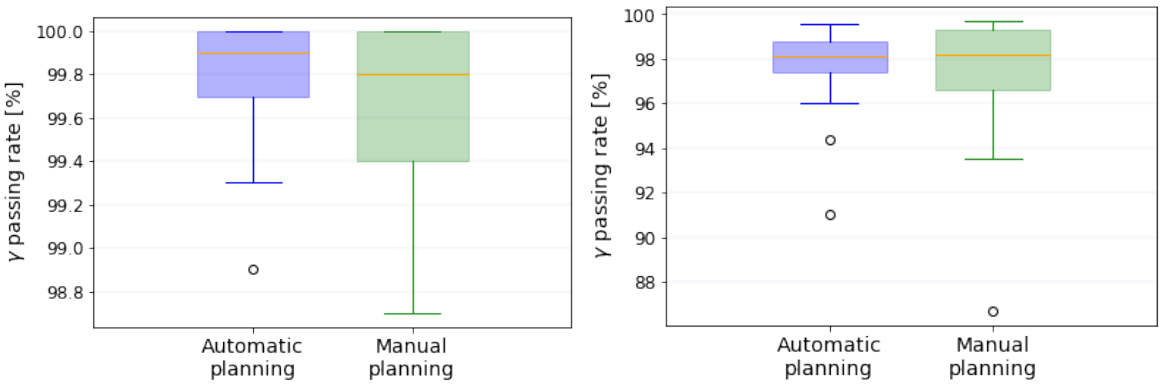

(a) γ passing rate 3% 3mm (p=0.0937)

(b) γ passing rate 2% 2mm (p=0.5305)

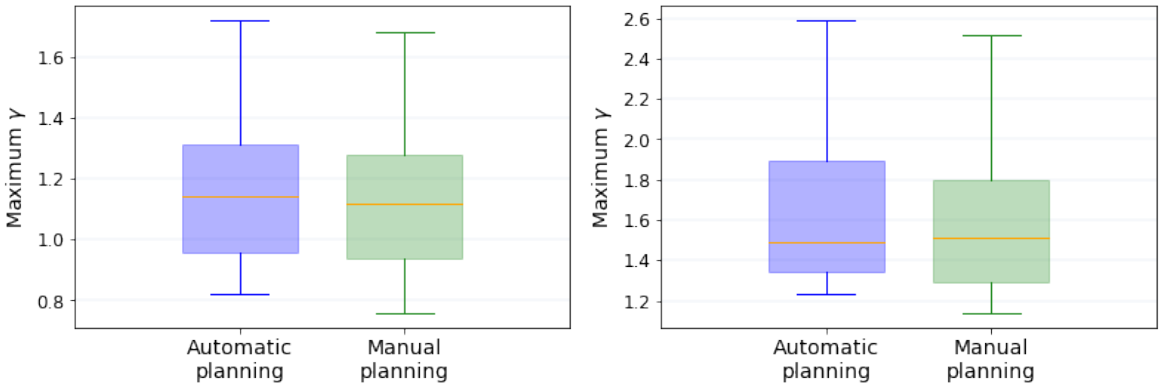

(c) Maximum γ 3% 3mm (p=0.6262)

(d) Maximum γ 2% 2mm (p=0.8296)

Figure 45: γ passing rate and maximum γ for the passing criteria 3% 3mm and 2% 2mm for automatic VMAT planning (blue) and manual VMAT planning (green) with associated p-values, N=25.

4.5 Blind test

Five physicists and three dose planners replied to the blind test. Figure 46 shows which plan the respondents preferred in each of the ten cases. A summary of the reasons behind the choice of plan is provided in Table D.1 in Appendix D.

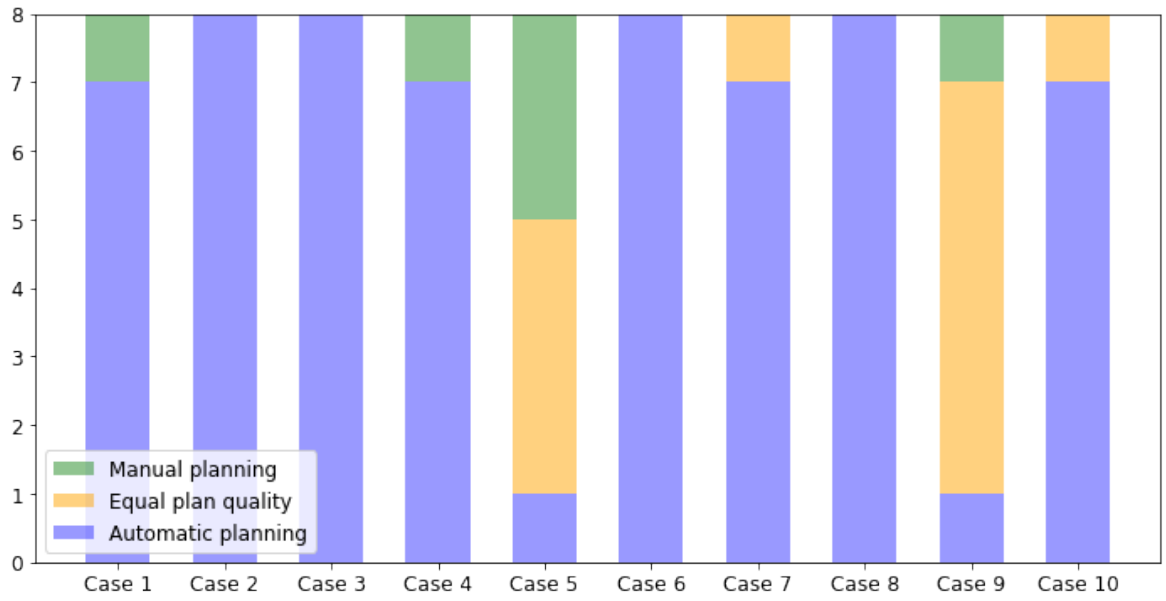

Figure 46: Stacked bar chart of the responses from the ten cases in the blind test. Blue and green represents those who preferred the automatic and manual VMAT plan, respectively. Yellow represents those who judged the automatic and manual VMAT plan quality as equal.

5 Discussion

This study aimed to develop a Python script that automatically made VMAT plans for LACC patients in RayStation. Equivalent automatic VMAT planning procedures are implemented for EBRT of breast and prostate cancer patients at the RT department at St. Olavs Hospital. For implementation in the clinic, the automatic VMAT plans must be of similar or better quality than the manually made VMAT plans that the retrospective patient group was treated with. The automatic VMAT planning script was designed to generate plans with just enough dose to target volumes according to the dose constraints from the Norwegian Directory of Health, and as low dose as possible to OARs. Lower dose to both target volumes and OARs with automatic VMAT than with manual VMAT planning were therefore expected.

The plan quality of the automatic and manual VMAT plans was assessed by evaluating dose statistics, including the conformity index, QA measurements, and a blind test. The main findings in the dose statistics were that automatic VMAT planning gave lower doses to both target volumes and OARs than manual VMAT planning. However, the doses to target volumes were above the minimum dose constraints. These results were expected and in line with the design idea of the automatic VMAT planning script. The automatic VMAT plans had significantly better conformity than the manual VMAT plans, predominantly caused by a lower dose to surrounding healthy tissue. Although the automatic VMAT plans were more complex than the manual VMAT plans, QA measurements showed no decrease in the linac's treatment delivery quality. The results of the blind test indicated that the recipients predominantly preferred the automatic over the manual VMAT plans.

5.1 The automatic VMAT planning script

One automatic VMAT plan was produced by the automatic VMAT planning script in 30-45 minutes, depending on the patient's LN situation. Hence, automatic VMAT planning considerably reduces the average of 6 hours of human planning needed to produce a manual VMAT plan for a LACC patient.

So far, the automatic VMAT planning script has only been tested on 25 clinical patients, and only eight patients without positive LNs. Hence, the script is optimised to work for these 25 cases. Every plan must therefore be carefully reviewed if used in the clinic to ensure that the priorities made by the script are acceptable for the individual

patient. The script's automatic VMAT plans should be considered a starting point of the treatment planning procedure. Even if the automatic VMAT plans are not fully clinically acceptable, the script has still significantly reduced the planning problem. From this starting point, a clinically acceptable plan is obtained with fewer human iterations than a manual VMAT planning approach. This reduction in treatment planning workload will release treatment planner resources from simple cases, providing more resources to improve the plan quality of more challenging cases [11].

In order to have time to test as many versions of the automatic VMAT planning script as possible, the script was mainly tested on one patient at a time. This procedure may have produced a script that was better suited for the two test patients than the whole patient group. For example, patient 19 had a strong relationship between the kidney and bowel doses. Therefore, finding the best compromise between low kidney and bowel doses was highly focused on during the development phase. The focus areas could have been different by choosing different test patients, affecting the design of the final script. However, it is difficult to say if a different focus area would influence the resulting automatic plans positively or negatively.

The dose statistics might have looked different if the manual VMAT plans were designed similarly to the automatic, with just high enough doses to target volumes and as low doses as possible to OARs. Even if all dose constraints are met, the clinic should have a common consensus on where to be in the compromise between high doses to target volumes and low doses for OARs to ensure consistency in the treatment planning. The automatic VMAT planning script makes different decisions, especially concerning target coverage and kidney doses, than the treatment planners in the clinic. Therefore, the clinic should discuss whether these decisions contribute to better patient outcomes or not before implementing the automatic VMAT planning script.

The script could have been developed further to adapt the number of iterations to the complexity of the VMAT plan. The automatic VMAT planning script had a fixed number of iterations, which resulted in equal run-time for patients with similar LN situations. Although two patients have similar LN situations, the positioning of the LNs affect the difficulty in meeting the dose constraints. Adapting the number of iterations to the difficulty in meeting the dose constraints have been done for automatic planning for prostate cancer [56]. This adaption gives fewer iterations to easier plans and more iterations to more difficult plans. Hence, run-time could be reduced for easy plans without negatively affecting the plan quality and increased for more complex

plans to increase plan quality.

The automatic VMAT planning script does not take the patients' medical history into account, which can influence the treatment outcome negatively. For further development of the script, interactive choices for the treatment planner could be added to input data on critical organs that can influence the scripts' input parameters. As an example, Table C.1 in Appendix C shows how the function weight of the kidney max EUD function influences V_{40Gy} and V_{30Gy} to the bowel for patient 19. If the patient has unhealthy kidneys, the importance of low mean kidney doses increases. If the treatment planner inputs that the kidneys are unhealthy, the script puts additional function weight (i. e. 10) to the kidney max EUD optimisation function to achieve an automatic VMAT plan with lower kidney doses with the cost of higher bowel V_{40Gy} and V_{30Gy}. Similar interventions could be done to other vulnerable OARs.

Treatment planner mimicking is not the only route to automatic VMAT planning. Other automatic VMAT planning methods, both other classical automatic planning solutions and modern AI solutions, have been presented in other studies [6–9, 12–14]. The Erasmus iCycle is an example of an *a priori* MCO solution to automatic planning developed in-house at the Erasmus MC cancer institute [57]. Erasmus iCycle was clinically implemented for IMRT planning for cervical cancer patients at the institute already in 2012 where it proved to reduce mean dose to OARs, especially to the bowel and sigmoideum. A similar approach was later developed for VMAT, which introduced a compromise between high plan quality with 20-beam IMRT and short treatment time with VMAT [58]. In a fully automated VMAT plan-of-the-day solution for cervical cancer patients, Erasmus iCycle was used as a pre-optimiser, and the resulting plans showed superior plan quality compared to manually made VMAT plans [5]. Knowledge-based planning solutions that require a library of treatment plans have produced treatment plans in a very short time, i.e. 1 minute for a BT treatment plan, which provides the opportunity to produce the treatment plan while the patient is at the treatment table [59]. One challenge with methods that require a library is that the quality of the output treatment plans depends on the quality of the treatment plans in the library. Ensuring high plan quality in the database is complicated as it involves discriminating the plan quality into whether it is good or bad. Another challenge with library-based methods is that the library has to be diverse to make good plans for special cases [11]. Collecting a large and diverse inter-institutional plan library is challenging due to privacy issues. Even though the treatment planner mimicking solution developed for LACC patients in this thesis may be the best available

option at St. Olavs Hospital today, other modern automatic planning solutions may be better suited for future planning problems.

5.2 Dose statistics

5.2.1 Target volumes

As expected from the design of the VMAT planning script, the dose received by target volumes is generally lower with automatic VMAT planning than with manual VMAT planning. This can be seen from the mean cumulative DVH curves in Figures 19 and 20 where the blue automatic planning curves mainly lie below the green manual planning curves. Ideally, as illustrated in Figure 5, the DVH curves for PTV_45 and CTV_45 should have a steep fall-off at 45 Gy. The DVH curves from manual VMAT planning are closer to this ideal than the automatic. This means more significant dose deviations inside the target volume for the automatic VMAT plans than for the manual. The shaded areas representing the first standard deviation in the DVH curves are narrower for automatic than manual VMAT planning. The standard deviation provides information on the plan consistency, and the results indicate that the automatic VMAT plans are more consistent than the manual.

$V_{95\%}$ and D_{98} are dose-volume parameters that also describe the shape of the DVH curve. Figure 21 shows that $V_{95\%}$ for PTV_45 for the patients without SIB tends to be lower with automatic than with manual VMAT planning. For the patients treated with SIB, $V_{95\%}$ is significantly lower with automatic VMAT planning (Table 10: $p<0.05$). Similar trends are seen from Figures 19a and 19b, where the fall-off begins at lower dose for automatic than for manual VMAT planning. However, too high $V_{95\%}$ has the expense of higher OAR doses. Therefore, when looking at $V_{95\%}$ and the soft dose constraint $V_{95\%} = 95\%$, automatic VMAT planning is preferred over manual because it gives room for lower OAR doses although it potentially kills fewer cancer cells. According to the dose-volume constraint, $V_{95\%}$ could be closer to 95% to give more room for low OAR doses. This was not done in this study due to traditions at St. Olavs to keep $V_{95\%}$ for PTV_45 above 98%.

D_{98} for PTVn and CTVn in Figures 22 and 23 shows that automatic VMAT planning gives significantly lower D_{98} than manual planning (Table 10: $p<0.05$). However, it fulfils the hard dose constraint $D_{98} > 100\%$ of prescribed dose. The narrow boxes just above the acceptance criteria confirms the design of the VMAT planning script to give just enough dose to target volumes, leaving room for low OAR doses. The plots also

show that the desired heterogeneous dose distribution with a central and peripheral dose of more than 100% and 90% of the prescribed dose, respectively, is obtained with both manual and automatic VMAT planning.

D_{max} to PTV_45 and the PTVns are shown in Figure 24. The hard dose constraint $D_{max} < 107\%$ avoid high hot-spots inside the target volumes. D_{max} for PTV_45 without SIB, PTVn_55 and PTVn_57.5 is generally below the maximum dose constraint for both automatic and manual VMAT planning. For xPTV_45 with SIB, D_{max} from manual VMAT planning is significantly higher, and above the maximum dose constraint, than from automatic VMAT planning (Table 10: $p<0.05$). xPTV_45 is the PTV_45 volume that excludes the PTVns. The high D_{max} to xPTV_45 with manual planning is due to low conformity. This low conformity is caused by spilled dose to healthy tissue that surrounds PTVn, which will be discussed in Section 5.3.

D_{50} for PTVn and CTVn is shown in Figure 25. The results imply that the soft dose constraint $D_{50} > 102\%$ is easier to accomplish for the CTVns than the PTVns. This is obvious as the heterogeneous dose distribution causes higher dose in the hottest 50% of the CTVn volume than the hottest 50% of PTVn volume as PTVn is a larger volume that encloses CTVn. PTVn does not meet the dose constraint to D_{50}. This indicates that the high-dose volume in the centre of PTVn is too small. Figure 47 illustrates a dose distribution of PTVn that meets the D_{50} soft dose constraint (left) and a dose distribution more similar to the dose statistics (right). The central and peripheral doses are similar, but the central high dose volume in the dose distribution that meets the soft dose constraint is larger. The optimisation functions that work to obtain high doses in PTVn and CTVn are min dose functions and uniform dose functions. Due to the desired heterogeneous dose distribution in the lymph nodes, uniform dose optimisation functions might not be suitable. Min DVH functions are more similar to the quantities used to state the soft dose constraint for D_{50}. Applying min DVH optimisation functions instead of uniform dose optimisation functions is recommended to be tested in further work to increase D_{50} to PTVn.

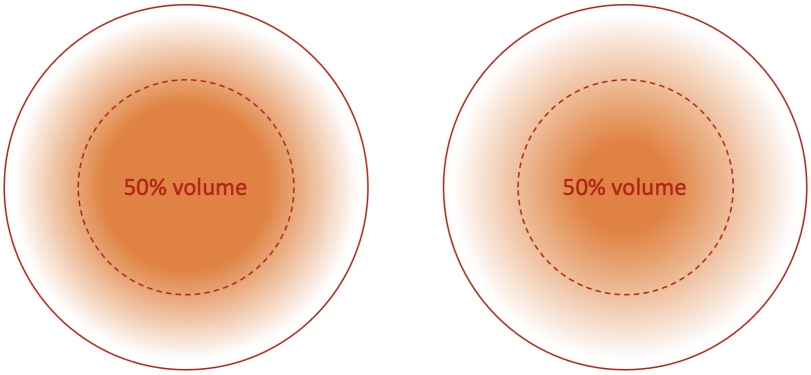

Figure 47: Illustration of a dose distribution that meets the D_{50} soft dose constraint to PTVn (left) and one dose distribution with too low D_{50} (right). The orange colour intensity represents the dose intensity. The dose distributions have similar central and peripheral dose, but different dose gradients. Volume fractions are not to scale.

D_{max} to xCTVp for patients treated without and with SIB is shown in Figure 26. The results show that both automatic and manual VMAT planning struggle to meet the soft dose constraint D_{max} < 103% (46.4 Gy). For patients treated without SIB, D_{max} to xCTVp were significantly higher with automatic than with manual VMAT planning (Table 10: p<0.05). According to the Norwegian Directory of Health, this soft dose constraint is made to prevent hot spots in OARs that receive additional dose from the BT boost [4]. Low D_{max} in OARs is of high priority in the automatic VMAT planning script and will be discussed in the next sections. Due to high priority if low dosen in the OARs, meeting the soft dose constraint to xCTVp has not been in focus during the development of the automatic VMAT planning script. Figures B.1 and B.2 in Appendix Section B show that the min dose function to xCTVp is far down the list of optimisation functions and has a low function value. For further work, the automatic VMAT planning script could increase the function weight of this optimisation function in the second phase to possibly get closer to the soft dose constraint.

5.2.2 Organs at risk

As expected from the design of the automatic VMAT planning script, the mean cumulative DVH curves in Figures 27 to 29 indicate that OAR doses are lower for automatic than with manual VMAT planning. The mean DVH curves and the first standard deviations for automatic VMAT planning overlaps or lies below the green manual VMAT planning curve for all OARs at all dose levels.

OAR dose statistics without SIB

For OARs with more serial than parallel arrangements, such as the rectum, bladder, sigmoideum and bowel, low D_{max} is essential for keeping the organ function. Figure 30 shows that both automatic and manual VMAT planning gives maximum doses lower than the hard dose constraint. Due to lower dose to target volumes in the automatic than manual VMAT plans without SIB, lower OAR doses were expected in the automatic VMAT plans. The results contradict this expectation and might suggest that manual planning gives lower D_{max}. This result is statistically significant for the bladder (Table 11: $p<0.05$) and fairly evident for the rectum (Table 11: $p=0.0596$). No significant differences were observed for sigmoideum and bowel.

The dose-effect relationship for late side effects of the bladder has been analysed as part of the EMBRACE studies [60]. The study observed an increased probability of urinary side effects with an increased dose to the hottest 0.1 cm^3 of the bladder. This trend should also apply for the hottest 0.03 cm^3 used to describe D_{max} in this thesis. From the results, manual VMAT planning gives lower D_{max} to the bladder for patients treated without SIB compared to automatic VMAT planning. However, the dose reduction is minor compared to the total bladder dose after BT. Hence, the dose reduction is not of high clinical relevance.

The dose-volume effect relationship for rectal morbidity has also been examined as part of the EMBRACE study [61]. The study showed that the dose to the hottest 2 cm^3 of the rectum volume was strongly related to the probability of grade 2-4 rectal morbidity. Dose to the hottest 2 cm^3 was not investigated in this thesis. However, the study showed a linear relationship between the dose to the hottest 2 cm^3 and the hottest 0.1 cm^3, which is closer to the D_{max} definition used in this thesis. According to the study, the reduced rectum D_{max} with manual VMAT planning does reduce the probability for rectal morbidity. However, the dose difference between automatic and manual VMAT planning is minor and not statistically significant. Hence, the dose reduction with manual VMAT planning has little clinical relevance.

The mean cumulative DVH curves in Figure 27 show that lower OAR doses for automatic than manual VMAT planning are found at larger volume fractions than the hottest 0.03 cm^3 that accounts for D_{max}. Figure 38 shows that the volume fractions of the rectum, bladder and bowel that receive maximum 40 Gy and 30 Gy are significantly lower for automatic than manual VMAT planning (Table 11: $p<0.05$, except for V_{40Gy} to rectum). Keeping the maximum doses or the average doses low is always a

compromise. The results for EBRT without SIB imply that automatic VMAT planning focuses slightly more on low average doses at the cost of slightly higher maximum doses than manual VMAT planning. As the OARs in Figure 27 are not solely structured in serial or parallel, both low maximum and mean doses are essential. Hence, focusing on lower mean doses when the D_{max} constraints are met is reasonable for these organs.

Maximum dose to the body volume is below the hard dose constraint for both automatic and manual VMAT planning, as seen from Figure 37. The results imply that automatic VMAT planning gives lower D_{max} to the healthy tissue in the body volume than manual VMAT planning, but the result is not statistically significant (Table 11: p=0.0847).

Maximum dose to the femoral heads are shown in Figure 35 and show that D_{max} to both the left and the right femoral head are below the hard dose constraint for both automatic and manual VMAT planning. The plot implies that automatic VMAT planning gives lower D_{max} to the femoral heads than manual VMAT planning, but the results are not statistically significant (Table 11: p=0.0771 and p=0.1733).

OAR dose statistics with SIB

Similarly as without SIB, lower OAR doses in the automatic VMAT plans for EBRT with SIB were expected due to lower dose to target volumes. The results from Figure 31 show little difference between automatic and manual VMAT planning in D_{max} to rectum, bladder, sigmoideum and bowel. Only D_{max} to the bladder for the patients with SIB was significantly lower for automatic than manual VMAT planning (Table 12: p<0.05). The clinical effect of lower D_{max} to bladder was discussed for patients treated without SIB. D_{max} is generally below the hard dose constraint for rectum, bladder and sigmoideum for both automatic and manual VMAT planning, but more frequently below for the bowel with automatic VMAT planning.

The results indicate that it is more challenging to attain the D_{max} hard dose constraint for the bowel with SIB to 57.5 Gy than with SIB to 55 Gy. The main explanation is that the bowel extends upwards in the abdomen near PTVn_57.5. Figure 33, which shows D_{max} for the xOARs (OAR excluding PTV_n + 15 mm), shows that all patients treated with SIB and automatic VMAT planning receive D_{max} below 47.3 Gy. This indicates that the hot-spots inside the bowel for automatic VMAT planning are near PTVn. The high D_{max} to the bowel above the hard dose constraint in Figures 31 and 32 therefore relates to the dose fall-off region between PTVn and the bowel. Similar observations are made for the sigmoideum and the bladder. For manual VMAT planning, the bowel

hot-spots are located further than 15 mm away from PTVn as D_{max} is generally above the hard dose constraint for xBowel in Figure 33. Such hot-spots further away from PTVn is less tolerable than hot-spots near PTVn with a prescribed high dose.

Figure 33 also shows that automatic VMAT planning always (except from one outlier) attains the D_{max} hard dose constraint to the xOARs, while manual VMAT planning does not. Table 11 shows that D_{max} to the sigmoideum and the bowel are significantly lower with automatic than with manual VMAT planning. The new dose-volume constraints from the Norwegian Directory of Health includes additional hard dose constraints to these exact xOAR volumes. Because these new guidelines were not implemented in the clinic when the manual VMAT plans were made, lower D_{max} to the xOARs with automatic VMAT planning was expected. This is because the VMAT planning script prioritises low D_{max} to these exact xOAR volumes with adaptive max dose optimisation functions. Similar observations, that automatic VMAT planning has the potential to significantly reduce dose to the bowel were also found in the validation of the Erasmus iCycle for cervical cancer patients [5].

The mean cumulative DVH curves for OARs and xOARs in Figures 28 and 29 indicate that most volume fractions receive a lower or similar dose with automatic than with manual VMAT planning. The rectum, bladder and bowel volume that receive minimum 30 Gy, V_{30Gy}, and 40 Gy, V_{40Gy}, are shown in Figure 39. From the results, V_{30Gy} in Figures 39b, 39d and 39f are significantly lower with automatic than manual VMAT planning for both rectum, bladder and bowel (Table 12: $p<0.05$). V_{40Gy} in Figure 39e is also significantly lower with automatic than manual VMAT planning for the bowel (Table 12: $p<0.05$). For rectum and bladder, V_{40Gy} are more similar between automatic and manual VMAT planning. Hence, lower V_{30Gy} and V_{40Gy}, which are dose-volume parameters related to the mean dose, are obtained for automatic planning without considerable negative effects on the maximum doses in Figures 31 to 33. This indicates high overall plan quality with automatic VMAT planning as the mean and maximum doses often are compromises of each other.

The maximum dose, D_{max}, to the spinal cord is shown in Figure 34. No statistically significant differences between automatic and manual VMAT planning were observed, but both are below the hard dose constraint. Keeping D_{max} to the spinal cord low is essential as it is a critical organ arranged in an especially serial structure [21]. From the result, nearly half of the patients received higher D_{max} with manual VMAT planning than any patient with automatic VMAT planning. This implies a higher risk of spinal

cord damage with manual VMAT planning. However, only seven patients had the spinal cord delineated in this study. Therefore, the automatic VMAT planning script needs further testing to provide confident statistics on the spinal cord.

The maximum doses, D_{max}, to the femoral heads are shown in Figure 35 and shows that D_{max} to both the left and right femoral head are below the hard dose constraint for both automatic and manual VMAT planning. The results show that D_{max} with automatic VMAT planning is significantly lower than with manual planning for both the left and right femoral head (Table 12: $p<0.05$). In a study of 650 long-term gynecologic cancer survivors, one of three patients reported hip pain after RT, which was four times more than the control group [62]. The median D_{max} was 45.3 ± 7.1 for those who reported hip pain and 44.5 ± 5.6 for those without hip pain. Hence, the manual VMAT plans give a higher risk of hip pain after RT than the automatic VMAT plans.

Both automatic and manual VMAT planning gives kidney doses below the hard- and soft dose constraints, but very low kidney doses compromise low doses to the body and bowel. The mean doses, D_{mean}, to the left and right kidneys are shown in Figure 36. D_{mean} to the right kidney is significantly lower with manual than with automatic VMAT planning (Table 12: $p<0.05$). For the left kidney, the median doses are 5.1 Gy and 3.9 Gy for automatic and manual VMAT planning, respectively, which implies that lower doses are obtained with manual VMAT planning also for the left kidney. However, this result is not statistically significant. Figure 37 shows that the maximum dose, D_{max}, to xBody is significantly higher with manual than with automatic VMAT planning (Table 12: $p<0.05$). When aiming for low kidney doses, some manual VMAT plans have dose accumulations in the body between the two kidneys, as seen in the dose distributions for patients 1 and 12 in Figures C.1 and C.2 in Appendix C. The dose fall-off from this accumulation stretches into the bowel, which explains the higher V_{40Gy} (white isodose) and V_{30Gy} (dark green isodose) to the bowel in the manual VMAT plans. Such dose accumulations are avoided in the automatic VMAT plans by allowing slightly higher kidney doses.

St. Olavs Hospital has a tradition to keep the mean kidney dose below 5 Gy, which explains the low kidney doses in the manual VMAT plans. The dose statistics implies that the low kidney doses have had a high cost to the bowel and body. The side effects of EBRT of cervical cancer are more often related to the intestines and bowel than to the kidneys (Oncologist M. Eide, personal communication, February 15, 2022). Allowing slightly higher kidney doses to spare the bowel is therefore a suggestion for

future patients.

5.3 Conformity index

The conformity index, defined by the *CN*, for PTV_45, PTVn_55 and PTVn_57.5 with automatic and manual VMAT planning are shown in Figure 40. The figure shows that the automatic VMAT plans have significantly higher conformity index than the manual VMAT plans (Table 13: $p<0.05$), meaning that the dose distribution is better confined to the target volumes. Figures 41 and 42 show the contribution from the first and second term of the *CN* Equation (2), respectively. The figures show that a larger fraction of the target volume is covered by the reference isodose with manual VMAT planning (Figure 41), i.e. better dose coverage in the target volumes, but that a larger fraction of the reference isodose is distributed inside the target volume with automatic VMAT planning (Figure 42), i.e. less dose leakage to healthy tissue surrounding the target volumes.

Figure 44 shows the 49.5 Gy isodose around PTVn_55 in patient 21. The images illustrate the two terms of the *CN* equation and examplifies how the reference isodose better covers PTVn_55 with manual VMAT planning. However, manual VMAT planning irradiates more healthy tissue surrounding PTVn_55 than automatic VMAT planning. The contribution to the *CN* from irradiating healthy tissue with manual VMAT planning is greater than the contribution from not covering the target volume with automatic VMAT planning. Therefore, manual VMAT planning obtains a low conformity index compared to automatic. Similar observations are seen in Figure 43 for PTV_45.

Numerous alternative conformity indexes exist to assess plan quality. One example is the COIN index which is similar to the *CN* used in this thesis, but also includes contributions from the reference isodose enclosed by each individual OAR [39, 63]. By also including OARs, the COIN index would better represent a quality measure of the whole treatment plan. The target volumes and OARs in this thesis considers different dose levels, indicating that the standard COIN index is not suitable. The standard COIN index could have been modified with different reference isodoses to different OARs, but this was not done in this thesis.

Essential information not related to geometric parameters is removed when reducing the measure of plan quality down to one index [39]. Qualitative aspects such as tissue

characterisation, tumour cell radiation sensitivity, and fractionation effects are not considered. This weakness reduces the clinical relevance of the conformity index and is why one number can not yet determine the plan quality.

5.4 QA measurements

Figure 18 shows that automatic VMAT planning has a significantly higher total number of MUs than manual VMAT planning (p<0.05). This was expected as the automatic VMAT plans had significantly higher conformity than the manual plans. High conformity is associated with narrow radiation fields, which require a larger number of MUs per unit of delivered dose to the patient. The larger number of MUs indicates higher plan complexity which could compromise the quality of treatment delivery. It could therefore be expected that the automatic VMAT plans would have lower γ passing rates and higher maximum γ than the manual VMAT plans when comparing the calculated and measured dose distributions. However, Figure 45 shows no difference between automatic and manual VMAT planning in neither γ passing rates nor maximum γ for both 3% 3mm and 2% 2mm. Hence, the automatic VMAT planning script produces automatic VMAT plans with higher complexity than manual VMAT plans without affecting the quality of treatment delivery.

5.5 Blind test

The blind test was responded to by five physicists and three treatment planners, which provides a reasonable basis for judging the difference in plan quality between the automatic and manual VMAT plans. Unfortunately, no physicians responded. Further work should ensure that the physicians' opinion agrees with the treatment planners' and physicists' opinions.

The results from the blind test in Figure 46 show that the majority of the recipients preferred automatic VMAT plans over the manual or judged them as equal in all ten cases. In eight cases, the automatic VMAT plans were distinctly preferred over the manual VMAT plans. In the two remaining cases, cases 5 and 9, four and six recipients, respectively, judged the plan quality equal. Cases 5 and 9 were included in the three cases (cases 4, 5, and 9) where the automatic VMAT plans were anticipated to score worst against the manual VMAT plans.

From the summary of reasons behind the choice of plan in Table D.1 in Appendix D,

it comes out clearly that better conformity and lower doses to OARs are the main strengths of the automatic VMAT plans compared to the manual. One disadvantage that was mentioned with the automatic VMAT plans was low target coverage. The target coverage is above the dose constraints for both automatic and manual VMAT planning but much closer to the acceptance limit with automatic VMAT planning. Lower but high enough, target coverage was part of the design idea of the planning script and was therefore expected. The benefits of the manual VMAT plans were lower kidney doses and better target coverage, which was also expected from the dose statistics.

5.6 Further work

This section includes a summary of further work already proposed during the discussion, in addition to new proposals.

First, it should be decided whether the script should be implemented in the clinic or not. If implemented, new automatic VMAT plans should be evaluated by a physician, both for plan validation and for identifying possible improvements of the script. Possible improvement areas of the script that are already identified and discussed are listed below.

- Increase D_{50} to PTVn by replacing the uniform dose optimisation functions with min DVH optimisation functions to PTVn.

- Reduce D_{max} to xCTVp by increasing the function weight of the max dose optimisation function to xCTVp.

- Adapt the number of iterations to the treatment plan complexity, i.e. from the total value of the objective function.

- Add interactive plan choices for the treatment planner to provide patient information to the script that affect the priority of different optimisation functions.

Adjusting the function weight of the max DVH optimisation functions based on the function value to reduce OAR doses in the first phase could be changed. The function value will be smaller for simple plans and higher for more challenging plans. Consequently, if the max DVH function weight is adapted based on a fixed function value,

as in the automatic VMAT planning script, less work will be put into decreasing OAR doses in simple plans with lower function value. This might be the reason why D_{max} to the OARs for the patients treated without SIB, which can be considered simple cases, tended to be higher with automatic than with manual VMAT planning. To avoid this, a suggestion for further development of the script is to replace the fixed function value with a fixed fraction of the total function value. For example, instead of increasing the function weight of max DVH to xBowel if the function value is less than i. e. 0.02, the function weight could be increased if the max DVH function value is less than 0.001% of the total value of the objective function.

The automatic VMAT planning script could also be tested for creating plans with different margins and different uterus positions. The positioning of the uterus and cervix has not been discussed in this thesis, but may change from day to day and hour to hour due to changes in bladder filling and bowel size. Oslo University Hospital has initiated a study investigating the effect of acute gastrointestinal toxicity by using the plan-of-the-day instead of one single treatment plan with large safety-margins covering all possible uterus positions [64]. The plan-of-the-day is a treatment plan with small margins adapted for the uterus position at the treatment time. This method includes creating multiple treatment plans, each accounting for a different uterus position, and the appropriate plan that matches the uterus position at the treatment time is used as the plan-of-the-day in each treatment session. Creating many VMAT plans with different uterus positions manually require extensive treatment planner resources. For this purpose, automatic VMAT planning would be favourable. To assist in the plan-of-the-day-study, the automatic VMAT planning script could be tested and further developed to produce automatic VMAT plans for multiple uterus positions.

6 Conclusion

A script for automatic volumetric modulated arc therapy (VMAT) planning in RayStation was developed for external irradiation of locally advanced cervical cancer (LACC) to improve clinical planning efficiency. The script aimed to deliver just enough dose to target volumes according to new dose-volume constraints from the Norwegian directorate of health published in June 2021 and as low dose as possible to organs at risk (OARs). The automatic VMAT planning script was tested on 25 retrospectively treated LACC patients, and the automatic VMAT plans were compared to the manually made VMAT plans used for treatment. From the dose statistics, the automatic VMAT plans followed the script design with lower but high enough doses to target volumes and generally lower OAR doses than the manual VMAT plans. The automatic plans scored significantly better on conformity than the manual VMAT plans. QA measurements showed that the higher complexity of the automatic compared to the manual VMAT plans did not negatively affect the delivering quality by the linear accelerator. A blind test performed by physicists and dose planners in the clinic showed that the automatic VMAT plans were predominantly preferred over the manual VMAT plans mainly due to better conformity and lower OAR doses. Hence, implementing the automatic VMAT script for treatment planning of LACC patients in the clinic would reduce the planning time without reducing the plan quality.

References

[1] W. Small et al. Cervical cancer: A global health crisis. *Cancer*, 123(13):2404–2412, 2017.

[2] G. Engholm et al. Nordcan: Cancer incidence, mortality, prevalence and survival in the nordic countries, version 8.2 (26.03.2019), 2016.

[3] K. Tanderup et al. Effect of tumor dose, volume and overall treatment time on local control after radiochemotherapy including MRI guided brachytherapy of locally advanced cervical cancer. *Radiotherapy and Oncology*, 120(3):441–446, 2016.

[4] The Norwegian Directorate of Health. Nasjonalt handlingsprogram med retningslinjer for gynekologisk kreft. `https://www.helsedirektoratet.no/retningslinjer/gynekologisk-kreft-handlingsprogram`, June 2021. [Online; accessed January, 2022].

[5] A. W. M. Sharfo et al. Validation of fully automated VMAT plan generation for library-based plan-of-the-day cervical cancer radiotherapy. *PloS one*, 11(12):e0169202–e0169202, 2016.

[6] P. A. Wheeler et al. Evaluating the application of pareto navigation guided automated radiotherapy treatment planning to prostate cancer. *Radiotherapy and oncology*, 141:220–226, 2019.

[7] Z. Ouyang et al. Evaluation of automated treatment planning and organ dose prediction for lung stereotactic body radiotherapy. *Curēus (Palo Alto, CA)*, 13(10):e18473–e18473, 2021.

[8] R. Bijman, A. W. Sharfo, L. Rossi, S. Breedveld, and B. Heijmen. Pre-clinical validation of a novel system for fully-automated treatment planning. *Radiotherapy and oncology*, 158:253–261, 2021.

[9] E. Y. Han et al. Clinical implementation of automated treatment planning for whole-brain radiotherapy. *Journal of applied clinical medical physics*, 22(9):94–102, 2021.

[10] M Hussein, B Heijmen, D Verellen, and A Nisbet. Automation in intensity modulated radiotherapy treatment planning-a review of recent innovations. *British journal of radiology*, 91(1092):20180270–20180270, 2018.

[11] Y. Fu et al. Artificial intelligence in radiation therapy. *IEEE Transactions on Radiation and Plasma Medical Sciences*, 6(2):158–181, 2022.

[12] X. Chen, K. Men, Y. Li, J. Yi, and J. Dai. A feasibility study on an automated method to generate patient-specific dose distributions for radiotherapy using deep learning. *Medical physics (Lancaster)*, 46(1):56–64, 2019.

[13] J. Fan, J. Wang, Z. Chen, C. Hu, Z. Zhang, and W. Hu. Automatic treatment planning based on three-dimensional dose distribution predicted from deep learning technique. *Medical physics (Lancaster)*, 46(1):370–381, 2019.

[14] A. M. Barragán-Montero et al. Three-dimensional dose prediction for lung IMRT patients with deep neural networks: robust learning from heterogeneous beam configurations. *Medical physics (Lancaster)*, 46(8):3679–3691, 2019.

[15] R. Pötter et al. The EMBRACE II study: The outcome and prospect of two decades of evolution within the GEC-ESTRO GYN working group and the EMBRACE studies. *Clinical and Translational Radiation Oncology*, 9:48–60, 2018.

[16] I. S. Hoem. Project thesis: Automatic VMAT planning in raystation for locally advanced cervical cancer, 2021.

[17] D. B. Richardson. Occupational health risks in nuclear power. In Cutler J. Cleveland, editor, *Encyclopedia of Energy*, pages 489–496. Elsevier, New York, 2004.

[18] E. B. Podgorsak. *Radiation Physics for Medical Physicists*. Graduate Texts in Physics. Springer International Publishing : Imprint: Springer, Cham, 3rd ed. 2016. edition, 2016.

[19] P. L. Olive. The role of DNA single- and double-strand breaks in cell killing by ionizing radiation. *Radiation Research*, 150(5):S42–S51, 1998.

[20] Stephen Joseph McMahon. The linear quadratic model: usage, interpretation and challenges. *Physics in medicine biology*, 64(1):01TR01–01TR01, 2018.

[21] A. Niemierko and M. Goitein. Calculation of normal tissue complication probability and dose-volume histogram reduction schemes for tissues with a critical element architecture. *Radiotherapy and oncology*, 20(3):166–176, 1991.

[22] M. Feng, G. Valdes, N. Dixit, and T. D. Solberg. Machine learning in radiation oncology: Opportunities, requirements, and needs. *Frontiers in oncology*, 8:110–110, 2018.

[23] S. Mallick, G. K. Rath, and R. Benson. *Practical Radiation Oncology*. Springer Singapore : Imprint: Springer, Singapore, 1st ed. 2020. edition, 2020.

[24] *Absorbed Dose Determination in External Beam Radiotherapy*. Number 398 in Technical Reports Series. INTERNATIONAL ATOMIC ENERGY AGENCY, Vienna, 2001.

[25] K. L. Moore. Automated radiotherapy treatment planning. *Seminars in Radiation Oncology*, 29(3):209–218, 2019. Adaptive Radiotherapy and Automation.

[26] Statens strålevern. Volum og doser i ekstern stråleterapi. `https://docplayer.me/15768007-Stralevernrapport-2012-9-volum-og-doser-i-ekstern-straleterapi-definisjoner-og-anbefalinger.html`, 2012. [Online; accessed January, 2022].

[27] M. R. Young and J. B. Yu. Chapter 45 - intensity modulated radiotherapy and image guidance. In Jack H. Mydlo and Ciril J. Godec, editors, *Prostate Cancer (Second Edition)*, pages 413–426. Academic Press, San Diego, second edition edition, 2016.

[28] D. Craft, P. Süss, and T. Bortfeld. The tradeoff between treatment plan quality and required number of monitor units in intensity-modulated radiotherapy. *International Journal of Radiation Oncology, Biology, Physics*, 67(5):1596–1605, 2007.

[29] T. Santos, T. Ventura, and M. C. Lopes. Evaluation of the complexity of treatment plans from a national IMRT/VMAT audit – towards a plan complexity score. *Physica medica*, 70:75–84, 2020.

[30] RaySearch Laboratories. *RayStation 11A software*. Stockholm, Sweden, May 2021. Version 11A SP1.

[31] RaySearch Laboratories. *RAYSTATION 9B, A guide to optimization in RayStation*. Stockholm, Sweden, 2019.

[32] A. Niemierko. Reporting and analyzing dose distributions: A concept of equivalent uniform dose. *Medical physics (Lancaster)*, 24(1):103–110, 1997.

[33] RaySearch Laboratories. *MULTI-CRITERIA OPTIMIZATION IN RAYSTATION*. Stockholm, Sweden, 2020.

[34] K. Fjellanger et al. PD-0748 iCycle-Eclipse: a novel approach to automated multicriterial treatment planning. *Radiotherapy and oncology*, 161:S577–S579, 2021.

[35] P. Voet, S. Breedveld, M. Dirkx, P. Levendag, and B. Heijmen. Integrated multicriterial optimization of beam angles and intensity profiles for coplanar and noncoplanar head and neck IMRT and implications for VMAT. *Medical physics (Lancaster)*, 39(8):4858–4865, 2012.

[36] D. F. Williamson, R. A. Parker, and J. S. Kendrick. The box plot: A simple visual method to interpret data. *Annals of internal medicine*, 110(11):916–921, 1989.

[37] T Dahiru. P - value, a true test of statistical significance? a cautionary note. *Annals of Ibadan postgraduate medicine*, 6(1):21–26, 2008.

[38] C. H. Goulden. *Methods of statistical analysis*. New York, second edition. edition, 1952.

[39] L. Feuvret, G. Noël, J. J. Mazeron, and P. Bey. Conformity index: A review. *International Journal of Radiation Oncology, Biology, Physics*, 64(2):333–342, 2006.

[40] A. Riet et al. A conformation number to quantify the degree of conformality in brachytherapy and external beam irradiation: Application to the prostate. *International Journal of Radiation Oncology, Biology, Physics*, 37(3):731–736, 1997.

[41] G. A. Ezzell et al. Guidance document on delivery, treatment planning, and clinical implementation of IMRT: Report of the IMRT subcommittee of the AAPM radiation therapy committee. *Medical physics (Lancaster)*, 30(8):2089–2115, 2003.

[42] ScandiDos. *Delta 4 Phantom+ User's Guide*. Uppsala, Sweden, 2019.

[43] ScandiDos. *ScandiDos Delta^4 software*. Uppsala, Sweden, November 2019. Version 1.00.0180.

[44] M. Hussein, C. H. Clark, and A. Nisbet. Challenges in calculation of the gamma index in radiotherapy – towards good practice. *Physica Medica*, 36:1–11, 2017.

[45] D. A. Low, W. B. Harms, S. Mutic, and J. A. Purdy. A technique for the quantitative evaluation of dose distributions. *Medical physics (Lancaster)*, 25(5):656–661, 1998.

[46] E. Bengtsson and P. Malm. Screening for cervical cancer using automated analysis of pap-smears. *Computational Mathematical Methods in Medicine*, pages 195–196, 2014.

[47] B. A Werness, A. J Levine, and P. M Howley. Association of human papillomavirus types 16 and 18 E6 proteins with p53. *Science (American Association for the Advancement of Science)*, 248(4951):76–79, 1990.

[48] C. S. Herrington. *Pathology of the Cervix*, volume 3 of *Essentials of Diagnostic Gynecological Pathology ;*. Springer International Publishing : Imprint: Springer, Cham, 1st ed. 2017. edition, 2017.

[49] Steven E Waggoner. Cervical cancer. *The Lancet*, 361(9376):2217–2225, 2003.

[50] National Cancer Institute. Definition of metastasis. `https://www.cancer.gov/publications/dictionaries/cancer-terms/def/metastasis`, 2020. [Online; accessed October 12, 2021].

[51] American Cancer Society. Lymph nodes and cancer. `https://www.cancer.org/cancer/cancer-basics/lymph-nodes-and-cancer.html`. [Online; accessed October 13, 2021].

[52] National Cancer Institute. Pelvis (female): Lymph nodes. https://visuals.nci.nih.gov/details.cfm?imageid=1770, 2020. [Online; accessed October 13, 2021].

[53] R. Pötter et al. MRI-guided adaptive brachytherapy in locally advanced cervical cancer (EMBRACE-I): a multicentre prospective cohort study. *The lancet oncology*, 22(4):538–547, 2021.

[54] L. C. Mendez and G. C. Morton. High dose-rate brachytherapy in the treatment of prostate cancer. *Translational andrology and urology*, 7(3):357–370, 2018.

[55] T. Girinsky et al. Overall treatment time in advanced cervical carcinomas: A critical parameter in treatment outcome. *International journal of radiation oncology, biology, physics*, 27(5):1051–1056, 1993.

[56] T. Kodama et al. Algorithm for an automatic treatment planning system using a single-arc VMAT for prostate cancer. *Journal of Applied Clinical Medical Physics*, 22(12):27–36, 2021.

[57] S. Breedveld, P. Storchi, P. Voet, and B. Heijmen. iCycle: Integrated, multicriterial beam angle, and profile optimization for generation of coplanar and noncoplanar IMRT plans. *Medical physics (Lancaster)*, 39(2):951–963, 2012.

[58] A. W. M. Sharfo et al. Comparison of VMAT and IMRT strategies for cervical cancer patients using automated planning. *Radiotherapy and Oncology*, 114(3):395–401, 2015.

[59] A. Nicolae et al. Evaluation of a machine-learning algorithm for treatment planning in prostate low-dose-rate brachytherapy. *International Journal of Radiation Oncology, Biology, Physics*, 97(4):822–829, 2017.

[60] P. Georg et al. Dose effect relationship for late side effects of the rectum and urinary bladder in magnetic resonance image-guided adaptive cervix cancer brachytherapy. *International journal of radiation oncology, biology, physics*, 82(2):653–657, 2012.

[61] R. Mazeron et al. Dose–volume effect relationships for late rectal morbidity in patients treated with chemoradiation and MRI-guided adaptive brachytherapy

for locally advanced cervical cancer: Results from the prospective multicenter EMBRACE study. *Radiotherapy and Oncology*, 120(3):412–419, 2016.

[62] A. C. Waldenström et al. Relative importance of hip and sacral pain among long-term gynecological cancer survivors treated with pelvic radiotherapy and their relationships to mean absorbed doses. *International journal of radiation oncology, biology, physics*, 84(2):428–436, 2012.

[63] D. Baltas et al. A conformal index (COIN) to evaluate implant quality and dose specification in brachytherapy. *International Journal of Radiation Oncology, Biology, Physics*, 40(2):515–524, 1998.

[64] K. Bruheim et al. Plan-of-the-day radiotherapy for patients with locally advanced cervical cancer - a prospective randomized controlled trial (the POD-protocol). 2021.

Appendices

A Example of Excel statistics

One example of the Excel sheets used in the optimisation process of the automatic planning script is provided in Figure A.1. The first plan, Cervix, is the manually made VMAT plan for this specific patient. Cervix (1) is the VMAT plan generated by the automatic VMAT planning script from the project thesis phase. The remaining VMAT plans are generated after different modifications of the VMAT planning script in the master's thesis phase.

Plan name	Rectum V40	Rectum V30	Rectum D0.03	Bladder V40	Bladder V30	Bowel V40	Bowel V30	Bowel D0.03	Body V47.3
Cervix	57,3	73,3	47,1	56,1	74,4	250,1	422	47,2	0
Cervix (1)	55,5	68	48,5	55,1	65,5	229,2	337,8	47,8	1,5
Cervix (2)	53,7	66,8	50,7	53,4	63	221,5	314,8	54,5	57
Cervix (3)	52,2	67	48,4	52	62,4	225,3	365,3	50,6	31,5
Cervix (4)	52,2	66,8	50,3	51,9	62,7	222,6	347,2	50,4	25,2
Cervix (5)	52,7	68,3	47,7	52,3	64,3	230,7	402,2	49,1	13,1
Cervix (6)	53,1	68,8	47,2	52,4	64,8	234,5	410,8	47,4	0,1
Cervix (7)	53,1	68,6	47,2	52,3	64,6	234,2	411,3	47,4	0,1
Cervix (8)	52,7	69,5	47,3	53,8	67,1	231	400,5	47,4	0,1
Cervix (9)	52,9	68,6	47,2	52,7	64,8	232,3	391,4	47,3	0,2
Cervix (10)	53,3	68,8	47	53	65,1	234,3	394,2	47,4	0,1
Cervix (11)	53,9	66,8	47,1	53	64,9	229,8	355,3	47,5	0,2
Cervix (12)	53,9	66,9	47	53,1	65,4	230,3	358,6	47,1	0,2
Cervix (13)	52,8	66,3	47	52,3	64,5	224,5	354,3	47,2	0,2
Cervix (14)	53,1	66,5	47	52,7	64,8	220,9	355,8	47,2	0,5

Figure A.1: Excel sheet with dose statistics for some organs at risk for different VMAT plans made for one specific patient. Different plans are enumerated with Cervix (#). A colour range from red to green is used to visualise high and low doses, respectively. V40 and V30 refer to the volumes that receive 40 Gy and 30 Gy, respectively, and D0.03 referd to the maximum dose.

B List of optimisation functions

Optimisation functions used in the automatic VMAT planning script for patients without and with positive lymph nodes are listed in Figures B.1 and B.2, respectively. The lists are arranged in the order of function value after the script has finished running, meaning that optimisation functions that were difficult to meet are positioned higher on the list. The xOAR volumes are labelled xOAR-PTVn, and the volume xBowelBag is the bowel volume minus PTVn and PTV 45.

ROI	Description	Robust	Weight	Value
				12.5175
Bladder	Max DVH 25.00 Gy to 50% volume		15.00	1.7945
Bladder	Max DVH 35.00 Gy to 36% volume		86.00	1.4903
xBowelBag	Max EUD 10.20 Gy, Parameter A 2		7.00	1.3686
PTV_45	Min dose 42.90 Gy		364045.00	1.2966
x40-PTV	Max dose 38.00 Gy		80.00	1.2227
Bladder	Max EUD 21.05 Gy, Parameter A 2		7.00	1.1770
xPTV_Ring0-1.5cm	Dose fall-off [H]43.00 Gy [L]23.00 Gy, Low dose distance 1.50 cm		120.00	1.1398
Body	Max EUD 7.67 Gy, Parameter A 2		3.00	1.0856
Rectum	Max EUD 20.48 Gy, Parameter A 2		7.00	0.8384
Rectum	Max DVH 35.00 Gy to 36% volume		86.00	0.6624
Body	Dose fall-off [H]45.00 Gy [L]20.00 Gy, Low dose distance 2.00 cm		200.00	0.3420
47.3	Max dose 46.80 Gy		30000.00	0.0535
CTV_45	Uniform dose 45.00 Gy		50.00	0.0230
CTV_45	Min dose 42.90 Gy		6331789.00	0.0157
CTV_45	Target EUD 45.00 Gy, Parameter A 1		10000.00	0.0039
xOAR47.3	Max dose 47.00 Gy		150000.00	0.0034
xCTVp	Max dose 46.00 Gy		10.00	1.3687E-4
PTV_45	Max dose 47.00 Gy		2000.00	6.8783E-6
Body	Max dose 47.00 Gy		300.00	6.3290E-8
xBowelBag	Max DVH 35.00 Gy to 32% volume		7.00	0.0000
FemoralHead_L	Max dose 45.00 Gy		10.00	0.0000
FemoralHead_R	Max dose 45.00 Gy		10.00	0.0000

Figure B.1: Optimisation functions used in the automatic VMAT planning script for a patient without positive lymph nodes. The functions are arranged in order of function value.

ROI	Description	Robust	Weight	Value
xBladder-PTVn	Max DVH 35.00 Gy to 50% volume		103.00	1.7068
xBowelBag	Max EUD 10.50 Gy, Parameter A 2		10.00	1.2406
xRectum-PTVn	Max DVH 35.00 Gy to 50% volume		50.00	1.1418
xPTV_Ring0-1.5cm	Dose fall-off [H]55.00 Gy [L]30.00 Gy, Low dose distance 1.50 cm		150.00	1.0288
x40	Max dose 38.00 Gy		100.00	1.0143
Body	Max EUD 8.11 Gy, Parameter A 2		3.00	0.9729
Bladder	Max EUD 25.18 Gy, Parameter A 2		10.00	0.9647
xBladder-PTVn	Max DVH 25.00 Gy to 50% volume		5.00	0.9331
Rectum	Max EUD 26.34 Gy, Parameter A 2		10.00	0.8041
PTV_45	Min dose 42.90 Gy		496827.00	0.7559
xBowelBag-PTVn	Max DVH 35.00 Gy to 7% volume		1452.00	0.5232
x47.3	Max dose 47.00 Gy		10000.00	0.2088
Kidney_R	Max EUD 3.09 Gy, Parameter A 1		1.00	0.1748
Kidney_L	Max EUD 2.53 Gy, Parameter A 1		1.00	0.1743
PTVn_57.5	Min dose 51.75 Gy		55062.00	0.1018
xRectum-PTVn	Max DVH 42.00 Gy to 22% volume		252.00	0.0995
Body	Dose fall-off [H]57.50 Gy [L]29.00 Gy, Low dose distance 2.00 cm		200.00	0.0907
xCTV!_45	Uniform dose 45.00 Gy		50.00	0.0231
CTVn2_57.5	Uniform dose 58.70 Gy		50.00	0.0149
xOAR47.3	Max dose 47.00 Gy		100000.00	0.0112
CTVn1_57.5	Uniform dose 58.70 Gy		50.00	0.0090
CTVn3_57.5	Uniform dose 58.70 Gy		50.00	0.0082
CTVn2_57.5	Min dose 57.60 Gy		18596.00	0.0073
CTVn1_57.5	Min dose 57.60 Gy		14789.00	0.0053
CTVn3_57.5	Min dose 57.60 Gy		12721.00	0.0038
xCTVp	Max dose 46.50 Gy		50.00	2.9790E-4
xPTV!_45	Max dose 47.20 Gy		2000.00	7.1715E-5
BowelBag	Max dose 57.40 Gy		1500.00	3.3069E-5
FemoralHead_L	Max dose 45.00 Gy		10.00	4.0769E-7
Body	Max dose 61.00 Gy		400.00	9.6237E-8
PTVn_57.5	Max dose 61.50 Gy		600.00	0.0000
SpinalCord_PRV	Max dose 45.00 Gy		1000.00	0.0000
CaudaEquina	Max dose 48.00 Gy		1000.00	0.0000
FemoralHead_R	Max dose 45.00 Gy		10.00	0.0000

Figure B.2: Optimisation functions used in the automatic VMAT planning script for a patient with positive lymph nodes. The functions are arranged in order of function value.

C Kidney doses

Screenshots from RayStation that show dose accumulations in the body volume between the kidneys are shown in Figures C.1 and C.2 for patient 1 and 12, respectively. How the function weight of the kidney max EUD optimisation function affects the kidney and bowel doses is shown in Table C.1.

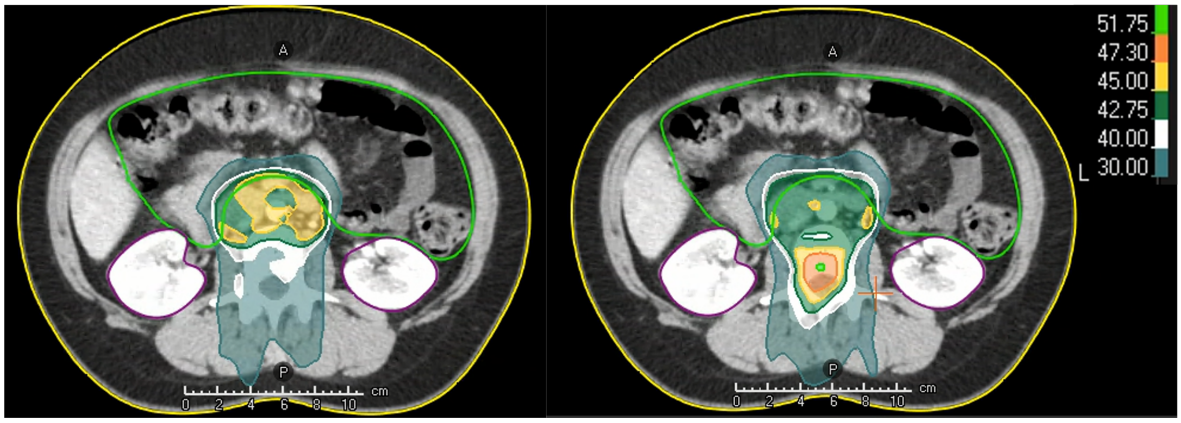

Figure C.1: Image of the dose distribution around the kidneys for patient 1 with automatic VMAT planning (left) and manual VMAT planning (right). Dose accumulates between the kidneys with manual VMAT planning. Image viewed in the transverse plane.

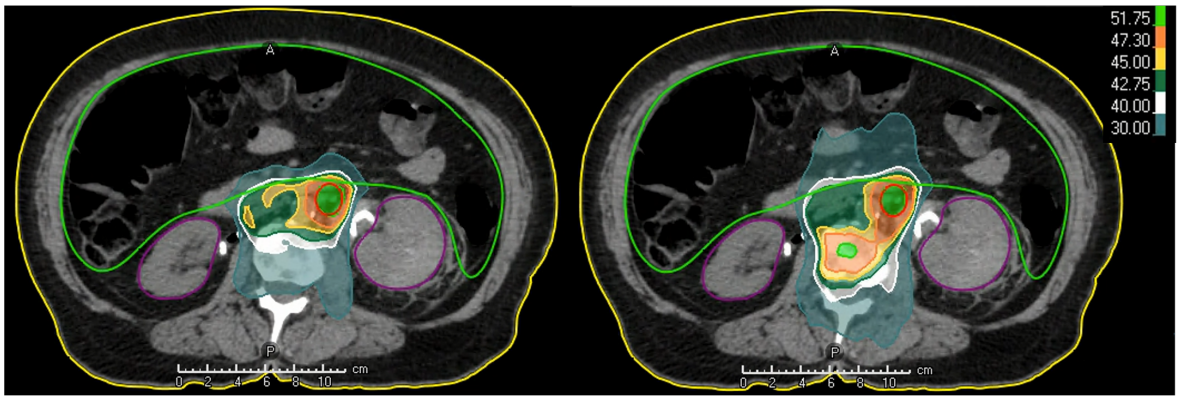

Figure C.2: Image of the dose distribution around the kidneys for patient 12 with automatic VMAT planning (left) and manual VMAT planning (right). Dose accumulates between the kidneys with manual VMAT planning. Image viewed in the transverse plane.

Table C.1: Dose data showing how the function weight of the kidney max EUD function affects the bowel and kidney doses in the automatic VMAT planning script for patient 19. All other parameters are kept constant.

Function weight kidney max EUD	**Bowel $V_{40\ Gy}$**	**Bowel $V_{30\ Gy}$**	**Kidney L D_{mean}**	**Kidney R D_{mean}**
10	234.2	657.0	5.7	5.1
5	222.5	570.4	5.8	6.9
1	219.1	540.7	6.5	7.1

D Blind test

The blind test form included a coloumn where the recipients could justify their choice of treatment plan. Table D.1 is a summary of the responses.

Table D.1: Summary of the reasons behind the choice of plan in the blind test. Reasons that weigh for and against the choice of a specific plan are marked with + and ÷, respectively.

	Automatic VMAT plans	**Manual VMAT plans**
Case 1	+ Better conformity + Lower bowel dose	+ Lower kidney doses ÷ Hot spot between the kidneys
Case 2	+ Better conformity + Lower OAR doses ÷ Lower target coverage	
Case 3	+ Better conformity + Lower OAR doses + Lower bowel dose ÷ Lower target coverage	+ Lower kidney doses ÷ Broad dose distribution
Case 4	+ Better conformity + Lower rectum dose ÷ Lower target coverage	÷ Lower target coverage to PTVn_57.5 ÷ Hot-spots in PTV_45
Case 5	+ Better conformity to PTV_45 + Lower rectum Dmax	+ Lower kidney doses + Better target coverage + Better conformity to PTVn ÷ Hot-spots in PTV_45
Case 6	+ Better conformity + Lower OAR doses + More homogenous dose to PTV_45 ÷ Lower target coverage	÷ Unacceptable hot-spots in PTV45 ÷ Low conformity
Case 7	+ Better conformity + Lower OAR doses	÷ Hotspot between the kidneys
Case 8	+ Better conformity + Lower OAR doses.	
Case 9	+ Better conformity	+ Better target coverage ÷ Hot-spots in PTV45
Case 10	+ Better conformity + Lower OAR doses	

E Automatic VMAT planning script

The automatic VMAT planning script that was developed for LACC patients in this master's thesis is available on request to Marit Funderud at the RT department at St. Olavs Hospital.

F Abstract for MedFys 2022

The following abstract was accepted for oral presentation at MedFys 2022 held in Hurdal from the 23rd to 25th of May 2022.

Automatic VMAT planning in RayStation for locally advanced cervical cancer.

Ingvild Straumsheim Hoem[1], Marit Funderud[2], Josefine Stahl Kornerup[3], Anne Beate Langeland Marthinsen[4]

[1] Department of physics, NTNU, ingvisho@stud.ntnu.no / ingvildhoem@gmail.com
[2] Radiation Therapy Department, St. Olavs Hospital, Marit.Funderud@stolav.no
[3] Radiation Therapy Department, St. Olavs Hospital, Josefine.Stahl.Kornerup@stolav.no
[4] Radiation Therapy Department, St. Olavs Hospital, Anne.Marthinsen@stolav.no / Department of Physics, NTNU; Anne.b.Marthinsen@ntnu.no

In radiation therapy, increased use of Volumetric Modulated Arc Therapy (VMAT) with conformal dose delivery has improved the dose distribution to target volumes while delivering acceptable lower doses to nearby organs at risk (OARs). However, treatment planning with VMAT is a complex and time-consuming process. This year, St. Olavs hospital in Trondheim has replaced manual with automatical VMAT treatment planning in RayStation for breast and prostate cancer patients. The automatic plans are script-based and developed from manual planning procedures. Automatic planning is time-saving, and the plans are of comparable quality to manual plans.

Locally advanced cervical cancer (LACC) involves irradiation of complex target volumes with simultaneous integrated boost (SIB) together with strict upper dose limits to OARs. This makes the treatment of LACC complicated. The current project aimed to make automatic VMAT plans for LACC in RayStation. An automatic treatment planning script that aims to reduce dose to OARs as much as possible while maintaining target coverage, conformity and homogeneity has been developed and teated on 15 LACC patients. The script follows cervical cancer radiation therapy guidelines from the Norwegian Directorate of Health (2021) and the EMBRACE II protocol. These automatically made plans are shown to be of similar quality as the corresponding manually made VMAT plans. When in clinical use, the automatic plans will significantly reduce planning time and variability due to the knowledge of the treatment planner. In

principle, with appropriate diagnosis specific adjustments and testing of plans, similar automatic planning procedures can be used for all cancer sites.

G Abstract for Biophysics and Medical Physics Spring Meeting 2022

The following abstract was accepted for oral presentation at the Biophysics and Medical Physics Spring Meeting in Trondheim from the 12th to 13th of May 2022.

Automatic VMAT planning in RayStation for locally advanced cervical cancer

Ingvild Straumsheim Hoem[1], Marit Funderud[2], Anette Guleng[3], Josefine Stahl Kornerup[4], Anne Beate Langeland Marthinsen[5]

[1] Department of physics, NTNU, ingvisho@stud.ntnu.no / ingvildhoem@gmail.com
[2] Radiation Therapy Department, St. Olavs Hospital, Marit.Funderud@stolav.no
[3] Radiation Therapy Department, St. Olavs Hospital, Marte.Anette.Dunseth.Guleng@stolav.no
[4] Radiation Therapy Department, St. Olavs Hospital, Josefine.Stahl.Kornerup@stolav.no
[5] Radiation Therapy Department, St. Olavs Hospital, Anne.Marthinsen@stolav.no / Department of Physics, NTNU; Anne.b.Marthinsen@ntnu.no

In radiation therapy, increased use of Volumetric Modulated Arc Therapy (VMAT) with conformal dose delivery has improved the dose distribution to target volumes while delivering acceptable lower doses to nearby organs at risk (OARs). However, treatment planning with VMAT is a complex and time-consuming process. In 2021, St. Olavs hospital in Trondheim replaced manual with automatic VMAT treatment planning in RayStation for breast and prostate cancer patients. The automatic plans were script-based and developed to mimic manual planning procedures. Automatic planning is time-saving, and the plans are of comparable quality to manual methods.

Treatment of locally advanced cervical cancer (LACC) involves irradiation of complex target volumes with simultaneous integrated boost (SIB) together with strict upper dose limits to OARs. Due to multiple dose levels and many nearby OARs, the treatment of LACC is complex. The current project aims to produce VMAT plans for LACC in RayStation automatically. An automatic planning script has been developed and tested on 40 LACC patients. The script follows radiation therapy guidelines for cervical cancer from the Norwegian Directorate of Health (2021) and the EMBRACE II protocol (2015). It aims at reducing dose to OARs as much as possible while maintaining target coverage, conformity and homogeneity. Treatment plans made with the automatic planning script has shown similar or better plan quality compared to the

corresponding manually made VMAT plans. When in clinical use, the automatic plans will significantly reduce planning time and plan variability caused by differences in experience between treatment planners. In principle, with appropriate diagnosis specific adjustments and testing of plans, similar automatic planning procedures can be used for all cancer sites.

Ingvild Straumsheim Hoem

Automatic VMAT planning in RayStation for locally advanced cervical cancer

NTNU
Kunnskap for en bedre verden

ST. OLAVS HOSPITAL
UNIVERSITETSSYKEHUSET I TRONDHEIM